Noname manuscript No.
(will be inserted by the editor)

Un-jamming due to energetic instability: statics to dynamics

Stefan Luding · Yimin Jiang · Mario Liu

Received: date / Accepted: date

Abstract Jamming/un-jamming, the transition between solid- and fluid-like behavior in granular matter, is an ubiquitous phenomenon in need of a sound understanding. As argued here, in addition to the usual un-jamming by vanishing pressure due to a decrease of density, there is also *yield* (plastic rearrangements and un-jamming that occur) if, e.g., for given pressure, the shear stress becomes too large. Similar to the *van der Waals transition* between vapor and water, or the critical current in superconductors, we believe that one mechanism causing yield is by the loss of the energy's convexity (causing irreversible re-arrangements of the micro-structure, either locally or globally).

We focus on this mechanism in the context of granular solid hydrodynamics (GSH), employing it in an over-simplified (bottom-up) fashion by setting as many parameters as possible to constant. Also, we complemented/completed GSH by using various insights/observations from particle simulations and calibrating some of the theoretical parameters – both continuum and particle points of view are reviewed in the context of the research developments during the last few years. Any other energy-based elastic-plastic theory that is properly calibrated (top-down), by experimental or numerical data, would describe granular solids. But only if it would cover granular gas, fluid, and solid states simultaneously (as GSH does) could it follow the systems evolution through all states into un-jammed, possibly dynamic/collisional states – and back to elastically stable ones. We show how the un-jamming dynamics starts off, unfolds, develops, and ends. We follow the system through various deformation modes: transitions, yielding, un-jamming and jamming, both analytically and numerically and bring together the continuum model with particle simulations, quantitatively.

Keywords constitutive model · state transitions · un-jamming · jamming · concave elastic energy · GSH

Dedication: SL *Bob was not only an inspiring researcher and colleague for me, he influenced my research on granular matter so much! Also he became a good friend over the 25 years I knew him. I will always remember the great research visits to Duke, but also the time we spent together on many international conferences, like in Cargese or at several Powders & Grains events. His passing away was a shock and leaves a big gap for me.*

Dedication: ML *It was in the heydays of helium physics when I, playing with some theories, first met Bob, the conscientious and meticulous experimenter, whose results are wise not to doubt, around which you simply wrap your model. But grains were his real calling. Many decades later, I am again busy fitting my pet theory to his data, and that of his group – such as shear jamming. Some things just never change.*

1 Introduction

The macroscopic Navier-Stokes equations allow one to describe Newtonian fluids with constant transport coefficients (e.g., viscosity). In many non-Newtonian systems, complex fluids [1], colloidal suspensions, review [2,3,4], and especially granular matter [5] in its flowing state [6], the transport coefficients depend on various

Stefan Luding
University of Twente, The Netherlands

Yimin Jiang
Central South University, Changsha, China

Mario Liu
University Tübingen, Germany

state variables such as the density and the granular temperature [7]. This interdependence and the presence of energy dissipation is at the origin of many interesting phenomena: clustering [8], shear-band formation [9], jamming/un-jamming [10], dilatancy [11], shear-thickening [12,13,3,4] or shear-jamming [10,14], plastic deformations [15,16,17,18,19,20], related also to creep/relaxation [21,22,11,23,24], and many others. The research on granular matter in the last decades – to a good fraction inspired by works of Bob Behringer and co-workers – will be briefly reviewed next.

1.1 A brief history of granular research

In order to describe solid-like granular matter on the macroscopic scale, concepts from elasto- and visco-plastic theories were used [25,26,15,27,28,16,29,30,31,32,33] including instabilities, yield and failure [34,35,36,37,38,28,39,40,41,42]. Recently, statistical mechanics/physics concepts [43], helped to better understand the probabilities for plastic deformations [17,44,45,18,19,46,20,33], force network change/growth [47,48], stress-based meso ensembles [49], or stress-relaxation [21,22,11,23]. A traditional subject of research are stress-fluctuations [50,51,52,53], and the quest for the "effective temperature" [54,55,44,45] of thermal or athermal granular packings [56,49,45]. Most recently, universal scaling laws [57] were reported, and compression and shear in particularly small systems [58] could be understood. Considering granular solids, their stiffness, and the elastic moduli [59,30,60] have to be considered in the presence of non-affine deformations [60]. For this, over-compression and shear [59,46,61,62,57] cyclic loading [63] or even thermal cyclic loading [64] were applied.

When sheared granular matter starts to flow and (for large enough strain) reaches a steady state, or critical state [65,66,67,13], the nowadays widely accepted "classical" $\mu(I)$-rheology [68] holds. It was recently extended to include friction, softness and cohesion [2,65,66,69,12,70], but it does not have a fully tensorial form [71,72], and doubts about its well-posed-ness are still discussed [73,74,75].

Modern experimental techniques [67,76,77,24], also with focus on low confining stress [78], shed new light on classical works on the response to local perturbations [79], jamming and un-jamming [80,81,79,22,82], in particular by shear [10,83,46,84,57,62,85], and transients, fabric/micro-structure evolution [52,86,87,30,46,88,89]. One of the classical experimental techniques involves photoelastic materials that allow to visualize stress [90,91,92], as complemented by a huge amount of particle simulations, e.g., see Ref. [9], or for a most recent example, see Ref. [93] and references therein.

One important success of granular research was to bring solid-like and flowing behavior of granular matter together, e.g., in a continuum theory with fluidity [94,44,18,45], and to understand anisotropy [86,66,88,89], also shape induced [95,96], as well as involving the rotational degrees of freedom and micro-polar models [2,97,98,99,100,101], not to forget wet particle systems [3,4], for which a thermodynamically consistent theory [102] and numerical solutions [103] were recently proposed.

1.2 Open challenges

Some open questions are: *How can we understand phenomena that originate from the particle- or meso-scale, which is intermediate between atoms and the macroscopic, hydrodynamic scale? And how can we formulate a theoretical framework that takes the place of the Navier-Stokes equations?*

A universal theory must involve all states granular matter can take, i.e., granular gases, fluids, and solids, as well as the transitions between those states. *What are the state variables needed for such a theory? And what are the parameters (that we call transport coefficients) and how do they depend on the state variables?*

Main goal of this paper is to propose a minimalist candidate for such an universal theory, able to capture granular solid, fluid, and gas, as well as various modes of transitions between these states. The model, remarkably, involves only four state variables, density, momentum density (vector), elastic strain (tensor), and granular temperature. It is a boiled down, simplified case of the more complete theory GSH [104,105,106,107,44,45], but complemented by insights based on DEM, see Ref. [46] and references therein, and modified such that it works below, above and during transitions. For the sake of transparency and treatability, we reduce most transport coefficients and parameters to constants whenever possible – without loss of generality.

Each transport coefficient is related to the propagation or evolution of one (or more) of the state variables that encompass the present state of the system. For simple fluids [1,108], it is possible to bridge between the (macroscopic) hydrodynamic and the (microscopic) atomistic scales; as an example, the diffusion coefficient quantifies mass-transport mediated by microscopic fluctuations.

In the case of low density gases, the macroscopic equations and the transport coefficients can be obtained using the Boltzmann kinetic equation as a starting point. For moderate densities, the Enskog

equations provide a good, quite accurate description of dense gases (or fluids) of hard atoms [1], or of particles including the effects of dissipation, which results in what is nowadays referred to as standard kinetic theory (SKT) [109,7]. Beyond SKT one can only reach out (empirically) towards realistic systems [110,8,111], and beyond, see, e.g., [12,4]. The limit of granular fluids is where other coefficients, like the viscosity, actually begin to deviate from SKT. This takes place well below jamming, and lead to a divergence [12, 112,113] when the granular fluid becomes denser [8, 114,111], approaching jamming, i.e., the state that we could call a granular solid, as described by classical solid mechanics [115]. Recent research also considers soft particles [113,70,116] for which jamming changes from a sharp to a rather smooth transition. One objective of this paper is to bring together fundamental theoretical concepts of continuum mechanics [117,31,45,118,102] with observations made from particle simulations for simple granular systems in the gas, fluid, and solid states, including also the transitions between those states [8,119,120,121,113,46,111].

1.3 About states of granular matter

When exposed to external stresses, grains are elastically deformed at their contacts. In static situations, there is only elastic energy; in flowing states, some of the elastic energy is transferred to kinetic energy and back[1], as sketched in Fig. 1 for the example of slow isotropic jamming, and – after an overcompression cycle – eventually un-jamming. Note that the jamming transition at very small (yet finite) compression rate appears smooth/continuous, whereas the un-jamming transition is rather sharp/discontinuous.

Grains yield differently for vanishing or finite T_g. In motion, for $T_g \neq 0$, yield is a continuous phenomenon, i.e., state variables vary continuously. If the grains are at rest initially, $T_g = 0$, yield is discontinuous – as evidenced by a layer of grains on a tilted plane. Discontinuity is mainly in the equilibrium value of the elastic stress. It is finite in the convex region and zero in the concave one, as it always relaxes away there. Any discontinuity of a phase transition is always in the equilibrium values of some quantities.

The behavior of very slowly compressed particles in Fig. 1 shows that even such little dynamics allows for a rich phenomenology below and above jamming, where the yellow area corresponds to a dense fluid with solid features – just below jamming, while the cyan area corresponds to a solid with fluid-like features – jammed, but strongly unstable (see the steps and wiggles in pressure and coordination number).

The capability of granular solids to remain quiescent, in mechanical equilibrium, under a given finite stress is precarious. For small perturbations they will return to their original state. If pressure or shear stress become too large, the grains will, suddenly, start moving – either locally or globally [17] – with a decaying elastic stress. This qualitative change in behavior is an unambiguous phase transition. We shall refer to the region capable of maintaining the global, overall equilibrium of static grains as *elastic*, and its boundary (in the space spanned by the state variables) as the *yield surface*. For local loss of elasticity we rather use the term plastic, irreversible events, see Refs. [19,58].

Granular systems will also un-jam for vanishing pressure and a continuous reduction of density, though we reserve the term yield for the (sudden) loss of elastic stability: Grains un-jam in either case, they *yield* only when the elastic stress, in particular the pressure, is finite.

[1] As **definition of states**, flowing states range from dilute granular gases via inertial, collisional granular fluids, to quasi-static flows and plastically (irreversibly) deforming granular solids, excluding only perfectly static, elastic granular solids (e.g., probed by elastic waves). The most interesting regime is around quasi-static flows where both solid and fluid features are important [83], with considerable permanent and fluctuating energy densities, w_e and w_T, respectively, summing up to the total $w = w_e + w_T$. Note that w_T contains all kinetic energy, $E_{\rm kin}$, and also the fluctuating part of the potential energy, $E^f_{\rm pot}$, i.e., $w_e = (E_{\rm pot} - E^f_{\rm pot})/V$, as discussed next. The density (equivalent to the volume fraction, $\rho \sim \phi$) alone is not sufficient to characterize the state of a particle system, even though "magic" densities like random close or lose, $\phi_{\rm RCP}$ and $\phi_{\rm RLP}$, respectively, are often used, but being highly material dependent they are not unique state descriptors. In addition to density, the ratio of kinetic to potential, elastic energy in the system, $K = E_{\rm kin}/E_{\rm pot}$, is one more possibility to characterize its state: gas ($\phi \ll 1$, $K \gg 1$), fluid ($\phi < \phi_{\rm RLP}$, $K > 1$) dense collisional flow ($\phi \sim \phi_{\rm RLP}$, $K \sim 1$), quasi-static flow ($\phi \sim \phi_{\rm RCP} > \phi_{\rm RLP}$, $K \ll 1$), granular solid ($K \approx 0$), static ($K = 0$), and the extreme, athermal case ($K \equiv 0$, maintained at all times), as can be realized by energy minimization, e.g., see Ref. [121] and references therein. The contribution of potential energy to the total energy is $1/(1+K)$, but using the fluctuating fraction of total energy defines the states as: gas ($w_T/w = 2/(1+K) \ll 1$, due to $E_{\rm pot} = E^f_{\rm pot}$), collisional ($w_T/w \sim 1$), intermediate quasi-static and solid-like ($w_T/w = 2K/(1+K) \approx 2K \ll 1$, due to equipartition $E_{\rm kin} = E^f_{\rm pot}$), static, solid ($w_T/w = 0$), and crystalline ordered, possibly at $\phi \gg \phi_{\rm RCP}$.
Main message of this paper is that, besides density, only two additional scalar state-variables are sufficient to encompass all possible (isotropic) states and transitions of a system, namely the isotropic elastic strain – encompassing the jamming density, ϕ_J, itself [46] – and a granular temperature $T_g \propto \delta v \propto \sqrt{w_T}$, encompassing the velocity fluctuations, δv [18]. For anisotropic (sheared) states at least one more state variable is needed.

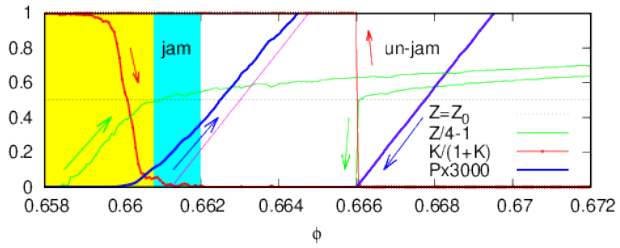

Fig. 1 Sketch of isotropic jamming and un-jamming, with dimensionless compression rate $I_v < I_v(\phi_J^0 = 0.6608) = \dot{\varepsilon}_v d_p/\sqrt{P_\Delta \rho_p} = 1.2 \times 10^{-5}$, of frictionless, polydisperse particles, from simulations in Ref. [46], with reversal at maximal density $\phi_{\max} = 0.9$, so that unjamming occurs at $\phi_J^1 = 0.666$. Displayed are the coordination number Z (green) that defines dynamic initial jamming at $Z(\phi_J^0) = Z_0$, the scaled dimensionless elastic pressure $P = P_\Delta d_p/k_n$ (blue), with $P(\phi_J^0) = 4 \times 10^{-5}$, and the fraction of kinetic energy $K/(1+K)$ (red), as discussed in footnote 1: For initial jamming, the yellow area designates the dense collisional flow state ($K \sim 1$), while the cyan area designates the quasi-static (isotropic) flow state ($K \ll 1$). The thin magenta line is a fit to Eq. (11) in Ref. [46] of all solid-like high-pressure data (using $K < 5 \times 10^{-4}$, i.e., $\phi \geq 0.665$), on the initial compression branch (data out of this plot, well above the rather unstable cyan area, up to much larger $\phi_{\max}$), yielding an extrapolated jamming density of $\phi_J^P = 0.66125$ (around which the cyan area is centered), and a dimensionless modulus $p_0 = 0.06272$ (note that $p_0 \to p_0/\phi_J^P$ in Ref. [46]), and the nonlinear coefficient $\gamma_p = 0.179$ that accounts for the large overlaps of particles in the simulation, for more details see Ref. [46]. Note that this full-range fitting perfectly collapses with the unloading branch (not visible), but that it is fundamentally different from the calibrated comparison between simulation and model solution, as presented in Sec. 6.

Starting from the elastic region, decompression (tension) reduces the density and the elastic deformations of the grains – until the latter vanish and the system unjams. Decompressing further just reduces the density accordingly. The system is now un-jammed in the sense that one can change the density without any restoring force, i.e., the elastic energy remains zero. In reverse, compression only increases the density, as long as it is smaller than the jamming density. At jamming both the elastic deformations and the associated energy start to increase with density. In contrast, there is a discontinuity leaving the elastic regime at finite values of elastic stress. It is a sudden transition from quiescent, enduringly deformed grains, to moving ones oscillatorily deformed due to "jiggling" particle motions. This transition needs to be explained, to have a model for. And it is clear that the transition must be encoded in the elastic energy – the only quantity characterizing the quiescent state – not in the dynamic/fluctuating contributions to energy.

In the elastic region, grains appear solid when at rest, but they will flow if subject to an imposed shear rate, and appear liquid. This *continuous change in appearance* is well accounted for by any competent dynamic theory or rheology, it is not a transition [2] . Moreover, flowing grains in the elastic region do feature a macroscopic elastic shear stress, with an associated elastic energy (even though granular contacts switch continually), something no Newtonian liquid is capable of. Also, the shear stress remains finite when the grains stop flowing, which is not the case in Newtonian fluids.

So there are two different flowing states, either with finite elastic stress/strain, or with vanishing ones, which includes granular gases as accounted for by the kinetic theory, see Refs. [8,111] and references therein. There is also a transition between them, as possibly related to (dry) liquefaction [35], but not to be confused with liquefaction due to a fluid between the particles, which is completely disregarded in this study of dry granular matter (even though the fluid stress can be considerable in wet system). We take both transitions, either leaving the quiescent state, or the flowing one, as the same transition, with the same underlying physics. In fact, encoding the transition in the elastic energy certainly affects the flowing state as well. The mechanism for yield is here related to elastic energy (irrespective whether the pressure or the shear stress is too large, or the density too small), as traditionally encompassed by concepts like plastic potentials, yield functions, or flow rules [29,117,31,33,101], see Fig. 2 below and textbooks like Ref. [117].

1.4 Relation to other systems in physics

We do not think that the transition is due to *spontaneously broken translational symmetry* – the usual mechanism giving rise to static shear stresses, as in any fluid-solid transitions. The quick argument is: Consisting of solid, grains already break translational symmetry. More importantly, the loss of equilibrium and granular static is caused by the shear stress or pressure being too strong.

This is an indication of an over-tightening phenomenon, of which the (pair-breaking) *critical current* is a prime example. If a superconductor conducts electricity without dissipation, it is in a *current-carrying equilibrium state*. If, however, the imposed current exceeds a maximal value, the system leaves equilibrium

[2] This is the macroscopic view on a representative volume much larger than the single particles; whether plastic granular flow and elastic instability transitions are connected on a local scale of a few grains is not excluded here, since there is ample evidence of local instabilities, force-chain buckling, trimer deformations, etc., see Refs. [34,122,39,123,42,14], on the particle scale, which is not addressed in this paper.

and enters a dissipative, resistive state. The superfluid velocity, $v_{sf} \sim \nabla\Psi$, given by the gradient of a quantum mechanical phase, Ψ, is the analogue of the strain. The dissipationless current, $j_{sf} = \partial w/\partial v_{sf}$, given by the derivative of the energy with respect to v_{sf}, is the analogue of the elastic stress. The over-tightening transition in superconductivity is well accounted for by an inflection point, at which the energy turns from stably convex to concave, see the classic paper by Bardeen [124]. The close analogy between the two systems is a good reason to employ the same approach here, to postulate that the surface of the cone in Fig 2 can be related to an inflection surface of the elastic energy.

1.5 About elastic granular matter

The granular solid state is contingent on granular matter capable of being elastic, for which there is ample evidence, see e.g. Refs. [125,6,126,79,127,128,49,120, 90] and references therein. In addition to the material stiffness, many other material properties (including cohesion, friction, surface-roughness, particle-shape) determine the elastic response of granular matter. For soft and stiff materials the deformations are, respectively, considerable and slight, but never zero. Because of their Hertz-like non-linear contacts, grains are infinitely soft in the limit of vanishing contact area (deformation). Therefore, at any given finite force, deformations are always sufficiently large to display the full spectrum of elastic behavior, including a considerable static shear stress (enabling a tilted surface), and elastic waves. Even the simplest model material, consisting of perfectly smooth spheres of isotropic, linearly elastic material, displays non-linearity due to their Hertz-type contacts, on-top of the contact network (fabric) and its re-structuring. Only in computer simulations is it possible to remove the first and focus on the second, see e.g. Ref. [46].

Elastic waves propagate in granular media, displaying various non-linear features, including anisotropy, dispersion and rotations, see e.g. Ref. [129,130,131,99, 132,133,100,134,101] and references therein. The discreteness and disorder of granular media add various phenomena – already for tiny amplitudes – such as dispersion, low-pass filtering and attenuation [135,99,136, 134]. With increasing amplitudes, a wide spectrum of further phenomena is unleashed, among which the beginning of irreversibility and plasticity, see Ref. [20] in this topical issue, and references therein, and the loss of mechanical stability [137], what we call "yield" in the following.

1.6 Yield: About the limits of elasticity

To envision the *yield surface*, we consider the space spanned by three parameters: pressure P, shear stress σ_s, and void ratio $e = (1-\phi)/\phi$ (where $\rho = \rho_p\phi$, with material density ρ_p and volume fraction ϕ), ignoring the granular temperature (i.e., fluctuations of kinetic energy), as discussed in Ref. [138] and so many papers following. Based on the observation of the *Coulomb yield* and the *virgin consolidation line*, we assume that the yield surface is as rendered in Fig. 2. Elastic, jammed states, maintained by deformed grains, are stable and static only inside it [3].

The Coulomb yield line, see Fig. 2(b), can be reached by increasing the shear stress at given confining pressure. When the shear stress exceeds a certain level, the system yields, un-jams and becomes dynamic. No static, stable elastic state exists above the Coulomb yield line, as evidenced by a sand pile's steepest slope.

It is imperative to realize that (what we call) the Coulomb yield line is conceptually different from the peak shear stress achieved during the approach to the critical state at much larger strains. Coulomb yield is the collapse of static states – such as when one slowly tilts a plate carrying grains until they start to flow (max. angle of stability). Its behavior is necessarily encoded in the system's energy, because this phenomenon does not at all involve the system's dynamics. The critical state, including the peak shear stress – though referred to as "quasi-static" – is a fully dynamic and irreversible effect. It is accounted for by *the stationary solution at given strain rates* in GSH. The angle of repose (always smaller than the max. angle of stability) is in GSH given by the critical friction angle [44,45].

In the absence of shear stresses, the maximally sustainable pressure depends on the void ratio, e, as rendered in Fig. 2(a). Starting from a given e, slowly increasing P, the grain-structure will collapse and yield at this pressure, to a smaller value of e, such that the final state is stable, static, and below the curve of Fig. 2(a). This is because when applying a slowly increasing pressure, the point of collapse is (ever so) slightly above the curve; and the end point below it is typically also close. This evolution resembles a stair-case, with the granular medium increasing its density by hugging this curve, which frequently referred to as the *virgin/primary consolidation line*, or simply the *pressure yield line*. The line cuts the e-axis at the random loosest void ratio, e_0, above which no elastic stable states exists.

[3] However, this does not exclude the possibility that there are plastic deformations possible inside (in finite systems) as evidenced from particle simulations, e.g., in Refs. [27,120].

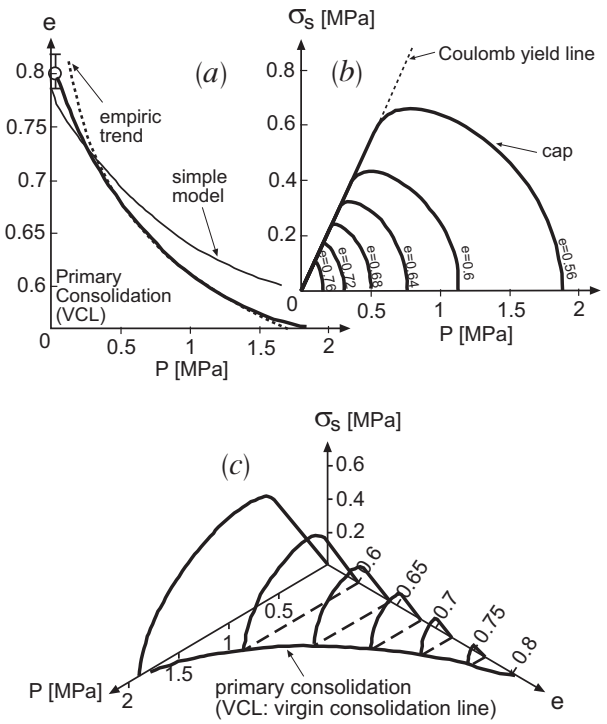

Fig. 2 Granular yield surface, or the jamming phase diagram, for $T_g = 0$, as a function of the pressure P, shear stress σ_s, and void ratio e, as rendered by an energy expression in [107]. Panel **(c)** is the 3D combination of **(a)** and **(b)**; with **(b)** depicting how the straight Coulomb yield line bends over, depending on the void ratio e – a behavior usually accounted for by *cap models* in elasto-plastic theories; while **(a)** depicts the maximal void ratio e (equivalent to the density) plotted against pressure P, or the so-called *virgin consolidation line* (VCL). In panel **(a)**, the dotted line is an empirical relation, $e = e_1 - e_2 \log(P/P_0)$, with $P_0 = 0.5\,\mathrm{MPa}$, $e_1 = 0.679$ and $e_2 = 0.097$, approximating the VCL, but not valid for $P \to 0$. The thick solid line cuts the e-axis at e_0, with the intersection being the lowest possible, random loosest packing value, see Ref. [107] for details, where also the thin solid line is discussed. Thus e_0 also defines the lowest possible jamming volume fraction, $\phi_{J0} = 1/(1+e_0)$, see Ref. [46], with static, elastic states possible only below the VCL, as will be shown in Secs. 5 and 6.

Because of the pressure yield line, the Coulomb yield curve cannot persist for arbitrarily large P at given e. Rather, it bends over to form a "cap", as rendered in Fig. 2(b), since an additional shear stress close to the pressure yield line will also cause the packing to collapse. (The shape of the cap depends on the interplay of isotropic and deviatoric deformations as well as the probability for irreversible, possibly large-scale restructuring events of the micro-structure, i.e., the contact network, including also the sliding of contacts, but also breakage of particles, which is, however, excluded from this study. Whether the picture sketched here is sound without breakage remains an open question.)

Merging 1(a) and 1(b) yields the elastic region below the yield surface, as given in Fig. 2(c). Although the e-axis, for $P, \sigma_s = 0$, see Fig. 2, is also referred to as the loci of (isotropic) un-jamming, the elastic stress goes continuously to zero here, because the grains are successively less deformed. There is, as already discussed above in subsection 1.3, no discontinuous phase transition or yield here, except for the coordination number, see Fig. 1. Point is, concerning only this one point of the plot, if the elastic stresses vanish, both in the convex and concave region, nothing much resembling a discontinuous transition happens there. Isotropic jamming and un-jamming, as well as the discontinuity in the coordination number on the isotropic e-axis is discussed in detail at various spots in this paper, see subsections 1.3, 3.2.3, and 4.1.1.

Next, we summarize all different symbols and nomenclatures.

1.7 Notation and symbols

This paper is a cooperation of co-authors, whose notational baggage from past publications clash with one another. In the dire need to compromise, we ask the readers to suffer – with us – using varying symbols and notations. Our state-variables are: density, ρ, momentum density, ρv_i, granular temperature, T_g, and the elastic strain, as summarized here.

1. The bulk density, ρ, is related to the volume fraction, $\phi = \rho/\rho_p$ (with ρ_p the particles' material density), the porosity $1-\phi$, and the void ratio $e = (1-\phi)/\phi$. (Later, we shall choose units such that $\rho_p = 1$, so that volume fraction and bulk density are identical [4].)
2. The conserved momentum density g_i defines the velocity $v_i = g_i/\rho$. The symmetric part of the velocity gradient is

   $$v_{ij} := v_{(i,j)} := \tfrac{1}{2}(\nabla_i v_j + \nabla_j v_i) = -\dot{\varepsilon}_{ij} = D_{ij}$$

   The total strain rate $\dot{\varepsilon}_{ij}$ is positive for compression and negative for tension.
   The symbol v_{ij} is usual in condensed matter physics, see [108,115,139]. It is also the one employed in most previous GSH-publications. The notation D_{ij} is common in theoretical mechanics [31,102], while $\dot{\varepsilon}_{ij}$, or $\dot{\gamma}$, are used, e.g., in soil mechanics and related literature [117,101].

[4] This choice requires a constant ρ_p as true for rather stiff materials or, e.g., for soft gel particles, however, for materials like soft foams and agglomerates, or under thermal expansion, ρ_p will become an independent state variable and the non-dimensionalization will work only with a reference density $\rho_p(P=0, T=T_0)$.

3. Subscripts, such as i,j,k,l, refer to components of tensors in the usual index notation, with double-indices implying summation, the comma indicating a partial derivative, as in $v_{(i,j)}$; the superscript * denotes the respective traceless (deviatoric) tensor. Using the summation convention, the volumetric strain rate is abbreviated as: $\dot{\varepsilon}_v = \dot{\varepsilon}_{ll} = -v_{ll} = -D_{ll} = -\mathrm{tr}\mathbf{D}$, where the last term is in symbolic tensor notation. The deviatoric strain rate is thus $\dot{\varepsilon}^*_{ij} = -v^*_{ij} = -D^*_{ij}$, with the norm $v_s := \sqrt{v^*_{ij}v^*_{ij}} = \dot{\gamma} = D_s = (2J_2^D)^{1/2}$, where J_2^D is the second deviatoric invariant, insensitive to the sign convention.
4. The elastic strain, $\varepsilon^e_{ij} \equiv -u_{ij}$, is the tensorial state variable on which the elastic (potential) energy depends [5]. It is always well-defined and unique, in contrast to the total or plastic strains, which are not, and thus will not be used as state variables for (constitutive) modeling. The respective strain rates, however, are well-defined and thus are used. The strain rate was already given (see item 2.), $\dot{\varepsilon}_{ij} = -v_{ij}$, so that the plastic strain rate is *defined* as: $\dot{\varepsilon}^p_{ij} = \dot{\varepsilon}_{ij} - \frac{d}{dt}\varepsilon^e_{ij}$ (see also item 7.).
5. The isotropic elastic strain

$$\Delta := -u_{ll} = \varepsilon^e_{ll} = \varepsilon^e_v = \log(\rho/\rho_J)$$

is positive for compression. It may be seen as the true strain relative to a stress-free reference configuration – if $\Delta > 0$. Arriving at $\Delta = 0$, the system un-jams at $\rho^u_J = \rho$ and the jamming density remains the actual one. [6]
6. The norm of the deviatoric elastic strain is, in accordance to the general scheme, $u_s = \sqrt{u^*_{ij}u^*_{ij}} = (2J_2^u)^{1/2}$.
7. In general, we take $\frac{\partial}{\partial t}$ as the partial time derivative, and $\frac{d}{dt}$ as the total one, including all convective terms. Hence, with the vorticity tensor given as $\Omega_{ij} \equiv v_{[i,j]} \equiv \frac{1}{2}(\nabla_i v_j - \nabla_j v_i)$, one has (as example) the total time derivative of the elastic strain

$$\frac{d}{dt}\varepsilon^e_{ij} = \left(\frac{\partial}{\partial t} + v_k\nabla_k\right)\varepsilon^e_{ij} + \Omega_{ik}\varepsilon^e_{kj} - \varepsilon^e_{ik}\Omega_{kj} \ . \qquad (1)$$

Being off the focus here, the convective and vorticity terms are neglected, so that $\frac{d}{dt} \equiv \frac{\partial}{\partial t}$. The dots in $\dot{\varepsilon}^p_{ij}$ and $\dot{\varepsilon}_{ij}$ are only a (convention preserving) indication of rates, but do not represent the mathematical operation above.
8. The total stress is not an independent state variable, but rather given by the energy density and entropy production, as discussed in the classical GSH literature. In the simplified version, it may be written as $\sigma_{ij} = \pi_{ij} + P_T\delta_{ij} + \sigma^{\mathrm{visc.}}_{ij}$, with elastic, kinetic/granular temperature and viscous contributions. The isotropic stress is referred to as pressure, $P = \frac{1}{3}\sigma_{kk}$, and the elastic pressure is $P_\Delta = \frac{1}{3}\pi_{kk}$, for three dimensions $\mathcal{D} = 3$.
9. The symbols B and G are used in the definition of the isotropic and deviatoric (shear) elastic energy density. In previous GSH-papers [107,44,45], the symbol A was used for G, the classical symbol, but since A is referred to as the anisotropy modulus in other studies, see Ref. [46], we stick to G here [7].
10. The granular temperature used in GSH is $T_g \propto \sqrt{w_T}$, encompassing both kinetic and potential fluctuating energy contributions. The granular temperature used in kinetic theory and DEM is different, denoted as $T_G = T_K = 2E_{\mathrm{kin}}/M\mathcal{D}$, with total mass of all particles, M, in dimension $\mathcal{D}$, ignoring the potential part. Comparing GSH-formulas in the gas limit to that of the kinetic theory [109,7,8,114,111], one should remember

$$T_g^2 \sim T_G \ . \qquad (2)$$

In the following, we will only use T_g, which has the units of velocity scaled by the particle diameter, i.e., that of an inverse time, or a rate, very similar to the fluidity, g, studied and discussed in Ref. [18], and references therein.) [8].

[5] Note the different signs in the last two terms, i.e., the isotropic elastic strain, $\Delta = \varepsilon^e_v$, is positive for compression, whereas u^*_{ij} is negative (if eigenvalues are considered).

[6] Generalizing GSH, we allow negative elastic strains $\Delta = \varepsilon^e_v$ here, interpreting those as the separation distance between particles – or their mean free path – in order to catch both jammed and un-jammed situations. Note that the elastic energy of a negative Δ is identically zero, and that a negative Δ is not independent of the density ρ. Compressing from an un-jammed state, the system jams at $\Delta = 0$, towards $\Delta > 0$ and $\rho > \rho_J$. In isochoric situations (constant density), an evolution of the state variable, Δ, the isotropic elastic strain, implies an evolution of the (enslaved, dependent) jamming density, $\rho_J = \rho\exp(-\Delta)$, as proposed and studied in detail in Ref. [46]. The physics clearly changes between positive (jammed) and negative (un-jammed) states, but for the sake of brevity, below jamming, we limit $\rho_J \geq \rho_{J0}$ and thus $\Delta(\rho) = \log(\rho/\rho_{J0})$, in cases where it would drop below its absolute limit, ρ_{J0}, which can be seen as the random loosest packing density.

[7] Note that (calligraphic) symbols $\mathcal{B} \neq B$, $\mathcal{G} \neq G$, and $\mathcal{A}$, in general, are the (tangent) moduli, representing the second derivatives of the elastic energy density with respect to isotropic and deviatoric elastic strains, or mixed, respectively; symbols $\mathcal{B}_\Delta$, $\mathcal{G}_\Delta$ are again different and are the secant moduli; for more details see subsections 3.2.2 and 3.2.3.

[8] The two temperatures T_g and T_G are different in the following sense. In thermal equilibrium of a static granular solid, one has $T_G = 0$, but $T_g = T$, since it is defined as equal to the true temperature in equilibrium, see Eq. (21) and Refs. [107,44,45]. In granular gases, if thermal equilibrium could ever be reached, one would have $T_G = T$, a relevant situation if one starts to consider dissipation and the consequent heating of the grains. By not claiming that T_G is a "temper-

1.8 Overview

In what follows, we shall, in Sec. 2, consider the significance of an inflection surface, of a convex-concave transition in the energy, as relevant for classical systems, transiently elastic systems and granular matter. We then present a review of GSH and new constitutive relations based on particle simulations, as well as a minimalist version, in Sec. 3, allowing for analytic solutions in Sec. 4, and numeric calculations to catch the transients in Sec. 5. A quantitative comparison and calibration with particle simulations is carried out in Sec. 6, before we conclude in Sec. 7.

2 Equilibrium conditions and dissipative terms

In this section, we first revisit the reason for thermodynamic energy's convexity, and derive the equilibrium conditions for three systems: elastic, transiently elastic and granular media. There is one equilibrium condition for each state variable, that maximizes its contribution to entropy or, equivalently, minimizes its contribution to energy. Examples for equilibrium conditions are uniform temperatures and uniform stresses. As these conditions represent extremal points, the energy needs to be convex to be minimal, for the system to be stable.

Then we make the general point that every equilibrium condition, if not satisfied, is a dissipative channel that gives rise to a negative/dissipative term in the evolution equation of the associated state variable. As a result, the state variable relaxes, towards satisfying the condition. In a closed system, all variables will eventually satisfy all their respective conditions, which is the state we called equilibrium.

If the energy is concave, equilibrium conditions represent maxima of the energy with respect to variation of a state-variable [9]. The dissipative terms will thus drive the system away from equilibrium, producing, e.g., non-uniformity in temperature and stress fields. When this happens, what micro-mechanical mechanisms it originates from, is necessarily more specific. How the dynamics further evolves depends on the system one considers. In the classical *van der Waals theory* of the gas-liquid transition, droplet formation is the basic mechanism. In granular media, we propose the following mechanism.

In the stable region, within the cone of Fig 2, the dissipative term in the equation for the elastic strain serves to maintain stress uniformity. It remains inconspicuous as long as one studies the evolution of uniform stresses. Outside the yield surface, it forces the system to leave stress uniformity. Non-uniform stresses accelerate grains in varying directions, producing jiggling and thus granular temperature which, in turn, allows the stress to relax, pushing the system back into the convex region.

This is what we believe happens in grains at yield and beyond the transition. Setting up a dynamical model for following the system through the transition to different states is the main purpose of this paper.

2.1 Elasticity

Consider an elastic system characterized by two state variables, the entropy density, s, and the elastic strain,

$$-\varepsilon^e_{ij} \equiv u_{ij} = \tfrac{1}{2}(\nabla_i U_j + \nabla_j U_i), \tag{3}$$

with a thermodynamic energy density that is a function of both, $w = w(s, u_{ij})$ [115].

A textbook proof of energy convexity considers only the entropy as a variable, and involves an elastic system connected to a heat bath. A temperature fluctuation (associated to entropy fluctuations) vanishes only if the energy is larger with it than without, which is shown to imply convexity [140]

In a more general consideration, we start with the assumption that the system is stable and has an equilibrium for given values of s and u_{ij}. Since the elastic stress, $\pi_{ij} \equiv -\partial w/\partial u_{ij}$ is symmetric, $\pi_{ij} = \pi_{ji}$, we may write the total differential of the energy density as:

$$\mathrm{d}w = T\mathrm{d}s - \pi_{ij}\mathrm{d}u_{ij} = T\mathrm{d}s - \pi_{ij}\mathrm{d}\nabla_j U_i\,, \tag{4}$$

with temperature $T = \partial w/\partial s$. We varied this energy by (i) keeping $\int s\mathrm{d}V = const.$, or $\delta\int(w - T_L s)\,\mathrm{d}V = 0$, with Lagrange parameter $T_L = const.$; (ii) forbidding external work, i.e., assuming a closed system:

ature" of the granular degrees of freedom, taking it only as a measure of the velocity fluctuation squared, $T_G \sim |\delta v_i|^2$, one may go on using T_G in denser ensembles too, ignoring the fluctuations of potential energy it has lost the meaning of a temperature. Conversely, one may use T_g in granular gases, anyway, taking it as $T_g \sim |\delta v_i| \gg T$.
While $T_g = T$ does hold in granular static equilibrium, $T_G = T$ can never be reached, as any finite T_G, for finite sized particles, translated into temperature, leads to values of order of the inner temperature of the sun. Only in the atomic/molecular limit of "particles" one has T_G analogous to $k_B T$. It is therefore more sensible to employ T_g throughout.

[9] Note that non-local terms in the sense of diffusion of granular temperature are very similar to the "non-local" diffusive evolution equation for fluidity, see the discussion in subsection 3.1. An essential difference here is that our particles are (strongly) deformable, which is not contained/considered in many other works; we do exclude breakage, however.

$\oint \pi_{ij}\delta U_i \,\mathrm{d}A_j = 0$; and (*iii*) using Gauss' theorem [10], the result is

$$0 = \int [T\delta s - \pi_{ij}\delta\nabla_j U_i - T_L\delta s]\,\mathrm{d}V$$
$$= \int [(T - T_L)\,\delta s + (\nabla_j \pi_{ij})\,\delta U_i]\,\mathrm{d}V. \quad (5)$$

With δs and δU_i varying independently, and $T_L = const.$, the equilibrium conditions may be written as

$$\nabla_i T = 0, \quad \nabla_j \pi_{ij} = 0. \quad (6)$$

These are extremal conditions. They represent an energy minimum and stable equilibrium, only if deviations from them yield an energy increase. Therefore, inserting $T = T^{eq} + \delta T$, $\pi_{ij} = \pi_{ij}^{eq} + \delta\pi_{ij}$, with $\nabla_i T^{eq} = 0$ and $\nabla_j \pi_{ij}^{eq} = 0$, we require

$$\delta^2 w = \delta T \delta s - \delta\pi_{ij}\delta u_{ij} > 0. \quad (7)$$

Assuming first $\delta u_{ij} \equiv 0$, we may write $\delta^2 w = \delta T \delta s = (\partial T/\partial s)(\delta s)^2 > 0$, implying

$$\frac{\partial^2 w}{\partial s^2} = \frac{\partial T}{\partial s} > 0,$$

or that the energy w is a convex function of s. As a result, temperature fluctuations will diminish, and the state characterized by a uniform temperature is a stable equilibrium. Conversely, if the energy is concave, $\partial^2 w/\partial s^2 < 0$, the condition $\nabla_i T = 0$ represents a maximum of energy, and the system is unstable. Any fluctuations in entropy will move it away from uniform temperature. In the case of the van der Waals transition between gas and liquid, a uniform single-phase system is moved to the coexistence of two phases, with different entropy densities, but the same temperature.

Next, as used explicitly below, in subsections 3.2.2 and 3.2.3, assuming $\delta s \equiv 0$, we order the six components of π_{ij} and u_{ij} each as a 6-tuple vector, denoted by Greek letters, and require

$$\delta^2 w = -\delta\pi_{ij}\delta u_{ij} = -\delta\pi_\alpha \delta u_\alpha = \frac{\partial \pi_\alpha}{\partial u_\beta}\delta u_\alpha \delta u_\beta > 0. \quad (8)$$

This implies that the 6x6 Hessian matrix

$$\frac{\partial^2 w_e}{\partial u_\alpha \partial u_\beta} = -\frac{\partial \pi_\alpha}{\partial u_\beta} \quad \text{has only positive eigenvalues,} \quad (9)$$

implying that the energy w is a convex function of the elastic strain u_{ij}. If there is at least one negative eigenvalue, the condition $\nabla_j \pi_{ij} = 0$ no longer represents a stable state, because along the associated eigenvector, the energy is a maximum. The system can and will depart from its previously elastic state, initially by violating $\nabla_j \pi_{ij} = 0$, typically rendering the stress non-uniform.

To obtain static elastic solutions, we solve $\nabla_i \pi_{ij} = 0$ for given boundary conditions. This is equivalent to looking for minima of the elastic energy. The solutions are stable if the elastic energy is convex. They are unstable otherwise, and devoid of physical significance.

The more general consideration, including both δs and δu_{ij}, leads to a 7x7 matrix that, for stable equilibria, must possess seven positive eigenvalues.

A complete consideration for elasticity requires also the inclusion of the density, ρ, and momentum density ρv_i as the energy's variables. This, being somewhat more lengthy, would distract from the present concern. The associated equilibrium conditions, with the gravitational acceleration, g_i, and the chemical potential given as $\mu = \partial w/\partial\rho$ (as derived in Refs. [141,118]) are:

$$\nabla_i \mu = -g_i, \quad (10)$$
$$-\dot{\varepsilon}_{ij} \equiv v_{ij} \equiv \tfrac{1}{2}(\nabla_i v_j + \nabla_j v_i) = 0, \quad (11)$$
$$\nabla_i P = s\nabla_i T + \rho\nabla_i \mu = -\rho g_i\ . \quad (12)$$

The force equilibrium $\nabla_i P = -\rho g_i$ is a direct result of $\nabla_i T = 0$ and $\nabla_i \mu = -g_i$. All three equations express minimal energy, or maximal entropy.

If any of the equilibrium conditions [11] are not satisfied, dissipative currents appear to counteract: heat diffusion $\sim \nabla_i T$ in the evolution equation for s, viscous stress $\sim v_{ij}$ in the evolution equation for ρv_i, and a term $\sim \nabla_k \pi_{ik}$, in the equation for the displacement,

$$\tfrac{\partial}{\partial_t} U_i - v_i = -\beta\nabla_k \pi_{ik}. \quad (13)$$

(Analogous to heat-conductivity, β quantifies the strength of the dissipation. Taking it as a scalar is an approximation.) All these terms serve the sole purpose of restoring the respective equilibrium conditions: $\nabla_i T, v_{ij}, \nabla_k \pi_{ik} = 0$.

The dissipative "displacement rate" $\sim \nabla_k \pi_{ik}$, as a necessary result of thermodynamics, has been first recognized in the classical 1972-paper: *"The unified hydrodynamic theory for crystals, liquid crystals, and normal fluids"*, by Martin, Paraodi and Pershan [139]. It drives

[10] According to Gauss' theorem, the surface integral transforms as: $\oint \pi_{ij}\delta U_i \,\mathrm{d}A_j = \int \nabla_j(\pi_{ij}\delta U_i)\mathrm{d}V = \int [(\nabla_j \pi_{ij})\delta U_i + \pi_{ij}\delta\nabla_j U_i]\,\mathrm{d}V = 0$. Using the definition of the stress or traction vector, $t_i = \pi_{ij}\hat{n}_j$, the surface integral can be rephrased, $\oint \pi_{ij}\delta U_i \,\mathrm{d}A_j = \oint t_i \delta U_i \,\mathrm{d}A$, allowing to add tractions (or point/contact forces) at the surface of V, which would pop up on the right hand side of Eq. (5) but are not used here.

[11] Deviations from $\nabla_i \mu = -g_i$ do not lead to a dissipative mass current, because the mass current is necessarily given by the momentum density ρv_i. The underlying reason is Galilean invariance, implying the local conservation of the *booster* [141,118].

the system, boundary conditions permitting, toward a constant stress. If the stress is not constant, such as in elastic waves, it contributes to wave damping. If one concentrates on the evolution of constant stresses, this term vanishes and is irrelevant. However, if the energy is concave, this term can drive the system away from uniform stresses and even will result in instabilities (numerical as well as physical). Writing the stress gradient in the notation of the 6x6 matrix, see Eq. (9), as:

$$\nabla_k \pi_{jk} \to \nabla_k \pi_\alpha = \partial \pi_\alpha / \partial u_\beta \nabla_k u_\beta \ , \tag{14}$$

we see that, if the matrix $\partial \pi_\alpha / \partial u_\beta$ has a negative eigenvalue, the corresponding term will its flip sign. Instead of keeping the stress uniform, it drives the stress towards non-uniformity. This in turn accelerates mass points, possibly leading to non-uniform velocities v_i and thus finite strain rates, $v_{ij} \equiv -\dot{\varepsilon}_{ij}$. Initially, the stress perturbation will grow along the direction associated with the negative eigenvalue, but for finite times, this is by no means true, as the system will try to move towards a stable equilibrium state, whatever that is. See the next sections 4 and 5 about what happens in granular matter without gradients. Discussing the possibility of a relation to gradient plasticity is beyond the scope of this paper.

Inserting Eq. (13) in the definition of the elastic strain, Eq. (3), reads

$$\begin{aligned} \tfrac{\partial}{\partial t} u_{ij} - v_{ij} &\equiv -\tfrac{\partial}{\partial_t} \varepsilon^e_{ij} + \dot{\varepsilon}_{ij} =: \dot{\varepsilon}^p_{ij} \\ &= -\nabla_i [\beta \nabla_k \pi_{jk}] - \nabla_j [\beta \nabla_k \pi_{ik}] \equiv \psi_{ij} \ , \end{aligned} \tag{15}$$

which seems to suggest that the dissipative current term, ψ_{ij}, is simply the plastic strain rate, $\psi_{ij} = \dot{\varepsilon}^p_{ij}$, which apparently exists even in classical solids if the stress is nonuniform. This could be confusing, as it is not related to typical plastic phenomena, such as connected to concepts of plastic potentials or flow functions (see Refs. [117,31,33]). The term plastic strain rate is more appropriate for the other dissipative contributions discussed in the next two sections, on transient elasticity and granular media.

Note that heat diffusion and viscous stress exist in any system, in which entropy and momentum are state variables: liquids, solids, granular media, irrespective of the microscopic interaction. Same holds for the dissipative term ψ_{ij}, which exists in any system in which the elastic strain is a variable. This is the reason it also exists in granular media. Generally speaking, every dissipative term strives to satisfy its equilibrium condition by changing the value or distribution of the associated state variable. Equilibrium is achieved if all equilibrium conditions are satisfied, as entropy is then maximal.

2.2 Transient elasticity and plasticity

There are many transiently elastic systems in nature. If quickly deformed, they are elastic and capable of restoring their original shape. But this does not happen if the deformation is kept longer; then the deformation is irreversible, plastic. One example are polymeric melts that consist of entangled elastic strands, which elastically deform, but disentangle if given enough time. This leads to a reduction, and eventually vanishing, of the elastic stress. For such systems, the equilibrium condition is:

$$\pi_{ij} = 0, \qquad \text{or, equivalently} \quad u_{ij} = 0 \ . \tag{16}$$

Consequently, the evolution equation (15) takes the form:

$$\dot{\varepsilon}^p_{ij} = \tfrac{\partial}{\partial t} u_{ij} - v_{ij} \equiv -\tfrac{\partial}{\partial_t} \varepsilon^e_{ij} + \dot{\varepsilon}_{ij} = -\lambda_e u_{ij} \ , \tag{17}$$

with the plastic strain rate now a relaxation term, with a positive coefficient λ_e. Employing essentially this equation, including the convective terms of Eq. (1), a wide range of polymer behavior including shear thinning/thickening and the Weissenberg or rod-climbing effect were reproduced [142,143].

It is noteworthy that the plastic strain rate in the form $\dot{\varepsilon}^p_{ij} = -\lambda_e u_{ij}$ is a diagonal Onsager term, hence off-diagonal ones such as

$$\dot{\varepsilon}^p_{ij} = \tfrac{\partial}{\partial t} u_{ij} - v_{ij} = -\lambda T_g u_{ij} - p_{ijkl} v_{kl} \tag{18}$$

are also permitted. They will turn out to be useful in granular physics.

The close link, even identity, between transient elasticity and strain relaxation on one hand, and plastic behavior of irreversible shape change on the other, is a useful insight. Similarly useful is the understanding of the difference between elasticity and transient elasticity. For the latter to be in equilibrium, the elastic stress has to vanish, while a constant stress suffices for the former. For verbal clarity, we denote

$$\begin{aligned} \text{elastic equilibrium}: &\quad \nabla_i \pi_{ij} = 0, \\ \text{“plastic equilibrium”}: &\quad u_{ij} \equiv -\varepsilon^e_{ij} = 0 \ , \end{aligned} \tag{19}$$

where “plastic equilibrium” is short for “transiently elastic, long-term equilibrium”.

There is a further subtlety that we must address here. If the polymer energy depends on both the density and the elastic strain, there are two contributions in the stress: the pressure as given by Eq. (12) and the elastic stress. Then the system may possess an equilibrium pressure even when Eq. (19) holds. However, if the density is not an independent state variable, implying $P \equiv 0$, an equilibrium pressure needs a finite $\Delta \equiv -u_{ll}$

to be sustained, and $u_{ij} = 0$ cannot be the equilibrium condition. Rather, it is given as

$$u^*_{ij} \equiv -\varepsilon^{e*}_{ij} = 0, \quad \text{implying} \quad \dot{\varepsilon}^p_{ij} = -\lambda_e u^*_{ij} \ , \tag{20}$$

the vanishing of the deviatoric part, while the trace Δ, not independent from the density, simply follows the dynamics of the density. It does not relax.

Note that the relaxation time of Δ and u_s need not be the same. If that of Δ is especially long, it may be neglected for certain phenomena, for which the dynamics is governed by $\dot{\varepsilon}^p_{ij} = -\lambda_e u^*_{ij}$ alone.

When the system is crossing an inflection surface, the term $-\lambda_e u_{ij}$, in Eq. (17) is not affected, and continues to push the elastic strain toward $u_{ij} = 0$.

2.3 Granular matter

GSH was set up in compliance with thermodynamics and conservation laws. Here, we discuss its structural part, necessary if one is to be consistent with the general principles of physics. In Sec. 3, a reduced complete version of GSH is presented, including a few, as simple as possible constitutive choices, which will be employed later to study the jamming and un-jamming dynamics.

Two basic pieces of physics characterize granular media: (1) They have two entropies: s_g for the granular degrees of freedom and s for the much more numerous microscopic ones. (2) Depending on circumstances, granular media may be elastic or transiently elastic. Both elastic and plastic equilibria of Eqs. (19) are therefore relevant. However, note that the equilibrium (limit) state is not necessarily ever reached, neither under permanent deformation, nor under free relaxation. In the former case, the system is permanently pulled away from the equilibrium (steady state is *not equal to* equilibrium), while in the latter, if T_g relaxes fast enough, the equilibrium cannot be realized by the other state variables either.

Including s_g as an extra state-variable, with $T_g \equiv \partial w/\partial s_g$, the equilibrium condition is $T = T_g$, obtained by maximizing $\int (s + s_g) \mathrm{d}V \approx \int s \, \mathrm{d}V$, where $s_g \ll s$ may be ignored. The equilibrium condition implies that all degrees of freedom, microscopic as well as granular ones, will eventually equilibrate with one another. Furthermore, since for particles of grain size well above molecular size, already for tiny velocity fluctuations (jiggling), one typically has $T_g \gg T$ by many orders of magnitude, $\sim 10^{10}$, see item 10. in subsection 1.7, we may set the equilibrium granular temperature to zero,

$$T_g = T \approx 0 \ . \tag{21}$$

In analogy to the relaxation terms discussed above, the evolution equation for s_g must therefore possess a relaxation term $\sim T_g$, pushing s_g towards $s_g \propto T_g = 0$. This dissipation/relaxation takes place due to collisions, with rate $\sim T_g$, in the collisional gas- and fluid-like regime. In addition, analogous to the viscous heating term in the hydrodynamic theory of Newtonian fluids, which transfers kinetic energy into heat, via $\eta v^*_{ij} v^*_{ij} \equiv \eta v_s^2 \to T \frac{\partial}{\partial t} s$, there is a term that transfers kinetic energy into "granular heat", $\eta_g v_s^2 \to T_g \frac{\partial}{\partial t} s_g$. Therefore, assuming $\nabla_i T_g = 0$, and ignoring other gradients, the evolution equation for granular energy reads

$$T_g \tfrac{\partial}{\partial t} s_g = -\gamma T_g^2 + \eta_g v_s^2 \ , \tag{22}$$

with coefficient $\gamma = \gamma(T_g)$ dependent on T_g, and the compressional viscosity neglected, like convective and diffusive terms, for the sake of brevity. To be used in the following, after division by T_g and some re-writing [12], the evolution equation for granular temperature reads:

$$b\rho \tfrac{\partial}{\partial t} T_g = -\gamma_1 T_g^* T_g + \eta_1 v_s^2 . \tag{23}$$

The effective rate of dissipation $T_g^* = T_g + T_e$ is discussed in more detail below in Secs. 3.1 and 4.

For given deviatoric (shear) strain rate, $v_s = |v^*_{ij}| = |-\dot{\varepsilon}^*_{ij}|$, the steady state solution is given and discussed in section 4.6 in the limit cases $\gamma_0 \ll \gamma_1 T_g$ and $T_e \ll T_g$:

$$T_g = T_g^{(ss)} = v_s \sqrt{\frac{\eta_g}{\gamma}} \approx v_s \sqrt{\frac{\eta_1}{\gamma_1}},$$

a result known to hold in granular gases [13], up to moderate densities [7,8,111]. In this case, the system is in the rate-independent elasto-plastic regime, where the granular temperature is proportional to the strain rate. For diminishing $T_g \ll T_e$ and $\gamma_0 \gg \gamma_1 T_g$, we have an exponential and much faster decay, $\frac{\partial}{\partial t} T_g \propto -T_g$, however, also here the steady state granular temperature persists and remains relevant, as $T_g^{(e)} \approx (T_g^{(ss)})^2/T_e$, see section 4.6.

[12] Preempting the discussion in Sec. 3, to write down the final evolution equation for T_g, for reasons detailed in [107, 44,45], and partially in Sec. 3, we use:

$$s_g = \rho b T_g, \ \eta_g = \eta_0 + \eta_1 T_g, \ \gamma = \gamma_0 + \gamma_1 T_g, \ \text{or, equivalently} \\ \gamma = \gamma_1 (T_g + \gamma_0/\gamma_1) \equiv \gamma_1 (T_g + T_e) \equiv \gamma_1 T_g^* \ ,$$

in order to work with parameters that do not depend on T_g anymore, and mostly ignoring the Newtonian type viscosity η_0 in the following. When inserting ρb into Eq. (22) for energy, the time derivative of this variable is assumed to be small and thus neglected.

[13] Note the difference in nomenclature: $T_G \sim T_g^2 \propto v_s^2$, see the text around Eq. (2).

Returning to the elastic strain u_{ij}, we note that granular media are elastic for quiescent grains, $T_g = 0$, as slopes of sand-piles demonstrate. If the particles "jiggle", $T_g \neq 0$, the elastic shear strain and stress will diminish, and eventually vanish: Tapping a vessel of grains (with a finite number) long (and strong) enough results in a flattened granular surface, like in transient elasticity. Combining both conditions of Eqs. (19), the evolution equation for the elastic strain contains both types of plastic strain rates, see also Ref. [102] and Eqs. (15), and (18),

$$\dot{\varepsilon}^p_{ij} = \dot{\varepsilon}_{ij} - \frac{\partial}{\partial t}\varepsilon^e_{ij} = \lambda T_g \varepsilon^e_{ij} + p_{ijkl}\dot{\varepsilon}_{kl} + \psi_{ij} \qquad (24)$$
$$= -v_{ij} + \frac{\partial}{\partial t}u_{ij} = -\lambda T_g u_{ij} - p_{ijkl}v_{kl} + \psi_{ij} \ ,$$

where the first term on the right, pushing u_{ij} towards the plastic minimum $u_{ij} = 0$, operates only for $T_g \neq 0$, representing the fluctuation driven plastic strain rate.

The second term represents strain-driven plastic deformations proportional to stress. Note that the probabilities p_{ijkl} occur well within the macroscopic, elastically stable regime – involving possibly local events, on the particle scale – and will be simplified [14] using only the respective purely isotropic and deviatoric (shear) plastic deformation probabilities, p_v and p_s, see subsection 4.1 [15]. The micro-mechanical origins of these probabilities, are not addressed here, rather see Refs. [27,46,20,123,18,14,19,33] and many more references therein. There – among other considerations – it is shown that (finite) granular systems can remain elastic for tiny strain, then have localized plastic events at larger strain with probability increasing, before (global) yield takes place with particular probabilities as cast into a meso-scale, stochastic master-equation approach, in Refs. [144,145,47].

The third term, ψ_{ij}, depends on the gradient of the elastic stress, see Refs. [107,44], and thus vanishes for constant elastic stress, as relevant in the following sections. As discussed above, around Eq. (15), the plastic strain rate, ψ_{ij}, pushes u_{ij} towards the elastic equilibrium of uniform stress in the energetically convex region, and away from it in the concave one, since the gradient of stress changes sign at the transition.

[14] The split up into an isotropic (volumetric) and a deviatoric (shear) contribution, results in $p_{ijkl} = p_v\delta_{ij}\delta_{kl} + p_s\hat{\delta}_{ij}\hat{\delta}_{kl}$, so that the strain-driven plastic deformation rate reduces to: $p_{ijkl}v_{kl} = p_v\delta_{ij}v_{ll} + p_s v^*_{ij} = -p_v\delta_{ij}\dot{\varepsilon}_v - p_s\dot{\varepsilon}^*_{ij}$. The symbols δ_{ij} and $\hat{\delta}_{ij}$, represent the unit isotropic and deviatoric tensors, with $\delta^2_{ij} = \mathcal{D}$, $\hat{\delta}^2_{ij} = 1$, and $\delta_{ij}\hat{\delta}_{ij} = 0$.

[15] The symbols p_v and p_s are probabilities so that, in order to avoid confusion with pressure, P, they are given with one subscript, and in color throughout.

2.3.1 Dynamics at constant shear rate or stress

Equation (24), in addition to the dynamics of T_g, Eq. (22), render granular behavior rather more complex than the superposition of behavior from polymers and elastic media. Imposing either a constant shear rate or a constant elastic stress in a polymer melt, Eq. (17), the steady state result is the same, $v_s = \lambda_e u_s$, in either case.

This symmetry does not hold for granular media – not even for the simplest case with $T_e = 0$, and $p = 0$. A constant shear rate, $\hat{v}_s$, where the hat indicates the fact that this quantity is fixed/controlled, with the stationary solution $T_g^{(s)} = \hat{v}_s\sqrt{\eta_1/\gamma_1}$ inserted into Eq. (24), ignoring the p-terms on the r.h.s., leads to a *rate-independent* evolution equation for u_{ij} that possesses the hypoplastic structure [146], since T_g is taking a value proportional to the absolute value of the strain rate. The steady state elastic shear strain is thus: $u_s^{(s)} = \sqrt{\gamma_1/\eta_1}/\lambda$. It accounts well for elasto-plastic motion [147], including the approach to the critical state and shear jamming [44,45,148,149].

On the other hand, controlling the stress or, equivalently, holding the elastic strain, $\hat{u}_s$, constant and inserting the stationary limit of Eq. (24), $v_s^{(u)} = \lambda T_g \hat{u}_s$, into Eq. (22), yields the relaxation rate: $\gamma_c = (\gamma_1 - \eta_1\lambda^2 u_s^2) = \gamma_1[1-(u_s/u_s^c)^2]$, negative if $\hat{u}_s < u_s^c = u_s^{(s)} = \sqrt{\gamma_1/\eta_1}/\lambda$, the case when we find T_g to relax to zero, pushing the system into a static state, $v_s^{(u)} \to 0$. The relaxation rate vanishes (i.e., the relaxation time diverges) as the stress (or elastic strain) approaches the critical value, u_s^c. With a further increase of u_s, the rate flips sign to positive above the critical value, see [44, 45], creating an ever increasing strain rate $v_s^{(u)}$. Accordingly, switching from an imposed shear rate (say during an approach to the critical state) to an imposed sub-critical stress will render the system static due to the relaxation of T_g, whereas a critical or super-critical stress will create T_g and thus accelerate the flow, since $v_s \propto T_g$.

2.3.2 Dynamics in the concave region

Within the cone of Fig. 2, in the energetically convex region, as long as one considers only the evolution of uniform stresses, the elastic dissipative term $\psi_{ij} = \nabla_i[\beta\nabla_k\pi_{jk}] + \nabla_j[\beta\nabla_k\pi_{ik}]$ remains zero. Serving to maintain stress uniformity, it may simply be neglected.

Perturbing the system by a (local) stress, $\delta\pi_{ij}$, from a static situation, in the convex, stable region, results in a relaxation of the elastic strain, due to the sign of ψ_{ij}. In contrast, in the concave region, because of Eq. (14),

this relaxation turns into an explosion, and drives the stress towards further, stronger non-uniformity.

This accelerates the grains, locally, leading to nonuniform velocities v_i and finite strain rates, $v_{ij} \equiv -\dot{\varepsilon}_{ij} \neq 0$. The latter serve as a source for granular heat, see Eq. (22), and create considerable T_g, which activates the first plastic term of Eq. (24), which relaxes the stress back into the stable, convex region. Hence, although the imposed perturbation creates a local stress response along the direction associated with the negative eigenvalue initially, it is the stress relaxation back to the convex region that dominates for finite times. If not strong/fast enough, the system will yield or un-jam dynamically. This is one way how GSH accounts for stability and un-jamming dynamics by instability, both mediated by the granular temperature

Unfortunately, including the elastic stress-gradient driven plastic strain rate renders Eq. (24) an unstable partial differential equation, the solution of which requires increased technical efforts. This is undesirable in a first, qualitative study, and an approximation scheme may prove useful. We suggest to go on neglecting the elastic dissipative terms, and to add a stress term to Eq. (22), such that T_g is directly produced by an elastic stress. The balance equations for s, s_g, for the energetically convex region, are given as

$$T\frac{\partial}{\partial t}s = R = \gamma T_g^2 + \beta_{ijkl}\pi_{ij}\pi_{kl} + \cdots , \tag{25}$$

$$T_g\frac{\partial}{\partial t}s_g = R_g = -\gamma T_g^2 + \eta_g v_{ij}v_{ij}. \tag{26}$$

The equally permissible alternative,

$$T\frac{\partial}{\partial t}s = \gamma T_g^2 + \cdots , \tag{27}$$

$$T_g\frac{\partial}{\partial t}s_g = -\gamma T_g^2 + \eta_g v_{ij}v_{ij} + \bar{\beta}_{ijkl}\pi_{ij}\pi_{kl}, \tag{28}$$

was not adopted, because any static π_{ij} would then produce T_g, leading to its decay. This is not observed in static granular media that can sustain finite stresses indefinitely (see sand-piles) – if not perturbed externally. Yet the reasoning is not valid outside the cone, where static stresses are not stable. Hence we combine Eq. (25) with (28), noting

$$\bar{\beta}_{ijkl} = 0 \text{ inside}, \quad \text{and } \beta_{ijkl} = 0 \text{ outside}, \tag{29}$$

the elastically stable cone. The explicit forms for β_{ijkl} and $\bar{\beta}_{ijkl}$, which carry the units of inverse stress (compliance) rate, are constitutive choices that will be discussed in the next section in some detail for β_{ijkl}, while a very simple model for $\bar{\beta}_{ijkl}$ will be presented in subsection 4.9 and studied in Sec. 5.

2.4 Second law of thermodynamics

The second law of thermodynamics (the balance of thermal and granular entropy) from Eqs. (25) and (26) can be summarized as $R > 0$ and $R_g + \gamma T_g^2 > 0$ (since both represent dissipative, irreversible processes), or combined:

$$R + R_g = (\beta_{ijkl} + \bar{\beta}_{ijkl})\pi_{ij}\pi_{kl} + \eta_g v_{ij}v_{ij} + \ldots \geq 0 , \tag{30}$$

noting that the dissipation of granular energy $-\gamma T_g^2$ irreversibly enters the thermal energy, thus cancelling itself in $R + R_g$.
More general, in the absence of gradients, the total production of entropy can be re-phrased [102] as:

$$R + R_g = \pi_{ij}\dot{\varepsilon}^p_{ij} + \sigma^D_{ij}\dot{\varepsilon}_{ij} \geq 0 , \tag{31}$$

with, however, more complex expressions needed for the evolution of the elastic strain, $\varepsilon^e_{ij} = \dot{\varepsilon}_{ij} - \dot{\varepsilon}^p_{ij}$, and the a-priori unknown viscous/dissipative stress, σ^D_{ij}, for both of which the isotropic and deviatoric parts can – and are assumed to – evolve independently from each other. As example, where the dissipative stress is not shown for the sake of brevity, inserting the constitutive relation from Eq. (24), leads to the following split-up:

$$\begin{aligned} R + R_g &\approx \pi_{ij}\left(\dot{\varepsilon}^p_{ij} + p_{ijkl}\dot{\varepsilon}_{kl}\right) + \ldots \\ &\approx \lambda_1 T_g P_\Delta \Delta + \lambda T_g \pi^*_{ij}\varepsilon^{e*}_{ij} + \pi_{ij}\left(p_v\dot{\varepsilon}_v\delta_{ij} + p_s\dot{\varepsilon}^*_{ij}\right) + \ldots . \end{aligned} \tag{32}$$

The first and second term in the last line of Eq. (32) represent entropy production by fluctuation driven relaxation and are always positive. In contrast, the third and fourth term are due to plastic (re-arrangements) driven by isotropic and deviatoric strain, respectively. They can be either positive or negative, dependent on the direction of the strain rate. The third term is negative for extension ($\dot{\varepsilon}_v < 0$), while the fourth term is negative, in particular, at strain reversal. If negative, these contributions must be compensated by positive production terms, such as the ones ignored [16], or the probabilities must be set to zero, as will be discussed in more detail in section 4.
A more general approach to construct the viscous/dissipative stress from an inserted plastic strain rate is using the Onsager matrix (to establish time-inversion symmetry), from the appendix in Ref. [102]. After ignoring gradients of temperature and thus heat fluxes, as well as all associated terms, one can transform

[16] For more details about possible choices of non-diagonal Onsager coefficients, see Appendix A in Ref. [102]. For example, the term $p_{ijkl}\dot{\varepsilon}_{kl}$, coupling the plastic strain rate with the strain rate, requires a similar term of opposite sign, coupling to the elastic stress and contributing to the viscous-dissipative stress: $\sigma^D_{ij}\dot{\varepsilon}_{ij} = -p_{klij}\pi_{kl}\dot{\varepsilon}_{ij} = -p_v P_\Delta \dot{\varepsilon}_v - p_s\pi^*_{ij}\dot{\varepsilon}^*_{ij}$.

all tensors into eigen-value form [17]. This results in only two independent invariants per state variable tensor, ignoring the third for the sake of simplicity, yielding a 4×4 matrix form to determine plastic strains and dissipative stresses:

$$\begin{pmatrix} \dot\varepsilon_v^p \\ \dot\varepsilon_s^p \\ \sigma_v^D \\ \sigma_s^D \end{pmatrix} = \mathcal{X} \cdot \begin{pmatrix} \Delta \\ \varepsilon_s^e \\ \dot\varepsilon_v \\ \dot\varepsilon_s \end{pmatrix} \quad , \quad \text{with} \tag{33}$$

$$\mathcal{X} = \begin{pmatrix} e_{vv} & e_{vs} & h_{vv} & h_{vs} \\ e_{sv} & e_{ss} & h_{sv} & h_{ss} \\ \alpha\pi_s - h_{vv}\mathcal{B}_\Delta & -h_{sv}\mathcal{G}_\Delta & \eta_{vv} & 0 \\ -h_{vs}\mathcal{B}_\Delta & \alpha_1 P_\Delta - h_{ss}\mathcal{G}_\Delta & 0 & \eta_{ss} \end{pmatrix}$$

$$= \begin{pmatrix} \lambda_1 T_g & -\alpha_1\dot\varepsilon_s & p_v & p_s\alpha_1\varepsilon_s^e \\ -\alpha\dot\varepsilon_v & \lambda T_g & p_v\alpha\Delta & p_s \\ \alpha\pi_s - p_v\mathcal{B}_\Delta & -p_v\alpha\Delta\mathcal{G}_\Delta & \eta_v & 0 \\ -p_s\alpha_1\varepsilon_s^e\mathcal{B}_\Delta & \alpha_1 P_\Delta - p_s\mathcal{G}_\Delta & 0 & \eta_s \end{pmatrix}$$

with 4-tuple vectors of the invariants of the state variables or their conjugates (pressure $P_\Delta = \mathcal{B}_\Delta\Delta$ and shear stress norm $\pi_s = \text{sign}(\pi)|\pi_{ij}| = \mathcal{G}_\Delta\varepsilon_s^e$), with secant moduli assumed constant in the momentary situation, above jamming (cases below jamming, $\Delta < 0$, are discussed at the end of this section).

The plastic strain rates (placeholder for strain-rate minus elastic strain, which is the state-variable) are thus:

$$\dot\varepsilon_v^p = \lambda_1 T_g\Delta - \alpha_1\varepsilon_s^e\dot\varepsilon_s(1-p_s) + p_v\dot\varepsilon_v \,,$$

and

$$\dot\varepsilon_s^p = \lambda T_g\varepsilon_s^e - \alpha\Delta\dot\varepsilon_v(1-p_v) + p_s\dot\varepsilon_s \,,$$

while the dissipative stresses are

$$\sigma_v^D = \eta_v\dot\varepsilon_v - p_v P_\Delta + \alpha\pi_s\Delta(1-p_v) \,,$$

and

$$\sigma_s^D = \eta_s\dot\varepsilon_s - p_s\pi_s + \alpha_1 P_\Delta\varepsilon_s^e(1-p_s) \,.$$

For the sake of brevity, some of the above terms are not used furtheron, i.e., while the α_1-term will be used, only a placeholder is given for $p_g = \alpha\Delta\dot\varepsilon_v(1-p_v)$; similarly, for the dissipative stresses, only the first terms are used in some (numerical) solutions (even though small), while the other terms are subject to ongoing studies. The only non-classical term used is the granular energy creation, active outside the elastically stable regime, abbreviated as $f_g = \bar\beta_{ijkl}\pi_{ij}\pi_{kl}$, below in Sec. 4.

Inserting the above expressions into Eq. (31) results in an always positive total entropy production:

$$\begin{aligned} R + R_g &= P_\Delta\dot\varepsilon_v^p + \pi_s\dot\varepsilon_s^p + \sigma_v^D\dot\varepsilon_v + \sigma_s^D\dot\varepsilon_s \\ &= \lambda_1 T_g\Delta P_\Delta + \lambda T_g\varepsilon_s^e\pi_s + \eta_v\dot\varepsilon_v^2 + \eta_s\dot\varepsilon_s^2 \\ &= \beta_v P_\Delta^2 + \beta_s(\pi_s)^2 + \eta_v\dot\varepsilon_v^2 + \eta_s\dot\varepsilon_s^2 \geq 0 \,, \end{aligned} \tag{34}$$

which is true by construction, since all terms are quadratic in either elastic strains (stresses) or strain rates. The first two terms are a simple constitutive choice for the more general forms in Eq. (30), with purely isotropic, $\beta_v = \lambda_1 T_g/\mathcal{B}_\Delta$, and deviatoric, $\beta_s = \lambda T_g/\mathcal{G}_\Delta$, compliance rates.

Below jamming, one has (per definition) no elastic stress with purely plastic deformations, with probabilities, $p_v = p_s = 1$, and thus only the viscous terms survive in Eq. (34). On the other hand, in the ideal elastic limit, above jamming, one has no plastic deformations, $p_v = p_s = 0$, so that the classical GSH shows up with only the λ-preceded relaxation terms surviving (and the α-preceded terms in plastic strains and dissipative stresses cancelling each other).

3 Granular solid hydrodynamics (GSH)

As review, GSH is a continuum mechanical theory for granular media, set up in compliance with thermodynamics and conservation laws. GSH possesses the *state variables*:
(i) density, ρ, or volume fraction, $\phi = \rho/\rho_p$,
(ii) momentum density, $\rho v_i = 0$, neglected here,
(iii) elastic isotropic strain $\Delta = -u_{ll} = \varepsilon_v^e = \log(\rho/\rho_J)$,
(iv) elastic deviatoric (shear) strain $u_s = \sqrt{2J_2^u}$,
(v) granular temperature $T_G \propto T_g^2$, and
(vi) temperature T, not used in the following,
with conventions and nomenclature given in Sec. 1.7.

The GSH used here reduces to various different, more classical theories, in the respective limits – when set appropriately, as was shown in: Refs. [147] for hypoplasticity, [150] for the $\mu(I)$-rheology, and [44] for fluidity, etc. The question is now if it is possible to catch the complex phenomenology at yielding, jamming, unjamming, elasticity and loss of elasticity with a simple model that only knows about four state variables: ρ, Δ, u_s, and T_g.

[17] Any rank-two tensor can be decomposed into (v = volumetric = isotropic, and s = shear = deviatoric) $T_{ij} = T_v\delta_{ij} + T_s\hat\delta_{ij}^0 + \ldots$, with unit tensor δ_{ij} and (reference) unit deviator in diagonal form: $\hat\delta_{ij}^0 = \sqrt{1/2}[1,0,-1]$, using the isotropic, first invariant $T_v = T_{ii}/\mathcal{D}$, ignoring its third invariant, and a signed version of the second invariant $T_s = \text{sign}(T)|T_{ij}^*| = \text{sign}(T)|T_{ij} - T_v\delta_{ij}| = \sqrt{T_{ij}^*T_{ij}^*} = \sqrt{2J_2^T}$, with $\text{sign}(T) = \hat\delta_{ij}^T\hat\delta_{ij}^0$, as used in [120]. In the eigensystem, $\text{sign}(T)$ switches sign whenever $\hat\delta_{ij}^T$ changes direction relative to the (constant) reference $\hat\delta_{ij}^0$.

For the sake of completeness, we first recollect the more complex, more complete classical GSH, as published in the previous years, in Sec. 3.1, before we reduce GSH to an over-simplified minimal model in Sec. 3.2, which will allow for a better understanding of the structure of GSH. Note that the nomenclature of classical GSH is applied in Sec. 3.1, whereas we switch to the positive compressive strain convention and nomenclature in Sec. 3.2.

3.1 About classical GSH

The complete equations of GSH may be found in Refs. [107,44], a simplified version in Ref. [45], from which we boil down to a minimalistic version in subsection 3.2, ignoring not only momentum density and gradients, but also the density dependence of most transport coefficients and parameters, since those represent top-down constitutive assumptions, rather than basic (qualitative, bottom-up) theory. First, we discuss a few complications in the classical GSH nomenclature, that are not necessary for our present focus, but will become important if a more quantitative model is the goal, so that we keep them as reference for the sake of completeness.

3.1.1 The classical GSH constitutive model

The energy density has a thermal and an elastic part:

$$w = w_T + w_\Delta, \qquad w_T = s_g^2/(2\rho b) \ ,$$
$$w_\Delta = \sqrt{\Delta}[2B(\rho)\Delta^2/5 + G(\rho)u_s^2], \quad B, G > 0 \ , \tag{35}$$

with $P_\Delta \equiv \pi_{\ell\ell}/3$. This represents the first constitutive assumption at the core of classical GSH. In the following, we drop the explicit ρ-dependence of B and G for convenience, but keep in mind and used it whenever needed. (In previous GSH-publications, G was denoted as $\mathcal{A}$.). The elastic stresses are defined as the derivatives of w with respect to the elastic strain u_{ij}:

$$\pi_{ij} \equiv -\partial w/\partial u_{ij} = P_\Delta \delta_{ij} - \pi_s u^*_{ij}/u_s \ , \tag{36}$$
$$P_\Delta = \sqrt{\Delta}(B\Delta + Gu_s^2/2\Delta), \quad \pi_s = 2G\sqrt{\Delta}\, u_s \ , \tag{37}$$
$$4P_\Delta/\pi_s = 2(B/G)(\Delta/u_s) + u_s/\Delta \ , \tag{38}$$

which represents no constitutive assumption, but is just a consequence of Eq. (35). Like the elastic stress, being conjugate to the elastic strain, the granular temperature is conjugate to the granular entropy, which allows to define the thermal pressure, P_T, as the derivative of the granular thermal free energy with respect to volume, at constant s_g or T_g, as:

$$T_g \equiv \partial w_T/\partial s_g = s_g/\rho b \ , \quad \rightarrow \quad w_T = \rho b T_g^2/2 \ , \tag{39}$$
$$P_T = -\left.\frac{\partial[w_T/\rho]}{\partial(1/\rho)}\right|_{s_g} \equiv -\left.\frac{\partial[(w_T - T_g s_g)/\rho]}{\partial[1/\rho]}\right|_{T_g} = -\frac{\rho^2 T_g^2}{2}\frac{\partial b}{\partial \rho} \ , \tag{40}$$

where we note that the granular entropy is not needed, replaced by the density dependent (positive) function $b = b(\rho)$, decaying with density, $\partial b/\partial\rho < 0$. The elastic energy w_Δ has been tested for: (1) static stress distributions in silos, sand piles, point loads on a granular sheet [151]; (2) incremental stress-strain relations from varying static stresses [152]; (3) propagation of elastic waves at varying stresses [153].

As already observed in Ref. [107], w_Δ is convex if:

$$u_s/\Delta \le \sqrt{2B/G} =: g_e, \quad \text{or} \tag{41}$$
$$\pi_s/P_\Delta \le \sqrt{2G/B} = 2/g_e \ .$$

For more details see subsection 3.4. Because the macroscopic friction, or yield limit, $\mu_0 \sim \sqrt{2G/B}$, is observed to be not (or only weakly) density dependent, in steady state, at least for cohesionless granular media, the next constitutive model assumption used is: $G/B = const.$, and

$$B = B_0\,[(\rho - \bar\rho)/(\rho_{cp} - \rho)]^{0.15} \ , \tag{42}$$

where $B_0 > 0$ is a constant, and $\bar\rho \equiv \frac{1}{9}(20\rho_{\ell p} - 11\rho_{cp})$, with $\rho_{cp} - \rho_{\ell p} \approx \rho_{\ell p} - \bar\rho$. ($\rho_{cp}$ is the *random-close packing density*, the highest one at which grains may remain uncompressed, $\rho_{\ell p}$ is the *random-loose packing density*, the lowest one at which grains may stay static.) The expression for B was empirically constructed to account for three granular characteristics: (1) It provides concavity, for any density smaller than $\rho < \rho_{\ell p}$, and convexity between $\rho_{\ell p}$ and ρ_{cp}, ensuring the stability of elastic solutions in this region. (2) The density dependence of sound velocities, c (as measured by Hardin and Richart [154]), is well approximated by $c = \sqrt{\mathcal{B}/\rho} \approx \sqrt{B\Delta^{1/2}/\rho}$. (3) The slow divergence at ρ_{cp} mimics the fact that the system is much stiffer for $\rho = \rho_{cp}$ than at loose packing $B(\rho = \rho_{\ell p})$. Comparing these constitutive assumptions for G and B with particle simulations is subject of ongoing work, but goes beyond the scope of this paper [18].

[18] To account for the un-jamming transition at the random loose density, $\rho_{\ell p}$, a density dependence of B was seen as necessary in the classical GSH literature. To account for the virgin consolidation curve, higher order elastic strain terms in the elastic energy were proposed, with density dependent coefficients, see [107,155]. The Coulomb yield could be accounted for with no density dependence, as in Eq. (41). Since

Finally, the function b was chosen as:

$$b = b_1/\rho + b_0\left[1-\rho/\rho_{cp}\right]^a , \tag{43}$$

with another small power law, $a \approx 0.1$, such that $P_T \approx w_T$ for $\rho \to 0$, and $P_T \approx w_T/(\rho_{cp}-\rho)$ for $\rho \to \rho_{cp}$, limits which reduces b to first or second term, respectively, for details see Refs. [8,156]. The thermal pressure is explicitly given as:

$$P_T = \frac{\rho^2 T_g^2}{2}\left[\frac{b_1}{\rho^2} + \frac{ab_0}{\rho_{cp}(1-\rho/\rho_{cp})^{1-a}}\right] =: \rho T_g^2 G_p , \tag{44}$$

which defines the abbreviation for the positive $G_p = G_p(\rho) = -(\rho/2)\partial b/\partial\rho$, that also is set to constant in the following sections, a good approximation for low densities only, where $G_p \approx b_1/2 \approx 1$ (in units of d^2). In the regime of standard kinetic theory being valid, one has $G_p = [1+(\mathcal{D}-1)(1+r)\phi g_2(\phi)]$, with restitution coefficient r and pair correlation at contact, $g_2(\phi)$, as specified for example in Refs. [8,113,111].

Adding some speculative connection to other works, the function b is qualitatively similar to the density dependence, $F = gd/\delta v$, of the scaled fluidity, g, as reported in Ref. [18]. However, note that the fluidity is based on shear stress and shear strain only, whereas the thermal stress, $P_T/G_p = \rho T_g^2 = \rho(\delta v/d)^2 \sim \rho(g/F)^2$ is also defined for isotropic deformations, i.e., non-sheared systems. Whether g and $F(\rho)$ are truly related with T_g and $G_p(\rho)$, and how exactly, is subject of ongoing research and goes beyond the scope of this paper.

3.1.2 The evolution equations

For completeness, we specify the evolution equations in the classical GSH nomenclature, where we note the sign conventions $\Delta = \varepsilon_v^e$, $u_{ij} = -\varepsilon_{ij}^e$ and $v_{ij} = -\dot{\varepsilon}_{ij}$, see Sec. 1.7. For the elastic strain one has:

$$\frac{\partial}{\partial t}u_{ij}^* = v_{ij}^* - \lambda T_g u_{ij}^*, \tag{45}$$

$$\frac{\partial}{\partial t}\Delta + v_{\ell\ell} = \alpha_1 u_{ij}^* v_{ij}^* - \lambda_1 T_g \Delta, \tag{46}$$

with α_1 as an off-diagonal Onsager coefficient, see subsection 2.4, accounting for Reynolds dilatancy. Mass and momentum conservation read:

$$\frac{\partial}{\partial t}\rho + \nabla_i(\rho v_i) = 0, \tag{47}$$

$$\frac{\partial}{\partial t}(\rho v_i) + \nabla_i(\sigma_{ij} + \rho v_i v_j) = -\rho g_i, \tag{48}$$

with the total stress: $\sigma_{ij} = \pi_{ij} + P_T\delta_{ij} - \eta_1 T_g v_{ij}^*$, with viscosity, $\eta_g = \eta_1 T_g$.

Finally, the evolution equation for T_g, with b as given by Eq. (39) and $T_g^* \equiv T_g + \gamma_0/\gamma_1 =: T_g + T_e$, is given by Eq. (23).

The coefficients $\alpha_1, \gamma_0, \gamma_1, \eta_1$, and ρb are all functions of the state variables, especially the density, which would require many more constitutive assumptions, so that they are over-simplified and taken as constants in the following sections. Alternative energy densities are compared next.

3.2 Minimal GSH type model for a material point

At the core of GSH, assuming a homogeneous representative volume, without convection, $\rho v_i = 0$ and gradients, $\nabla_i(...) = 0$, one has a postulated energy density,

$$w = w_e + w_T , \tag{49}$$

with an elastic and a dynamic, kinetic/granular contribution. The total stress is thus not an independent (state) variable, but can be abbreviated as

$$\begin{aligned}\sigma_{ij} &= \pi_{ij} + P_T\delta_{ij} + \sigma_{ij}^{\text{visc.}} \\ &=: P_\Delta\delta_{ij} + \pi_{ij}^* + \rho T_g^2 G_p\delta_{ij} + \chi\dot{\varepsilon}_v\delta_{ij} + \eta\dot{\varepsilon}_{ij}^* ,\end{aligned} \tag{50}$$

where the five terms represent isotropic and deviatoric elastic stresses, kinetic/granular stress (with an over-simplified $G_p = 1$, which should depend – at least – on density, see Eq. (44)), and isotropic (v=volumetric) and deviatoric (s=shear) viscous stresses, with viscosities $\chi = \eta_v$ and $\eta = \eta_1 = \eta_s$, respectively, where the subscript 1 was used above.

Now, a few versions of the energy density are discussed, before elastic energy stability is considered in the next subsection 3.4.

3.2.1 The linear elastic energy

For completeness, in the (too) simple case of a linear elastic energy density:

$$w_{lin} = \left((1/2)B_{lin}\Delta^2 + G_{lin}u_s^2\right) \quad \text{if } \Delta > 0 , \tag{51}$$

and $w_{lin} = 0$ if $\Delta \le 0$, with $u_s^2 = \varepsilon_{ij}^{e*}\varepsilon_{ij}^{e*}$, one can easily derive the elastic stress $\pi_{ij} = \partial w/\partial u_{ij}$. The parameters B_{lin}, G_{lin} carry the units of stress, while their possible dependencies on other state-variables (like density) are ignored here.

The isotropic elastic pressure (defined in $\mathcal{D}$ dimensions) is:

$$P_\Delta^{lin} = \frac{\pi_{ll}}{\mathcal{D}} = \frac{\partial w_{lin}}{\partial\Delta} = B_{lin}\Delta ,$$

our illustrative examples are focused on the latter, hence B is set to constant in Secs. 4 and 5. A quantitative comparison with particle simulation data will show which assumptions or terms are really needed.

and the deviatoric elastic stress is:

$$\pi_{ij}^{*\,lin} := \frac{\partial w_e}{\partial \varepsilon_{ij}^{e*}} = 2G_{lin}\varepsilon_{ij}^{e*} \,.$$

Further differentiation yields the (constant) moduli: $\mathcal{B}_{lin} = B_{lin}$, $\mathcal{G}_{lin} = 2G_{lin}$, and no anisotropy $\mathcal{A}_{lin} = 0$, which is surely too simple for granular matter.

The anisotropic linear elastic energy density:

$$w_A = \left((1/2)B_{lin}\Delta^2 + A_{lin}\Delta\varepsilon_{ij}^{e*}\hat{\varepsilon}_{ij}^{e} + G_{lin}u_s^2\right) \,, \qquad (52)$$

if $\Delta > 0$ with $\hat{\varepsilon}_{ij}^{e} = \varepsilon_{ij}^{e*}/|\varepsilon_{ij}^{e*}|$, as proposed in Refs. [86, 120, 157]. yields:

$$P_\Delta^A = \frac{\pi_{ll}}{\mathcal{D}} = B_{lin}\Delta + A_{lin}\varepsilon_{ij}^{e*}\hat{\varepsilon}_{ij}^{e} \,,$$

and the deviatoric elastic stress:

$$\pi_{ij}^{*\,A} = \frac{\partial w_e}{\partial \varepsilon_{ij}^{e*}} = 2G_{lin}\varepsilon_{ij}^{e*} + A_{lin}\Delta\hat{\varepsilon}_{ij}^{e} \,.$$

Further differentiation yields the (constant) moduli: $\mathcal{B}_A = B_{lin}$, $\mathcal{G}_A = 2G_{lin}$, and anisotropy $\mathcal{A}_A = A_{lin}$, which is the simplest possible anisotropic elastic model, with cross-coupling between isotropic and deviatoric elastic strains and stresses, as compared to particle simulations and discussed in detail in Refs. [86, 120, 157]. However, the anisotropy modulus is not constant and thus requires an evolution or state equation by itself, e.g., $A_{lin}/B_{lin} = F_{dev}$, with deviatoric fabric, F_{dev}, as observed from 3D particle simulations in Refs. [120, 30].

3.2.2 The non-linear (Hertzian) elastic energy

One can derive the elastic stress $\pi_{ij} = \partial w/\partial u_{ij}$, from the simplest (non-linear) elastic energy density:

$$w_e = \sqrt{\Delta}\left((2/5)B\Delta^2 + Gu_s^2\right) \quad \text{if } \Delta > 0 \,, \qquad (53)$$

and $w_e = 0$ if $\Delta \le 0$, with $u_s^2 = \varepsilon_{ij}^{e*}\varepsilon_{ij}^{e*}$, and $B = B(\rho)$, $G = G(\rho)$ carrying the units of stress, while their possible functional dependencies on other state-variables (like density) are not carried along in the rest of this study. Two choices (out of many more) of the density dependence of the energy density (and its coefficients) are discussed below, where appropriate, but in other cases the density dependence is avoided completely in order to learn what the effect of this simplifaction would be. The isotropic elastic pressure (defined in $\mathcal{D}$ dimensions) is:

$$P_\Delta = \frac{\pi_{ll}}{\mathcal{D}} = \frac{\partial w_e}{\partial \varepsilon_v^e} = B\Delta^{3/2} + \frac{1}{2}Gu_s^2\Delta^{-1/2} =: \mathcal{B}_\Delta\Delta \,,$$

and the deviatoric elastic stress is:

$$\pi_{ij}^* := \frac{\partial w_e}{\partial \varepsilon_{ij}^{e*}} = 2G\Delta^{1/2}\varepsilon_{ij}^{e*} =: \mathcal{G}_\Delta\varepsilon_{ij}^{e*} \,,$$

implicitly defining the (Δ-dependent) bulk and shear secant moduli $\mathcal{B}_\Delta$ and $\mathcal{G}_\Delta$, which mimic a linear Δ- or ε_{ij}^{e*}-dependence of isotropic or deviatoric stress, respectively, not to be confused with the (true) tangent moduli:

$\mathcal{B} = B\Delta^{1/2}\left[(3/2) - (1/4)(G/B)(u_s/\Delta)^2\right] \neq \mathcal{B}_\Delta$,
$\mathcal{G} = 2G\Delta^{1/2} = \mathcal{G}_\Delta$, and $\mathcal{A} = G\Delta^{1/2}(u_s/\Delta)$.

The notation details and alternative definitions of the state variables $\varepsilon_v^e = \Delta$ and $u_s = |\varepsilon_{ij}^{e*}| = |-u_{ij}^*|$ are given in Sec. 1.7.

3.2.3 The granular linear elastic energy

From particle simulations, using the linear contact model, see Refs. [46, 158, 159, 120] and references therein, the (linear) elastic energy density is complemented by a pre-factor, dependent (non-linearly) on the coordination number

$$C := C(\phi, \phi_J) = C(\Delta) = C_0 + C_1\Delta^{\alpha_C} \,, \qquad (54)$$

with positive constants [19] , see subsection 6, so that:

$$w_C = \phi\left(\frac{1}{2}CB_C\Delta^2 + (C - C_0)G_Cu_s^2\right) \text{ if } \Delta > 0 \,, \quad (55)$$

and $w_C = 0$ if $\Delta \le 0$, with $u_s^2 = \varepsilon_{ij}^{e*}\varepsilon_{ij}^{e*}$, and B_C, G_C carrying the units of stress, while their possible dependencies on other state-variables – like density, explicitly spelled out in Eq. (55) – are ignored in the rest of this study, for the sake of simplicity, without loss of generality, while density-dependent coefficients are discussed in the context of the Hertzian energy density.

Note that the above w_C implies that the first term gets an additional, constant contribution in C due to the implied linear contact model; this contribution is not present in the second term that vanishes for $\Delta \to 0$ (for frictionless materials) [120]. Otherwise the linear and the Hertzian energy densities resemble each other for $\alpha_C = 1/2$, as detailed below.

The isotropic elastic pressure is:

$$\begin{aligned} P_\Delta^C &= \frac{\partial w_C}{\partial \Delta} = \phi C B_C\Delta + \phi C' B_C\left[\Delta^2/2 + (G_C/B_C)u_s^2\right] \\ &= \phi C_0 B_C\Delta + \phi C_1 B_C\Delta^{1+\alpha_C}\left[1 + \frac{\alpha_C}{2} + \alpha_C\frac{G_C}{B_C}\frac{u_s^2}{\Delta^2}\right] \\ &\approx \phi C_0 B_C\Delta \quad \text{for } \Delta \ll 1 \quad \text{and } \alpha_C > 0 \,, \end{aligned} \qquad (56)$$

and the deviatoric elastic granular stress is:

$$\pi_{ij}^{*\,C} = \frac{\partial w_e}{\partial \varepsilon_{ij}^{e*}} = 2\phi C_1 G_C\Delta^{\alpha_C}\varepsilon_{ij}^{e*} \,, \qquad (57)$$

[19] The derivatives of C are:
$C' = \alpha_C C_1\Delta^{\alpha_C - 1} = \alpha_C(C - C_0)\Delta^{-1}$, and
$C'' = \alpha_C(\alpha_C - 1)C_1\Delta^{\alpha_C - 2} = \alpha_C(\alpha_C - 1)(C - C_0)\Delta^{-2}$.

both featuring very similar non-linearities as the Hertzian type energy density, qualitatively different only in the first, linear term of P_Δ^C.

The tangent moduli are:

$$\mathcal{B}_C = \phi C_0 B_C + \phi C_1 B_C \Delta^{\alpha_C} \times \left[(1+\alpha_C)(1+\frac{\alpha_C}{2}) + \alpha_C(\alpha_C-1)\frac{G_C}{B_C}\frac{u_s^2}{\Delta^2}\right] ,$$
$$\mathcal{G}_C = 2\phi C_1 G_C \Delta^{\alpha_C} \text{ , and}$$
$$\mathcal{A}_C = 2\alpha_C \phi C_1 G_C \Delta^{\alpha_C}(u_s/\Delta) \quad (58)$$

Note that inserting $\alpha_C = 1/2$, which fits almost perfectly particle simulation data [46], results in

$$\mathcal{B}_C = \phi C_0 B_C + \phi C_1 B_C \Delta^{1/2}\left[\frac{15}{8} - \frac{1}{4}\frac{G_C}{B_C}\frac{u_s^2}{\Delta^2}\right] ,$$
$$\mathcal{G}_C = 2\phi C_1 G_C \Delta^{1/2} \text{ , and}$$
$$\mathcal{A}_C = \phi C_1 G_C \Delta^{1/2}(u_s/\Delta) , \quad (59)$$

with the first term ($C_0 > 0$) being the only difference to the non-linear Hertzian moduli in subsection 3.2.2, after translation: $(4/5)B = \phi C_1 B_C$ and $G = \phi C_1 G_C$.

3.2.4 Granular Hertzian energy density

The combination of the two previous subsections, i.e., non-linear contacts combined with granular (coordination number dependent) energy, goes beyond the scope of this study and will be discussed elsewhere.

3.3 Simplest GSH equations and discussion

For a material point, in absence of gradients, using $\partial_t \sim \partial/\partial t \sim d/dt$, the evolution of density with strain rate:

$$\partial_t \rho = \rho \dot{\varepsilon}_v \quad (60)$$

has no free parameters. Here, positive strain rate corresponds to compression and negative to extension, i.e., density increase and decrease, respectively; density can also be seen as the volume fraction, related to each other by the (constant) material density, i.e., $\phi = \rho/\rho_p$. Later, in section 5, units will be chosen explicitly, such that $\rho_p = 1$, so that $\phi = \rho$, as implied from now on.

In the evolution equation for the isotropic elastic strain:

$$\partial_t \Delta = \dot{\varepsilon}_v - \lambda_1 T_g \Delta + \alpha_1 \varepsilon_{ij}^{e*} \dot{\varepsilon}_{ij}^* \quad (61)$$

the *first term* couples elastic and total strain together, while the *second term* is relaxing Δ towards zero [20] – in case of finite T_g, with rate $\lambda_1 T_g$. The *third term* can be positive (or negative, e.g., at strain reversal [21]), and thus works against (or with) the relaxation term.

The third equation defines the evolution of the deviatoric (shear) elastic strain

$$\partial_t \varepsilon_{ij}^{e*} = \dot{\varepsilon}_{ij}^* - \lambda T_g \varepsilon_{ij}^{e*} , \quad (62)$$

where the *first term* creates deviatoric elastic strain, co-linearly with the strain rate, while the *second term* relaxes the deviatoric elastic strain, with rate λT_g. A dilatancy term analogous to the third in Eq. ((61)) is permitted by the Onsager relation, and was previously added for symmetry in Refs. [44,45,120], as discussed in subsection 2.4, and used in section 4.

The fourth equation represents the evolution of the granular temperature

$$\partial_t T_g = -R_T T_g T_g^* + f_T(\dot{\varepsilon}_{ij}) \quad (63)$$
$$= R_{T0}\left[-(1-r^2)T_g T_g^* + f_s^2 \dot{\varepsilon}_{ij}^* \dot{\varepsilon}_{ij}^* + f_v^2 \dot{\varepsilon}_v \dot{\varepsilon}_v\right]$$

with $T_g^* = T_g + T_e$, as specified in the following section 4, and the abbreviation for the dissipation rate, $R_T = \gamma_1/(\rho b) = R_{T0}(1-r^2)$, proportional to the energy dissipation factor $(1-r^2)$, where r is the (effective) restitution coefficient. The energy creation terms are condensed into the tensor function $f_T(\dot{\varepsilon}_{ij})$, independent on r, so that one could separate them into two energy creation rates, $R_{T0} f_s^2 = \eta_s/(\rho b)$ and $R_{T0} f_v^2 = \eta_v/(\rho b)$, for shear and volumetric strain rates, respectively.

3.4 Minimal elastic model with two variables

One could decompose the elastic stress and strain tensors into invariants (and their orientations). Under the assumption of fixed and co-linear tensor-eigensystems, and ignoring the third invariant for the sake of brevity, what remains are the isotropic and deviatoric stresses, $\sigma_\alpha = \{P_\Delta, \pi_s = \pi_s^*\}$, and elastic strains, $u_\alpha = \{\Delta, u_s = u_s^*\}$, each as 2-tuple vectors, denoted by Greek indices. This provides the criteria for energy minima:

$$\delta^2 w = -\delta\pi_{ij}\delta u_{ij} = \delta\pi_\alpha \delta u_\alpha = \frac{\partial \pi_\alpha}{\partial u_\beta}\delta u_\alpha \delta u_\beta > 0. \quad (64)$$

[20] Relaxation of $\Delta \to 0$, at fixed density, ρ, implies that the granular temperature (jiggling) causes the jamming density to relax as $\rho_J \to \rho$, in both jammed and un-jammed states, increasing and decreasing, respectively. A decrease (an increase) of the elastic strain, Δ, at fixed density, ρ, corresponds to an increase (a decrease) of the jamming density, ρ_J, see Ref. [46]. On the other hand, at fixed confining pressure, P, a jammed system, at finite, but small T_g (tapping) will develop to a state such that the elastic pressure, $P_\Delta = P - P_T \approx P$, remains constant; relaxation of Δ then corresponds to an increase of density, i.e., compaction.

[21] After large strain, one has a positive product, $\varepsilon_{ij}^{e*}\dot{\varepsilon}_{ij}^* > 0$, but at strain reversal the same term will be negative, for a while, until the elastic deviatoric strain reverts direction.

Using the (positive) invariants yields the simple 2x2 Hessian matrix (for second order elastic work):

$$\frac{\partial^2 w_e}{\partial u_\alpha \partial u_\beta} = \frac{\partial \pi_\alpha}{\partial u_\beta} = \begin{pmatrix} \partial P_\Delta/\partial \Delta & \partial P_\Delta/\partial u_s \\ \partial \pi_s/\partial \Delta & \partial \pi_s/\partial u_s \end{pmatrix} =: \begin{pmatrix} \mathcal{B} & \mathcal{A} \\ \mathcal{A} & \mathcal{G} \end{pmatrix} = \mathbf{C} \,. \quad (65)$$

If it has only positive eigenvalues, the (elastic) energy w_e is a convex function of the elastic strain-invariants Δ and u_s. With other words, the elastic stability criterion is $\det(\mathbf{C}) = \mathcal{B}\mathcal{G} - \mathcal{A}^2 > 0$.

3.4.1 Eigen-values and -vectors at elastic instability

First, we compute the eigen-values and -vectors from the matrix $\mathbf{C}$, before we introduce constitutive assumptions about the energy density and discuss those, separately, in the next sub-subsections.

Basic linear algebra yields the two eigen-values, $C_{1,0} = (\mathcal{B}+\mathcal{G})/2 \pm \sqrt{(\mathcal{B}-\mathcal{G})^2/4 + \mathcal{A}^2}$, as solution of the quadratic equation $0 = (\mathcal{B}-C)(\mathcal{G}-C) - \mathcal{A}^2 = C^2 - C(\mathcal{B}+\mathcal{G}) + \mathcal{B}\mathcal{G} - \mathcal{A}^2$, with $C_1 = \mathcal{B}+\mathcal{G}$ and $C_0 = 0$, at the point of instability, where $\mathcal{B}\mathcal{G} = \mathcal{A}^2$.

Using C_1, and $\mathcal{A} = \sqrt{\mathcal{G}\mathcal{B}}$, with the two equations $-\mathcal{G}\hat{n}_1^{(1)} + \mathcal{A}\hat{n}_2^{(1)} = 0$ and $\mathcal{A}\hat{n}_1^{(1)} - \mathcal{B}\hat{n}_2^{(1)} = 0$, results in the corresponding eigen-vector (with $\hat{n}_2^{(1)} = \hat{n}_1^{(1)}\mathcal{G}/\mathcal{A} = \hat{n}_1^{(1)}\mathcal{A}/\mathcal{B} = \hat{n}_1^{(1)}\sqrt{\mathcal{G}/\mathcal{B}}$), which defines the "direction" (in elastic strain invariants) of maximal stability: $\hat{n}^{(1)} = \pm(1, \sqrt{\mathcal{G}/\mathcal{B}})/\sqrt{1+\mathcal{G}/\mathcal{B}}$.

Note that *eigenvectors* are normalized, come with unspecified direction ($\pm$), are associated to an eigenvalue (superscript (0) or (1)), and are situated in the space of isotropic and deviatoric elastic strains (Δ, u_s), where the brackets indicate a line-vector, with components separated by the komma. Some examples are given below in Fig. 3.

Using $C_0 = 0$, and $\mathcal{A} = \sqrt{\mathcal{G}\mathcal{B}}$, with the two equations $\mathcal{B}\hat{n}_1^{(0)} + \mathcal{A}\hat{n}_2^{(0)} = 0$ and $\mathcal{A}\hat{n}_1^{(0)} + \mathcal{G}\hat{n}_2^{(0)} = 0$, results in the corresponding eigen-vector (with $\hat{n}_2^{(0)} = -\hat{n}_1^{(0)}\mathcal{B}/\mathcal{A} = -\hat{n}_1^{(0)}\mathcal{A}/\mathcal{G} = -\hat{n}_1^{(0)}\sqrt{\mathcal{B}/\mathcal{G}}$), which gives the "direction" of instability (in the space of elastic strain-invariants): $\hat{n}^{(0)} = \pm(-\sqrt{\mathcal{G}/\mathcal{B}}, 1)/\sqrt{1+\mathcal{G}/\mathcal{B}}$, perpendicular to the direction of maximal stability. Note the special role the ratio of shear to bulk modulus takes in this analysis.

More explicitly, incremental changes in the elastic strain space, in directions $\hat{n}^{(0)}$, i.e., $\delta u_\alpha^{(0)} = (\delta\Delta^{(0)}, \delta u_s^{(0)}) = \delta\varepsilon^e\, \hat{n}_\alpha^{(0)}$, at the point of elastic instability, can be done without change of elastic stress, $\delta\pi_\alpha^{(0)} = 0$, and energy, $\delta^2 w^{(0)} = (\delta\varepsilon^e)^2 \hat{n}_\alpha^{(0)} \hat{n}_\beta^{(0)} C_{\alpha\beta} = 0$. Such increments are thus permitted from energy/thermodynamic arguments; for examples, see Fig. 3. With other words, any other elastic strain increment will require energy; for energy considerations, see also Ref. [102,42,101] and references therein.

3.4.2 GSH with Hertzian type elastic instability

In the case of a Hertzian type elastic energy density, w_e, see Eq. (53), as typically used in the GSH literature [44], one has:

$\mathcal{B} = (3/2)B\Delta^{1/2} - (1/4)Gu_s^2\Delta^{-3/2} \neq \mathcal{B}_\Delta$,
$\mathcal{G} = 2G\Delta^{1/2}$, and $\mathcal{A} = G\Delta^{-1/2}u_s$,

i.e., the stability condition, $\mathcal{B}\mathcal{G} - \mathcal{A}^2 > 0$, translates to

$$(u_s/\Delta)^2 < g_e^2 := 2B/G \,, \quad (66)$$

as previously shown in Eq. (12) in Ref. [45], and in Eq. (41) above, for elastic, static systems above jamming, for $\Delta > 0$. Below jamming, for $\Delta \leq 0$, one has $w_e = 0$ and thus trivially $\det(\mathbf{C}) = 0$, while at the point of instability: $\sqrt{\mathcal{G}/\mathcal{B}} = \mathcal{A}/\mathcal{B} = \mathcal{G}/\mathcal{A} = 2\Delta/u_s = 2/g_e$.

Using w_e in Eq. (53), the non-zero eigenvalue can be re-written as: $C_1 = [B+2G]\Delta^{1/2} = B[1+4/g_e^2]\Delta^{1/2}$, with $g_e = \sqrt{2B/G}$, while the zero eigenvalue will be more relevant for understanding failure mechanisms at elastic instability.

The eigen-vectors in elastic strain space are:
$\hat{n}^{(1)} = \pm(1, 2/g_e)/\sqrt{1+4/g_e^2}$, and
$\hat{n}^{(0)} = \pm(2/g_e, -1)/\sqrt{1+4/g_e^2}$,
at the point of elastic instability, where incremental strains parallel to $\hat{n}^{(0)}$ change neither stress, $\delta\pi_\alpha^{(0)} = 0$, nor energy, $\delta^2 w^{(0)} = (\delta\varepsilon^e)^2 \hat{n}_\alpha^{(0)} \hat{n}_\beta^{(0)} C_{\alpha\beta} = 0$, and are thus permitted.
In other words, considering the shear vs. normal stress space, one could see the limit of elasticity as one possible definition of the maximal (elastic) macroscopic (bulk) friction, defined by the ratio: $\mu_e := \pi_s^*/P_\Delta = \mathcal{G}_\Delta u_s/(\mathcal{B}_\Delta\Delta)$, with the limit value taken at the loss of elastic stability: $\mu_e^0 = \sqrt{2G/B} = 2/g_e$. Incremental changes of elastic strain along the eigenvector $\hat{n}^{(1)}$, with norm $\delta\varepsilon^e$, result in stress increments, $\delta\pi_\alpha^{(1)} = C_1\delta\varepsilon^e\hat{n}_\alpha^{(1)}$, parallel to the slope $\mu_e^0 = \sqrt{\mathcal{G}/\mathcal{B}}$.

3.4.3 GSH with granular elastic energy instability

In the case of a granular (coordination number dependent) elastic energy density, w_C, see Eq. (55), and the respective moduli, see Eq. (59), the stability condition, $\mathcal{B}_C\mathcal{G}_C - \mathcal{A}_C^2 > 0$, translates to:

$$C_0 + C_1\Delta^{\alpha_C} \times \left[(1+\alpha_C)(1+\frac{\alpha_C}{2}) - \alpha_C(1-\alpha_C)\frac{G_C}{B_C}\frac{u_s^2}{\Delta^2}\right] - 2\alpha_C^2 C_1\Delta^{\alpha_C}(G_C/B_C)(u_s/\Delta)^2 > 0\,, \quad (67)$$

that can be solved by a rather complex function

$$C_0+C_1\Delta^{\alpha_C}(1+\alpha_C)(1+\frac{\alpha_C}{2}) > \alpha_C C_1\Delta^{\alpha_C}(1+\alpha_C)\frac{G_C}{B_C}\frac{u_s^2}{\Delta^2}\,, \quad (68)$$

which simplifies to

$$u_s < \frac{C_0}{\alpha_C C_1(1+\alpha_C)}\frac{B_C}{G_C}\Delta^{1-\alpha_C/2}\,, \quad (69)$$

close to jamming, for $\Delta \ll 1$, given $0 < \alpha_C < 1$. This renders w_C a strange choice, since it implies stronger stability to shear strain closer to jamming, and a non-linear behavior of the elastic stability – subject of ongoing studies.

3.5 Anisotropic, elastic-plastic moduli from DEM

In Refs. [46,120,157], an incremental (athermal) elasto-plastic evolution model for the isotropic and deviatoric stresses was proposed (in their eigen-system, p and τ) as

$$\partial_t p = \mathcal{B}\dot\varepsilon_v(1-p_v) + \mathcal{A}\dot\varepsilon_s(1-p_s)\,, \quad (70)$$
$$\partial_t \tau = \mathcal{A}\dot\varepsilon_v(1-p_v) + \mathcal{G}\dot\varepsilon_s(1-p_s)\,, \quad (71)$$

with additional evolution equations for the anisotropy modulus $\mathcal{A}$ [120,157], and the jamming density [46] – both not detailed here. In order to relate this model to the present GSH based evolution equations, assume (overly simplified, for the sake of clarity) that $\partial_t p \approx \mathcal{B}\partial_t\Delta$ and $\partial_t\tau \approx \mathcal{G}\partial_t\varepsilon_s^e$, to arrive at the evolution equations of the elastic strains:

$$\partial_t\Delta = \dot\varepsilon_v(1-p_v) + \frac{\mathcal{A}}{\mathcal{B}}\dot\varepsilon_s(1-p_s)\,, \quad (72)$$
$$\partial_t\varepsilon_s^e = \dot\varepsilon_s(1-p_s) + \frac{\mathcal{A}}{\mathcal{G}}\dot\varepsilon_v(1-p_v)\,, \quad (73)$$

where the first terms represent their elastic and plastic responses, with probabilities for plastic deformations p_v (see Sec. 4.1.1) and p_s (see Sec. 4.1.2), while the second terms are anisotropy terms, cross-coupling isotropic and deviatoric strain actions and reactions.

In Ref. [120], the elements of the constitutive moduli matrix, $\mathbf{C}$, were directly deduced from particle simulations, and took a form (slightly simplified here by implying that the fabric and the elastic strain are proportional): $\mathcal{B} = B_0\phi Z$ (with the product of volume fraction, ϕ, and coordination number, Z, which is a non-linear function of Δ), $\mathcal{G}/\mathcal{B} = G_0(\Delta)(1-g_s(u_s/\Delta)^2)$, and $\mathcal{A}/\mathcal{B} = u_s/\Delta$, with $G_0(\Delta) = g_0(1-\exp(-\Delta/\Delta_g))$ and constants B_0, g_0, g_s and Δ_g. Note that for this model no energy density is available so far – work in progress.

In the elastic limit case one has $p_v = p_s = 0$, and can identify the cross-term in Eq. (72) with the last term in Eq. (61), i.e., $\alpha_1\varepsilon_s^e\dot\varepsilon_s = \frac{\mathcal{A}}{\mathcal{B}}\dot\varepsilon_s$, causing pressure dilatancy under shear strain. From the second cross-term in Eq. (4.1), one can deduce a missing cross-term in Eq. (62), as $\alpha_d = \frac{\mathcal{A}}{\mathcal{G}}\dot\varepsilon_v$, causing shear stress "dilatancy" under isotropic strain.

From this, the condition for elastic instability, $\mathcal{G}/\mathcal{B} - (\mathcal{A}/\mathcal{B})^2 = 0$, translates to: $g_e^2 := (u_s^g/\Delta)^2 = G_0(\Delta)/[1+g_sG_0(\Delta)]$, which implies a very narrow elastic regime for small Δ, since $G_0(\Delta) \to g_0\Delta/\Delta_g$, for vanishing $\Delta/\Delta_g \ll 1$, so that $g_e \propto \sqrt{\Delta/\Delta_g}$. For large $\Delta/\Delta_g \gg 1$, one has instead $g_e^2 \approx 1/[g_s + 1/g_0]$, independent of Δ.

The "direction" (in elastic strain invariants) of maximal stability becomes: $\hat n^{(1)} = \pm(1,\sqrt{\mathcal{G}/\mathcal{B}})/\sqrt{1+\mathcal{G}/\mathcal{B}} = \pm(\Delta,u_s^g)/\sqrt{\Delta^2+(u_s^g)^2}$, and with the perpendicular "direction" of maximal in-stability: $\hat n^{(0)} = \pm(-\sqrt{\mathcal{G}/\mathcal{B}},1)/\sqrt{1+\mathcal{G}/\mathcal{B}} = \pm(-u_s^g,\Delta)/\sqrt{\Delta^2+(u_s^g)^2}$, after using $\sqrt{\mathcal{G}/\mathcal{B}} = \mathcal{A}/\mathcal{B} = u_s^g/\Delta$.

This model, derived from frictionless particle simulations [120], thus would result in a non-linear $u_s^g = g_e\Delta$ in Fig. 3 – different from the other models presented before in this section. However, all models have in common that the stress response to a strain-increment in the direction of the unit-vector $\hat n^{(1)}$, is parallel to the slope $\mu_e^0 = \sqrt{\mathcal{G}/\mathcal{B}}$ in stress space.

Further consideration of this particle simulation based constitutive model for stress and fabric – and the question if an additional fabric state variable (tensor) is needed at all – go beyond the scope of the present study, but are subject of ongoing research. Nevertheless, the cross-terms discussed above will be considered in the next section in some situations.

3.6 Special cases

In order to reduce the model complexity, and to understand what the eigen-vectors from the last subsection mean, it is instructive to consider a few simple special cases. Some of these cases will be later studied analytically and numerically. They represent simplifications that boil down a complicated theoretical framework to a simpler, possibly even transparent form that allows for better understanding and sometimes even for analytical solutions. We propose to apply those special cases to any new theory before one really applies the whole framework. Furthermore, the special cases allow to isolate a few of the terms and possibly calibrate the model parameters one by one. One traditional work on more complex, so-called proportional loading paths is

Ref. [35], however, we reduce ourselves to the simplest cases only.

For the rest of this section, we use the stability results from the Hertz-like elastic energy density, as discussed in subsection 3.4.2. Most of the cases are illustrated schematically in Fig. 3.

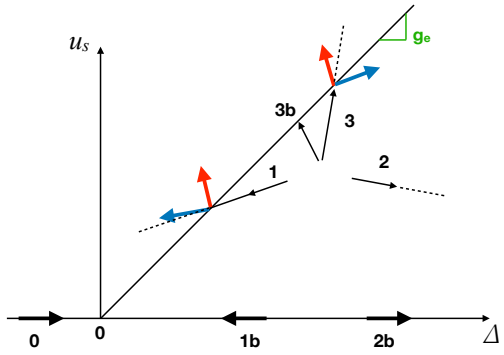

Fig. 3 Sketch of (strain-driven) deformation cases in the space of the elastic strain invariants, i.e., u_s plotted against Δ. The slope g_e indicates the elastic instability limit. The numbers at the black arrows indicate the case-number, where dashed, thin lines are continuing the trends outwards into the concave zone (elastically instable). The blue and red arrows give the eigen-vectors of stability $\hat{n}^{(1)}$, and instability, $\hat{n}^{(0)}$, respectively, where their unspecified direction ($\pm$) maybe directed outwards or into the convex zone (elastically stable), dependent on the situation and the boundary conditions.

Except for a few cases, most start from a jammed, elastically stable state with finite initial elastic strains $\Delta(0) > 0$ and $u_s(0) > 0$.

(case 0) Assume the system unjammed, $\Delta(0) < 0$, and apply a constant compressive strain rate, $\dot{\varepsilon}_v = -v_{ll} > 0$. The density and the elastic strain, $\Delta = \log(\rho/\rho_J)$, will grow together until the system jams at ρ_J, from which on its evolution equation kicks in. It was shown in Refs. [160,161], and earlier works cited therein, that already below jamming, the jamming density (and thus Δ) depends on the procedure of preparation, in particular on the strain rate and on the granular temperature, however, this fact goes beyond the present focus and is thus not studied further.

(case 1) Assuming a purely isotropic de-compression, $\dot{\varepsilon}_v = -v_{ll} < 0$, from a jammed state, one expects the elastic isotropic strain, Δ, to decrease faster than its deviatoric (shear) counterpart, u_s, until at $u_s^2 = (2B/G)\Delta^2$, or $u_s = g_e\Delta$, the looser system cannot sustain the shear-stress anymore, so that un-jamming due to instability with respect to shear occurs. In order to remain at least marginally stable, one needs a decrease of $u_s \to u_s^0 = g_e\Delta$, a situation that could be referred to as shear-yielding [10,95,46].

(case 1b) In the situation without initial elastic shear strain, $u_s(0) = 0$, the stability criterion is always true and the system remains stable until isotropic unjamming takes place at $\Delta = 0$.

(case 2) In the case of isotropic compression, the model remains stable, unless the virgin consolidation line is reached, where the system restructures to be able to carry the increasing stress. This situation is not detailed further, but the **(case 2b)** of loading without shear is studied in subsection 4.1 to display the role of plastic deformations due to isotropic compression.

(case 3) Assuming a purely deviatoric (volume conserving) shear strain rate, $\dot{\varepsilon}^*_{ij} = -v^*_{ij}$, from a state with initial $\Delta_0 > 0$, one expects the elastic deviatoric (shear) strain, u_s, to increase faster than its isotropic counterpart, Δ, could build up, until at $\Delta \to \Delta_0(1 + \epsilon_\Delta) = u_s/g_e$, the system cannot sustain pressure (isotropic stress) anymore, so that an instability with respect to volume change occurs, and one has a consequent decrease of ϕ_J, due to a possible further increase of Δ, i.e., one origin of dilatancy. The evolution of Δ inside the cone and at the limit of elastic stability are qualitatively different, as will be studied numerically later on.

(case 3b) Under the same purely deviatoric deformation, the isotropic elastic strain Δ could also decrease, corresponding to ϕ_J increasing. This leads to elastic instability at smaller elastic strains, $\Delta \to \Delta_0(1 - \epsilon_\Delta) = u_s/g_e$, not much changing the considerations in case 3, but rather leading to compactancy instead of dilatancy, as to be expected for very loose packings. Furthermore, this could lead to isotropic unjamming, if ϕ_J drops below ϕ.

Several of the cases discussed above will be next studied analytically (as far as possible) and numerically in section 5.

4 Analytical results for special cases

After a summary of the equations that will be used in this section, we take several special cases, starting from the athermal limit, $T_g = 0$. Various versions and limits of the model are discussed and analytically treated (in some special cases where this is possible), while also several new terms and regularization schemes are proposed, to be later used in the numerical solutions.

The set of model equations is summarised here for reference, with the colored terms representing exten-

sions from the black terms (representing model 0):

$$\partial_t \rho = \rho \dot{\varepsilon}_v \ , \tag{74}$$
$$\partial_t \Delta = \dot{\varepsilon}_v(1-p_v) - \lambda_1 T_g \Delta p_g + \alpha_1 \varepsilon^{e*}_{ij}\dot{\varepsilon}^*_{ij}(1-p_s) \ , \tag{75}$$
$$\partial_t \varepsilon^{e*}_{ij} = \dot{\varepsilon}^*_{ij}(1-p_s) - \lambda T_g \varepsilon^{e*}_{ij} + \alpha_d \ , \tag{76}$$
$$\partial_t T_g = -R_T T_g^2 (T^*_g/T_g) + f_T(\dot{\varepsilon}_{ij}) + f_g(g_*) \ , \tag{77}$$

before some meaningful special cases (purely isotropic and deviatoric loading) are discussed below, for which analytical solutions are provided, if possible. The colored terms are not present in the original Eqs. (60)-(63), which is referred to as model 0 (having thus no valid athermal limit), which is used as starting point to study transients in Sec. 5.

The blue terms p_g and α_d are introduced here as place-holders for elements discussed below, in subsection 4.7, or to be added in future, as introduced in Refs. [46,120,157].

The rate of cooling is modified in the elastic, jammed state ($\Delta > 0$) by adding an "elastic dissipation rate" T_e, referred to as model e, as $T^*_g/T_g = 1 + T_e/T_g = 1 + T_{e0}\Delta^h/T_g$ where only the special case $h = 0$, i.e., $T_e = T_{e0}$, will be treated below [22]. The presence of T_e does not affect the dynamics too much for finite $T_g \gg T_e$ (Haff's free homogeneous cooling state (HCS), well below jamming), but in the limit of very small $T_g \to 0$, for elastic, jammed systems, this (phonon/wave-driven) dissipation becomes important, generalizing HCS, providing an exponential decay of $T_g \to 0$ in absence of other driving mechanisms (and $\Delta > 0$), see subsection 4.4. The dissipated granular energy $\partial_t w = \rho b T_g \partial_t T_g = -\rho b T_g^3 (T^*_g/T_g)$ is balanced by an equal positive term creating thermal energy or entropy, i.e., this term does not contribute to the second law of thermodynamics, see subsection 2.4.

The new magenta term $f_g(g_*)$, in Eq. (77), is only active if the system is outside of the elastically stable regime, where $g_* = u_s/\Delta - g_e > 0$, with the limit of elastic stability g_e. It is continuous, inactive in the convex region, active outside. This term generates more granular temperature, jiggling, the more the system gets elastically unstable, due to concavity of the elastic energy.

The terms $(1-p_v)$ and $(1-p_s)$ represent the probabilities for elastic deformations, with p_v and p_s the probabilities for isotropic/deviatoric plastic deformations, respectively, see Ref. [46], as specified in Sec. 2.3, Eq. (24), and discussed next, in section 4.1.

[22] For a Hertzian type bulk modulus, the time-scale of momentum (wave) propagation, for $u_s = 0$, can be estimated as $t_e = 1/T_e = d/v_e \propto d/\sqrt{\mathcal{B}_\Delta/\rho} = d\sqrt{\rho/B\Delta^{1/2}} \propto \Delta^{-1/4}$, i.e., an exponent $h = 1/4$. This estimate, together with a Hertzian elastic pressure, $P_\Delta \propto \Delta^{3/2}$, yields an estimated wave speed $v_e \propto P_\Delta^{1/6}$ or moduli $\mathcal{B} \propto P_\Delta^{1/3}$.

4.1 The granular athermal limit $T_g = 0$

Enforcing the athermal case, $T_g = 0$, the system of equations reduces to:

$$\partial_t \Delta = \dot{\varepsilon}_v(1-p_v) + \alpha_1 \varepsilon^{e*}_{ij}\dot{\varepsilon}^*_{ij}(1-p_s) \ , \tag{78}$$
$$\partial_t \varepsilon^{e*}_{ij} = \dot{\varepsilon}^*_{ij}(1-p_s) + \alpha_d \ , \tag{79}$$

see Eqs. (72) and (4.1), where the cross-term α_d is usually neglected, and the off-diagonal Onsager coefficients p_v and p_s were previously introduced in Ref. [107], but taken equal to α_1, while here they are, alternatively, interpreted as the probabilities for (isotropic and deviatoric) plastic (re-structuring) events in the packing, as in subsection 2.3, , and in Refs. [46,157]. Note that in Eqs. (78) and (79), the probabilites for isotropic and deviatoric plastic deformations are systematically attached to isotropic and deviatoric strain rates, respectively.

In the few plots in this section, dimensionless units are used, such that $\rho = \phi$, and stress is in units of 1 MPa, as discussed in detail at the beginning of section 5. The quantitative calibration of the GSH based theory by particle simulation data as well a alternative units, are discussed in section 6.

4.1.1 Athermal isotropic loading

For *isotropic loading* ($\dot{\varepsilon}^*_{ij} = 0$), the system of equations reduces even further to $\dot{\varepsilon}^p_v := \dot{\varepsilon}_v - \partial_t \Delta = \dot{\varepsilon}_v p_v = \partial_t \log(\rho_J)$ [23].

The elastic limit, with probability $p_v = 0$, translates to constant ρ_J, whereas the fully plastic limit, $p_v = 1$, translates to $\dot{\varepsilon}^p_v = \dot{\rho}/\rho = \dot{\varepsilon}_v$. In all other cases, the probability for plastic deformations should be a function of the state-variables and the sign of deformation rate (i.e., compression or tension).

A simple constitutive assumption, $p_v \dot{\varepsilon}_v = -\lambda_1 T_e \Delta$, could be directly merged into the relaxation term as $-\lambda_1 T^*_g \Delta$, with $T^*_g = T_g + T_e$, and solved analytically [24]. This model displays the transient elastic behavior of polymer melts or glasses for which (in absence of any isotropic strain rate, for finite, constant T_e) $\Delta \to 0$. However, since the reality of granular matter, as measured from particle simulations in Ref. [46], is somewhat more complex, already for frictionless spheres – and even more for realistic frictional non-spherical particles – we have to come up with a better relation for the probability for isotropic plastic rearrangements.

[23] The chain rule yields an identity between the plastic strain rate and the time-evolution of the jamming density: $\partial_t \Delta = (\partial_t \rho)/\rho - (\partial_t \rho_J)/\rho_J = \dot{\varepsilon}_v - \partial_t \log(\rho_J)$.

[24] Inserting the expression from above, this yields the athermal evolution of the elastic strain: $\partial_t \Delta = \dot{\varepsilon}_v - \lambda_1 T_{e0} \Delta^{1+h}$.

The (un-)jamming density was reported, see Eq. (5) in Ref. [46], to reach after infinitely many isotropic loading/un-loading cycles the limit density:

$$\rho_\infty = \rho_{J0} + b_\infty \left[\frac{\rho}{\rho_{J0}} - 1\right]_+^{\beta_\infty} , \qquad (80)$$

with the half-sided linear function $[x > 0]_+ = x$, and $[x \leq 0]_+ = 0$, otherwise, $\rho_\infty = \rho_{J0}$ for $\rho < \rho_{J0}$ [25]. Using Eq. (80), and noting that the first loading is characterized by $\rho_J - \rho_{J0} = p_{v0}(\rho_\infty - \rho_{J0})$, with $p_{v0} = 1 - e^{-1}$, see Eq. (6) in Ref. [46], one can deduce the probability for plastic deformations from:

$$\frac{\partial \log(\rho_J)}{\partial t} = \frac{1}{\rho_J}\frac{\partial \rho_J}{\partial t} = \frac{\rho}{\rho_J}\frac{\partial \rho_J}{\partial \rho}\frac{1}{\rho}\frac{\partial \rho}{\partial t} = p_v \dot{\varepsilon}_v , \qquad (81)$$

yielding:

$$\begin{aligned} p_v &= \frac{\rho}{\rho_J}\frac{\partial \rho_J}{\partial \rho} = p_{v0}\beta_\infty \frac{\rho}{\rho_J}\frac{\rho_\infty - \rho_{J0}}{\rho - \rho_{J0}} \qquad (82)\\ &= (e-1)\beta_\infty \frac{\rho}{\rho_J}\frac{\rho_\infty - \rho_J}{\rho - \rho_{J0}} \approx \frac{1}{2}\frac{\rho}{\rho_{J0}}\frac{\rho_\infty/\rho_J - 1}{\rho/\rho_{J0} - 1} \\ &= \frac{p_{v0}}{1-p_{v0}}\beta_\infty \frac{\rho_\infty/\rho_J - 1}{1 - \rho_{J0}/\rho} \approx 0.5\frac{\Delta - \Delta_\infty}{1 - \rho_{J0}/\rho} , \end{aligned}$$

expressed in terms of the difference between the limit and the actual jamming density $\rho_\infty - \rho_J = e^{-1}(\rho_\infty - \rho_{J0})$, with $\Delta_\infty = \log(\rho_\infty/\rho_J)$.
Below jamming, we postulate $p_v(\rho < \rho_{J0}) = 0$. Just above jamming, the divergent probability in Eq. (83) is limited to $p_v(\rho/\rho_{J0} - 1 \ll 1) = 1$, until it decays to finite positive values $0 < p_v \leq 1$ at higher densities. After shear reversal, the plastic strain rate becomes negative $p_v \dot{\varepsilon}_v < 0$, which we also simplify to $p_v(\dot{\varepsilon}_v < 0) = 0$, i.e., no plastic events for de-compression. Cast into one formula, as implemented in the numerical solutions, this reads: $\min(1, \max(0, p_v))\max(0, \dot{\varepsilon}_v)$.

4.1.2 Athermal deviatoric (pure shear) loading

Another special case that allows for analytical treatment is pure *deviatoric (isochoric) shear*, $\dot{\varepsilon}_v = 0$, the elastic strains develop as $\partial_t \Delta = \alpha_1 \varepsilon^{e*}_{ij}\dot{\varepsilon}^*_{ij}(1 - p_s)$ and $\partial_t \varepsilon^{e*}_{ij} = \dot{\varepsilon}^*_{ij}(1 - p_s)$ or, equivalently, for the plastic strain rate $\dot{\varepsilon}^p_{ij} = \dot{\varepsilon}^*_{ij} - \partial_t \varepsilon^{e*}_{ij} = \dot{\varepsilon}^*_{ij} p_s \sim v_s p_s$.

Postulating the existence of a constant "critical" steady state for the macroscopic friction, i.e., the quasi static limit stress ratio, $\mu^c_0 := \mu^c(v_s \to 0) = \mathcal{G}^c_\Delta u^c_s/(\mathcal{B}^c_\Delta \Delta^c)$ [26], [27], this allows to express the probability for plastic (shear) events as:

$$p_s = \frac{\mu}{\mu^c_0}\left[\varepsilon^{\hat{e}*}_{ij}\hat{\dot{\varepsilon}}^*_{ij}\right]_+ := \frac{1}{\mu^c_0}\frac{\mathcal{G}_\Delta}{\mathcal{B}_\Delta}\frac{\left[\varepsilon^{e*}_{ij}\dot{\varepsilon}^*_{ij}\right]_+}{\Delta v_s} \approx \frac{u_s}{u^c_s} , \qquad (83)$$

for $\Delta > 0$, and $p_s = 1$ otherwise, where the hats denote unit-tensors, the ratio of the tangent moduli depends on the constitutive choice of the energy density, and the last approximation is only valid after sufficiently long steady shear, close to the critical state, and/or if $\Delta \approx \Delta^c$ vanishes from Eq. (83), but not for strain reversal. The term in brackets limits $p_s \geq 0$, as to keep it positive, i.e., $[x > 0]_+ = x$, and $[x \leq 0]_+ = 0$, and

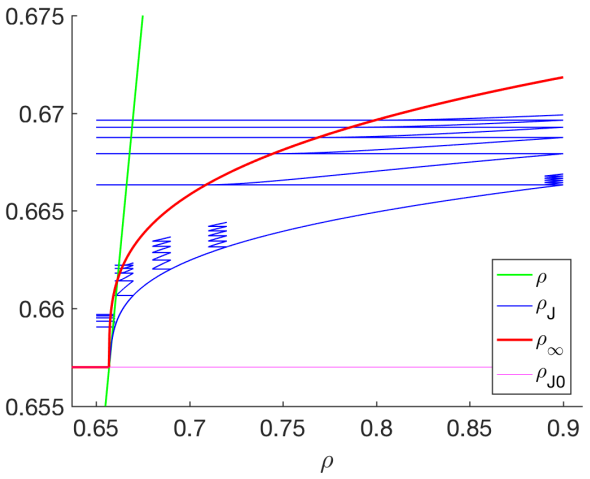

Fig. 4 Jamming density $\rho_J = \rho\exp(-\Delta)$, plotted against density, ρ, during loading up to $\rho_{max} = 0.66, 0.67, 0.69, 0.72$ and 0.90, with subsequent un-/re-loading cycles with amplitude, $\delta\rho = 0.01$. The cycles on top correspond very much to the case $\rho_{max} = 0.90$ and $\delta\rho = 0.25$ displayed in Fig. 2a in Ref. [46]. The solid red line represents ρ_∞ in Eq. (80), with $\rho_{J0} = 0.657$, and coefficients $b_\infty = 0.02$, $\beta_\infty = 0.30$. Note the flat blue lines for un-loading and for $\rho_J < \rho_\infty$, i.e., cases where one has $p_v = 0$ for unloading and in unjammed situations. (The jamming density can be deduced from simulations using Eq. (104), see Sec. 6.)

[25] Thus, while $\rho_{J0} \sim \rho_{\ell p}$, corresponds to random loose packing, $\rho_\infty \sim \rho_{cp}$ takes the place of random close packing, ρ_{cp}, continuously grows with density. The higher densities could be achieved by over-compression of soft particles (rubber, gel, etc.), whereas hard particles (metal, glass, etc.) would break (not considered here). For hard/rigid particles, one could replace Eq. (80) with a step function equal to ρ_{cp} for $\Delta > 0$.

[26] For the Hertzian energy density, see Eq. (53), using $\mu := \pi^*_\Delta/P_\Delta$, the ratio of moduli, $\mathcal{G}_\Delta/\mathcal{B}_\Delta = 2G/[B + (1/2)G(u_s/\Delta)^2]$, implies a relation, $\mathcal{G}^c_\Delta/\mathcal{B}^c_\Delta = \mu^c_0\Delta^c/u^c_s = 2G/[B + (1/2)G(u^c_s/\Delta^c)^2] = 4/[g_e^2 + (u^c_s/\Delta^c)^2]$, between shear and bulk modulus, and allows to determine from the quadratic equation: $\mu^c_0(u^c_s/\Delta^c)^2 - 4u^c_s/\Delta^c + \mu^c_0 g_e^2 = 0$ the shear to isotropic elastic strain ratio $u^c_s/\Delta^c = 2/\mu^c_0 \pm \sqrt{(2/\mu^c_0)^2 - g_e^2}$, with real solutions for $\mu^c_0 \leq 2/g_e$, as realized in cases modelled here (data not shown).

[27] For the granular energy density, see Eq. (55), the ratio of tangent moduli and the solution for μ^c_0 are not spelled out here, for the sake of brevity.

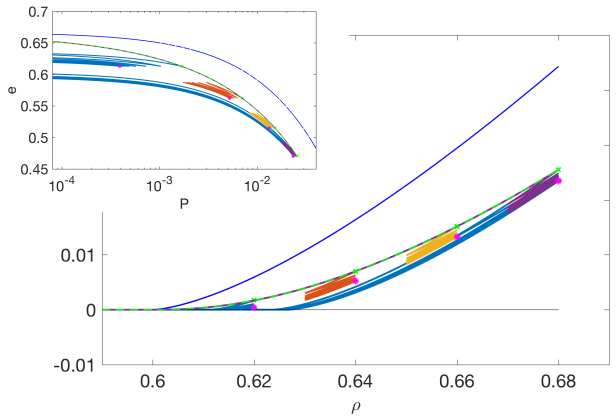

Fig. 5 Pressure plotted against density, ρ, similar as in Fig. 4, but with $\rho_{J0} = 0.60$, during loading up to $\rho_{max} = 0.62$, 0.64, 0.66, and 0.68, with subsequent un-/re-loading cycles with amplitude, $\delta\rho = 0.01$. The horizontal blue lines on top correspond to $\rho_{max} = 0.68$ and $\delta\rho = 0.08$. The dashed green curve represents the initial loading, up to ρ_{max} (green dots), with six un-/re-loading cycles, ending at the magenta dots. Note that the lowest $\rho_{max} = 0.62$ is un-jamming and re-jamming during the cycles. The upper (blue) curve represents the elastic limit case, with $p_v = 0$, i.e., without plastic rearrangements and the analytical pressure state-line: $P_\Delta = B\Delta^{3/2}$, with $B = 1$. The lowermost curves represent cyclic un-/re-loading from $\rho_{max} = 0.68$ with large amplitude, $\delta\rho = 0.08$, down to $\rho_{min} = 0.60$, well below the jamming-point, un-jamming and re-jamming during every cycle. The inset represents the void fraction, e, plotted against (logarithmic) pressure, P, similar to Fig. 2a.

thus valid also for strain-reversal and during early transients, for which negative argument values result in perfectly elastic response, $p_s = 0$, as done similarly in Refs. [46,157,120] and references therein – based on, and in agreement with, DEM simulations [28]. The probability for plastic events in Eq. (79), specified above in Eq. (83), can be very small at the beginning of shear, but increases due to the build-up of elastic shear strain, u_s, before it asymptotically approaches $p_s = 1$ for large strain in the perfectly plastic, critical state. At reversal of shear, the argument of the bracket-function becomes negative, i.e., the system is elastic with $p_s = 0$, until the shear strain adjusts to the new direction [29].

In cases where density and thus Δ is reduced in magnitude after the system has reached the critical state (not studied here), also $u_s^c \propto \Delta^c$ will reduce, and the term $1 - p_s = 0$, can become negative, resulting in the decay of u_s, however, this is skipped here for the sake of brevity.

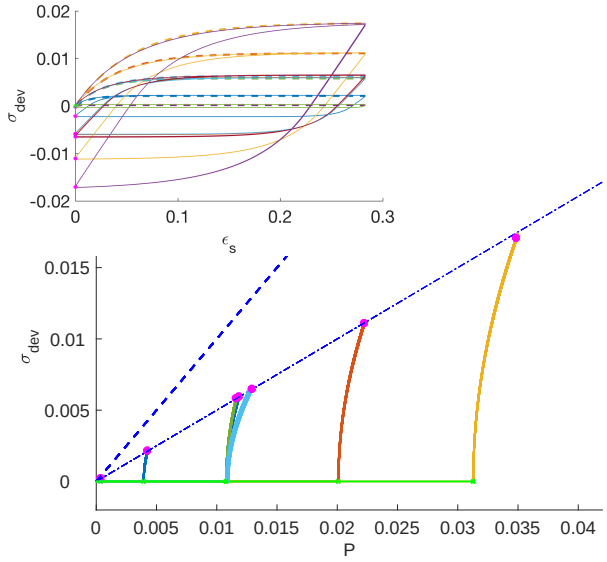

Fig. 6 Shear stress, $\sigma_{\rm dev} := \pi_s = |\pi^*_{ij}|$ (units are specified in section 5 and a comparison to particle simulations is presented in section 6), plotted against pressure, P, from athermal solutions to cases compressed up to $\rho_{max} = 0.61$, 0.63, 0.65, 0.67, and 0.69 (green dots), and subsequent cyclic pure shear with amplitude, $\delta\gamma \sim 0.28$, where the magenta dots represent the end-situation after six forward-backward shear cycles. The dashed line indicates the pre-set slope $\mu_0^c = \sigma^c_{\rm dev}/P^c = 0.5$. The only other parameter active in this model is $\alpha_1 = 2$, where the case $\rho_{max} = 0.65$ was simulated with two other values of $\alpha_1 = 0.5$ and 8, to display the enhancing effect on pressure-dilatancy of this parameter. Note that the imposed macroscopic friction, here $\mu_0^c = 0.5$ (dash-dotted blue line), is chosen smaller than the elastic stability limit, $2/g_e = 1$ (dashed blue line), such that the latter is never reached. The inset represents the shear stress evolution with strain, during the cyclic forward-backward shearing, where the higher density cases reach larger stress levels; the thick dashed lines represent the analytical solutions from Eq. (84) during initial shear from the isotropic states.

Analytical treatment is possible close to steady state, for $\Delta \approx \Delta^c$ assumed constant, where the deviatoric elastic strain evolves as: $\partial_t u_s = v_s(1 - p_s) \approx v_s(1 - u_s/u_s^c)$, with analytical solution:

$$u_s(t) = u_s^c - [u_s^c - u_s(0)]\exp(-v_s t/u_s^c) \ , \qquad (84)$$

and critical state elastic shear strain:

$$u_s^c = \Delta^c \left[2/\mu_0^c - \sqrt{(2/\mu_0^c)^2 - g_e^2}\right] \ ,$$

as plotted in the inset of Fig. 6 as dashed lines, for the initial shear stress evolution $\sigma_{\rm dev} = \pi_s^* = 2G\Delta^{1/2}u_s$. This analytical solution is very similar to the solutions

[28] If one can assume: $\Delta \approx \Delta^c$, i.e., that the isotropic elastic strain is almost constant, close to its critical state limit already, Eq. (79) can be solved analytically, yielding an exponential approach of u_s to its critical state limit, see Ref. [46].

[29] Like for p_v, this could be merged into the relaxation term $-\lambda T_g^* u_{ij}^*$, if one would assume: $-v_{ij}^* p_s = -\lambda T_e u_{ij}^*$, the discussion of which goes far beyond this paper.

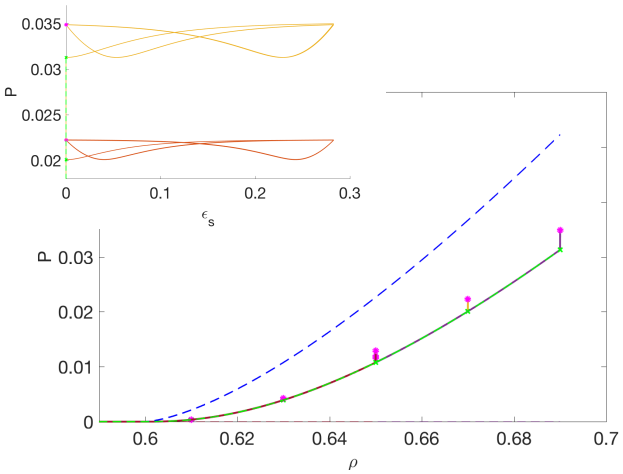

Fig. 7 Pressure plotted against density, from the same model solution as in Fig. 6. The lower curve represents the initial loading, up to ρ_{max} (green dots), with six cyclic forward-backward shear cycles, ending at the magenta dots, displaying the pressure-dilatancy caused by isochoric shear. The upper (dashed blue) curve represents the elastic limit compression, with $p_v = 0$. The inset displays the pressure during the shear cycles for the largest two densities.

presented in Refs. [120,46,157], however, further discussion is beyond the scope of this paper [30].

What remains is to also consider the variation/evolution of Δ during pure (volume conserving) shear, due to variations in the jamming density. Noting the similarity between p_s and the α_1-term in Eq. (78), in order to solve the problem analytically, one can rewrite the evolution equation for the isotropic elastic strain as: $\partial_t \Delta = \alpha_1 u_s v_s (1-p_s) \approx \alpha_1 u_s^c v_s p_s (1-p_s) \approx \alpha_1 u_s^c p_s \partial_t u_s \approx \alpha_1 u_s \partial_t u_s$, for constant v_s (not valid for strain-reversal). This equation has a critical state solution, $\Delta = \Delta^c$, due to the term $(1-p_s) \approx 0$, as well as a stable elastic solution with $\partial_t \Delta \approx 0$ for $p_s \propto u_s \approx 0$, in an initial isotropic state, see the infinite slopes in Fig. 6, for small shear strain and thus small shear stress. Due to the quadratic proportionality to u_s, the variation in Δ is much smaller than the variation in u_s itself – at least as long as $u_s/\Delta < 1$. During shear starting from an isotropic state, the variation in Δ is strictly positive, in the athermal limit, correspinding to dilatancy, i.e., the jamming density decreases, while at shear strain-reversal the evolution is opposite, changing sign during evolution, allowing for "butterfly-shape" loading-unloading cycles of Δ or P_Δ, see the inset in Fig. 7, as consistent with particle simulations [120]. Note that the above assumptions are reasonable well above jamming, $\Delta > 0$, but not close to jamming, where the un-jamming can happen during every branch of the cycles, as shown in Ref. [46].

[30] Note that since u_s^c depends (weakly) on Δ, the system of equations is still coupled and the analytical solution is only approximate.

4.2 The granular thermal limit $\dot{T}_g = 0$

Assume that one could maintain a constant granular temperature steady state, e.g., by homogeneous driving/tapping, see Refs. [162], which would result in the set of equations:

$$\partial_t \Delta = \dot{\varepsilon}_v (1-p_v) - \lambda_1 T_g \Delta p_g + \alpha_1 \varepsilon_{ij}^{e*} \dot{\varepsilon}_{ij}^* (1-p_s) \quad (85)$$

$$\partial_t \varepsilon_{ij}^{e*} = \dot{\varepsilon}_{ij}^* (1-p_s) - \lambda T_g \varepsilon_{ij}^{e*} + \alpha_d \ . \quad (86)$$

For vanishing strain rate $\dot{\varepsilon}_{ij} = 0$, the equations decouple and only the relaxation terms survive, This corresponds to the "plastic equilibrium" limit case $\Delta = 0$, $\varepsilon_{ij}^{e*} = 0$, which is approached exponentially fast, with rates $\lambda_1 T_g$ and λT_g. The term $p_g = 1$ allows to choose the plastic equilibrium of transiently elastic systems, for which $\Delta \to 0$, or is needed in a form $p_g = 1 - \Delta_\infty/\Delta$, or $p_g = 1 - p_v$, so that a granular type plastic limit with $\Delta > 0$ can be achieved, see subsection 4.7.

For finite $\dot{\varepsilon}_{ij}$, the system will establish thermal, elasto-plastic dynamic states that are not discussed further for the sake of brevity.

Strictly controlling density, i.e., fixing e, the situation is interesting again for granular matter. Any perturbation, as tapping or small-amplitude cyclic shear, will typically result in a decrease of both the elastic strain, Δ, and consequently the pressure, $P_\Delta = \mathcal{B}_\Delta \Delta$, with elastic bulk-modulus $\mathcal{B}_\Delta \propto B\Delta^{1/2} + \dots$. In this situation, the pressure curve shifts to smaller densities (larger e), and changes slope, both moving it away further from the elastic state-line, like shown in Fig. 5 (which represents a zoom into the previous Fig. 4, but with different parameter $\rho_{J0} = 0.60$, which would more resemble frictional granular material. On the other hand, large strain shear results in (pressure) dilatancy, shifting the state-line to higher densities (or the void fraction to the right, towards the VCL, but not beyond), defining the critical state line (CS) – see magenta points in Fig. 7. The amplitude of pressure dilatancy increases with density (pressure), and so does the characteristic shear strain at which the system transits into a new state.

4.3 Isotropic jamming/un-jamming in minimal GSH

The model equations for isotropic compression/tension, with strain rates $\partial_t \rho = \dot{\varepsilon}_v \neq 0$, and $\dot{\varepsilon}_{ij}^* = 0$, reduce to:

$$\partial_t \Delta = \dot{\varepsilon}_v (1-p_v) - \lambda_1 T_g \Delta \quad (87)$$

$$\partial_t \varepsilon_{ij}^{e*} = -\lambda T_g \varepsilon_{ij}^{e*} + \alpha_d \quad (88)$$

$$\partial_t T_g = -R_T T_g^2 (T_g^*/T_g) + f_T(\dot{\varepsilon}_{ij}) + f_g(g_*) \quad (89)$$

The density is coupled to strain rate directly, while the second equation (88) is decoupled (for $\alpha_d = 0$) just relaxing an existing elastic shear strain to zero.
TODO: *I dont know where this came from - remove it for submission:* From the coupled evolution equations (87) and (89) for Δ and T_g, we observe that the situation at the end of an isotropic compression is independent of the density reached if $p_v = 0$. The coupled evolution equations (87) and (89) could be (quantitatively) calibrated to particle simulations like in Ref. [46], in a future study, however, in Sec. 6 they are calibrated to the athermal case, that isolates the evolution of Δ, as is relevant also for extremely small compression rates, $\dot{\varepsilon}_v$, and thus $T_g \approx 0$, if $p_v \neq 0$. For finite positive (compressive) strain rate, the inhomogeneous solution leads to a divergent increase of T_g with time due to the continuous energy input. The energy production term due to elastic instability in Eq. (89) would become active for finite u_s, when $\Delta < g_e u_s$, but is ignored here, assuming $u_s = 0$ (which is not strictly true in real systems, where there can be some small, local, random elastic deviatoric strain).

For finite positive (compressive) strain rate, one has a continuous energy input due to the viscous source term f_T, that can lead to increase or decrease of T_g, and thus affects also the evolution of Δ. For negative (expansive) strain rate, the same is true, however, as soon as the system approaches un-jamming, the behavior qualitatively changes due to $T_e \to 0$, which is qualitatively, not quantitatively accounted for in the present version with constant parameters, in particular f_v and R_{T0}; more details are beyond the scope of this study.

4.4 Homogeneous cooling below and above jamming

In the absence of any strainrate mode, or other means of energy input [162], and assuming that T_g is so small that Δ is practically constant, the evolution equation for T_g, abbreviating $\gamma = R_T = R_{T0}(1-r^2)$, and assuming $T_e = 0$, results in an algebraic evolution:

$$\frac{T_g}{T_g^0} = \frac{1}{1 + R_T T_g^0 t} \ , \tag{90}$$

in the free, homogeneous cooling state, as relevant for systems below jamming in the granular gas state [31]. On the other hand, assuming the simplest model for $T_g^* \approx T_e$, with $h = 0$ (or for constant Δ), for a small perturbation from an elastic base state, one has

$$\frac{T_g}{T_g^0} = \exp\left(-R_T T_e t\right) \ , \tag{91}$$

[31] Remember that the granular temperature in the standard kinetic theory literature is $T_G \propto T_g^2$, but we do not consider all those details here and rather refer to the relevant literature, e.g., Refs. [7,8,110,111] and references therein.

as relevant for elastically stable systems, well above the jamming density, for which small perturbations decay exponentially fast.

4.5 Pure shear transients from an isotropic state

This case was studied in detail by particle simulations in Refs. [120,46], and should be studied analytically too with respect to questions about the build-up of anisotropy, and the degradation of the (shear) modulus, but is skipped for the sake of brevity.

4.6 Steady state pure shear (model 0 and e)

In case of deviatoric pure shear, the density equation vanishes, since $v_{ll} = 0$ the density is conserved, $\partial_t \rho = 0$, and the terms with isotropic strain rate in the equations drop out. The remaining equations yield the steady state solution for the granular temperature:

$$\partial_t T_g = 0 = R_{T0}\left[-(1-r^2) T_g T_g^* + f_s^2 \dot{\varepsilon}_{ij}^* \dot{\varepsilon}_{ij}^*\right]$$

with $T_g^* = T_e + T_g$, so that (for $T_e = 0$):

$$(T_{g0}^{(ss)})^2 = \frac{f_s^2 (\dot{\varepsilon}_{ij}^* \dot{\varepsilon}_{ij}^*)}{(1-r^2)} = \frac{f_s^2 v_s^2}{(1-r^2)} \ , \tag{92}$$

or (for $T_g^* = T_g + T_e$):

$$(T_g^{(ss)})^2 + T_g^{(ss)} T_e - (T_{g0}^{(ss)})^2 = 0 \ ,$$

yields

$$T_g^{(ss)} = \pm\sqrt{(T_e/2)^2 + (T_{g0}^{(ss)})^2} - T_e/2 \ , \tag{93}$$

where only the positive solution is reasonable.

In the "collisional" limit $T_g \gg T_e$, one has the dynamic steady state: $T_g^{(ss)} \approx T_{g0}^{(ss)} \propto v_s$, while for $T_g \ll T_e$, the steady state temperature in the "elastic" steady state is: $T_{ge}^{(ss)} \approx (T_{g0}^{(ss)})^2 / T_e \propto v_s^2$, i.e., it vanishes quadratically for $v_s \to 0$.

For the deviatoric elastic strain one has:

$$\partial_t \varepsilon_{ij}^{e*} = 0 = \dot{\varepsilon}_{ij}^* - \lambda T_g \varepsilon_{ij}^{e*} \ ,$$

so that:

$$u_s^{(ss)} = v_s/(\lambda T_g^{(ss)}) \text{ and } u_{s0}^{(ss)} = \sqrt{1-r^2}/(\lambda f_s) \ , \tag{94}$$

while for the isotropic elastic strain one has:

$$\partial_t \Delta = 0 = -\lambda_1 T_g \Delta + \alpha_1 \varepsilon_{ij}^{e*} \dot{\varepsilon}_{ij}^* \ ,$$

so that inserting Eqs. (92) and (94) yields the isotropic elastic strain in steady state:

$$\Delta^{(ss)} = \frac{\alpha_1 v_s^2}{\lambda_1 \lambda (T_g^{(ss)})^2} \text{ and } \Delta_0^{(ss)} = \frac{\alpha_1 (1-r^2)}{\lambda_1 \lambda f_s^2} \ , \tag{95}$$

the former valid for model e, the latter for the simplest model 0, where the subscript 0 indicates $T_e = 0$; model e is not indicated since it represents the default case.

In the "elastic" limit $T_g \ll T_e$, for $v_s \to 0$, the other two state variables, in model 0, behave as: $u_s^{(ss)} \to v_s^{-1}$, $\Delta^{(ss)} \to v_s^{-2}$, and thus $g^{(ss)} = u_s/\Delta \to v_s$, i.e., a leading order linear increase with (shear) strain rate.

4.7 Steady state pure shear (model 1)

In model 1, only the evolution equation of the isotropic elastic strain has to be modified:

$$\frac{d}{dt}\Delta = 0 = -\lambda_1 T_g \Delta p_g + \alpha_1 u_{ij}^* v_{ij}^*$$

so that inserting Eqs. (92) and (94) yields the isotropic elastic strain in steady state:

$$\Delta_1^{(ss)} = \frac{\alpha_1 v_s^2}{\lambda\lambda_1 (T_g^{(ss)})^2 p_g} = \frac{\Delta^{(ss)}}{p_g} \ , \tag{96}$$

for model 1 for constant or Δ-indepdendent p_g.
In some of the numerical implementations, we used $p_g = \Delta - \Delta_\infty$, in order to make Δ relax towards a finite value, with $\Delta_\infty = \log(\rho_\infty/\rho)$, as defined in Eq. (80). This allows to re-write $p_g = \log(\rho_J/\rho_\infty)$, which makes the relaxation term vanish for $\rho_J = \rho_\infty$, negative for larger values and increasingly positive for smaller jamming densities. Unfortunately, it also requires to solve a quadratic equation, resulting in

$$\Delta^{(ss)} = (1/2)\Delta_\infty[1 + \sqrt{1 + 4\Delta^{(ss)}/\Delta_\infty}] \ ,$$

i.e., an increased steady state elastic strain, representing strain-dilatancy. Note that this approach to achieve finite Δ under steady state shear, increasing with density – as to be expected – is different in philosophy than making the bulk modulus factor B density dependent.
In other of the numerical implementations, we used $p_g = 1 - \Delta_\infty/\Delta$, in order to make Δ relax towards a finite value, resulting in the simpler steady state expression:

$$\Delta_1^{(ss)} = \Delta^{(ss)} - \Delta_\infty = \log(\rho_\infty/\rho_J^{(ss)}) \ ,$$

with $\Delta_\infty < 0$ for $\rho > \rho_\infty$, which even can change sign dependent on the relative magnitudes of $\Delta^{(ss)}$ and Δ_∞. Note that this approach to achieve finite Δ under steady state shear, increasing with density – as to be expected – is different in philosophy than making the bulk modulus factor B density dependent.

4.8 Discussion of the steady state

Dividing Eq. (94) by (95) yields the deviatoric to elastic strain ratio in steady state (in order to evaluate whether the system is elastically stable or not):

$$g^{(ss)} := \frac{u_s^{(ss)}}{\Delta^{(ss)}} = \frac{\lambda_1 T_g^{(ss)}}{\alpha_1 v_s} \ . \tag{97}$$

If the ratio of elastic strains in Eq. (97) is smaller than the elastic stability limit $g^{(ss)} \leq g_e = \sqrt{2B/G}$ the system remains in a possibly stable (elastic, jammed) state, while it looses stability if the ratio reaches and/or exceeds the limit value.

Solving numerically the system of equations, including the transient evolution, confirms that the steady state is independent of the density, for model 0, see Sec. 5, as ρ does not appear in the steady state solutions above.

The elastic strain ratio, Eq. (97), which determines whether the system becomes elastically instable in steady state, is not the same as the macroscopic friction at which the material flows plastically. Dividing the steady state shear stress by pressure defines the macroscopic (bulk) "friction": $\mu = \sigma_{ij}^*/P$, which results in the steady state bulk friction:

$$\mu^{(ss)} = \frac{\sigma_{ij}^*}{P} = \frac{\pi_{ij}^{*\,(ss)} + \eta v_{ij}^*}{P_\Delta + P_T} = \frac{\mathcal{G}_\Delta u_{ij}^{(ss)} + \eta v_{ij}^*}{\mathcal{B}_\Delta \Delta^{(ss)} + P_T} \ . \tag{98}$$

In the slow strain rate limit, $\dot{\varepsilon}_{ij} \to 0$, of Eq. (98), above jamming, $\Delta > 0$, the second terms in nominator and denominator vanish, linearly and quadratically with $T_g \to 0$, respectively, and one has

$$\begin{aligned} \mu_0^{(ss)} &= \frac{\mathcal{G}_\Delta u_s^{(ss)}}{\mathcal{B}_\Delta \Delta^{(ss)}} \\ &= \frac{2(G/B)(\Delta^{(ss)})^{-1} u_s^{(ss)}}{1 + (1/2)(G/B)(u_s^{(ss)})^2 (\Delta^{(ss)})^{-2}} \\ &= \frac{4(G/2B) g^{(ss)}}{1 + (G/2B)(g^{(ss)})^2} = \frac{4g^{(ss)}}{g_e^2 + (g^{(ss)})^2} \ . \end{aligned} \tag{99}$$

For the special case $g^{(ss)} = g_e$, when the elastic limit of stability and the steady state ratio of elastic strains coincide, this translates to: $\mu_0^{(ss)} = 2/g_e$.

4.9 Temperature unjamming regularization (model g)

In order to regularize the elastic unjamming instability, we introduce a measure for the distance from the elastic limit $g_s = (g - g_e) = (u_s/\Delta - \sqrt{2B/G})$, which influences the temperature evolution

$$\frac{d}{dt} T_g = R_T \left[-T_g^2\right] + f_T(\dot{\varepsilon}_{ij}) + f_g(g_*) \ , \tag{100}$$

with $f_g(g_*) = f_g\theta(g_s)g_s$, and the step-function $\theta(g_s > 0) = 1$, and 0 else, so that one has for steady-state pure shear (with model 0):

$$(T_g^{(ss)})^2 = \frac{f_s^2 v_s^2 + f_g\theta(g_s)g_s}{(1-r^2)} \ , \qquad (101)$$

i.e., just an elevated granular temperature that affects, in turn, the other state-variables (elastic strains) via their respective relaxation terms, as will be shown in the next section 5.

5 Numerical solutions of GSH

In order to better understand GSH, including transients and transitions, and to validate the analytical solutions in the previous section 4, we solve the system of equations numerically (with matlab, using ode45) and – focusing on a few terms only – discuss the features of the simplest GSH type model with mostly constant coefficients, see table 1, and the energy density from Eqs. (53). Symbols with a prime are dimensional, whereas all presented results are dimensionless (without prime), as explained next.

Units are indicated by subscript-u and are here chosen as particle diameter, e.g., $x_u' = d_p' = 10^{-3}$m, and density, $\rho_u' = \rho_p' = m_p'/V_p' = 2000\,\mathrm{kg\,m^{-3}}$, with volume, V_p', of a single particle, so that its mass is: $m_p' = \rho_p' V_p' = (\pi/6)\rho_p'(d_p')^3 = (\pi/6)m_u' \approx 10^{-6}\,\mathrm{kg}$, with unit of mass: $m_u' = \rho_u'(x_u')^3 = 2\times10^{-6}\,\mathrm{kg}$. When the final unit is chosen as stress, $\sigma_u' = 1\,\mathrm{MPa}$ (or $10\,\mathrm{kPa}$), this results in the unit of time being: $t_u' = (m_u'/x_u'/\sigma_u')^{1/2} \approx 50\times10^{-6}\,\mathrm{s} = 50\,\mu\mathrm{s}$ (or $t_u' = 500\,\mu$s).

The protocol of the numerical solutions consists of three stages: The initial preparation by isotropic compression (green) is followed by the testing mode (various colors for different parameters), and finally by a relaxation phase without any strain rate (magenta). The testing mode is in the following examples pure deviatoric (volume-conserving) shear, for large strains, to approach the critical state.

5.1 Effect of elastic dissipation and unjamming

Next goal is to understand the behavior of the simplest version of the GSH model and the effects of the elastic dissipation parameter T_e and the temperature regularization, f_g, that controls the dynamics at elastic unjamming.

The initial preparation starts from an un-jammed state at $\rho(0) = 0.58$, with isotropic jamming taking place at density $\rho_{J0} = 0.60$, up to different target densities $\rho = 0.61$, 0.62, 0.63, 0.68, 0.74, and 0.80 during $t_p = 1000$. From this point on, pure shear is applied for $t_s = 5000$ and the final relaxation is applied for $t_r = 4000$.

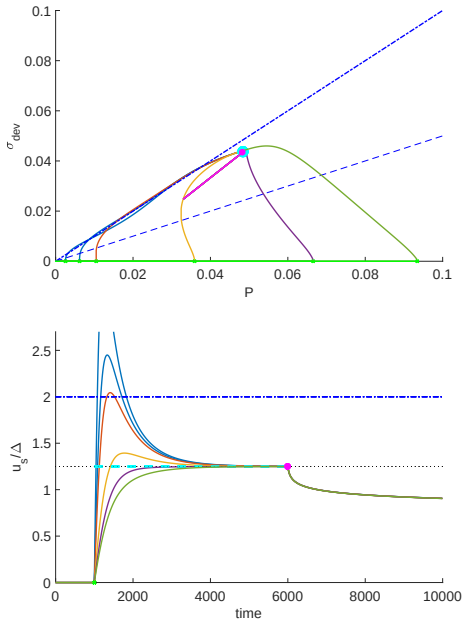

Fig. 8 Case A (model 0): Shear stress plotted against pressure (top) and deviatoric-to-isotropic elastic strain ratio plotted against time (bottom). The green lines (on the horizontal axis) represent the isotropic preparation, the magenta lines (overlapping) the final relaxation, and the big solid (cyan) dot, or dashed cyan line in the lower panel, show the theoretically predicted steady state $\sigma_{\rm dev} = \mu_0^{(ss)} p$ from Eq. (99), being density-independent for the over-simplified models. The dash-dotted (blue) lines represent the elastic stability limit g_e, while the dashed thin blue line indicates $\mu_0 = 0.5$ (not relevant here) for $T_e = 10^{-6}$.

First, the effect of T_e on the system is studied in Figs. 8 and 9, by plotting shear stress against pressure and the ratio of the deviatoric-to-isotropic elastic strains against time. Due to the density-independent parameters, in particular B, all the different density configurations approach to the same steady state, as analytically predicted (solid point in upper panel). The overshoot in the transient decreases with increasing density, before the steady state ratio of u_s/Δ is reached, and the relaxation kicks in after shear is stopped . In the former, Fig. 8, $T_e = 10^{-6}$ (case A) is practically zero and has no effect, whereas in the latter, Fig. 9, the finite T_e (case B) causes a reduced T_g in steady state, as well as a much more rapid relaxation (exponential due to T_e, instead of algebraic, like in the free cooling

	m.	T_e	f_g	B	G	λ	λ_1	α_1	R_{T0}	r	R_T	f_s	f_v	η_s	χ	g_e	$g^{(ss)}$	μ_0
A	0	10^{-6}	0	1	0.5	3	1	2	50	0.6	32	2	1	1	0.1	2	1.250	0.90
B	$0e$	2×10^{-4}	0	1	0.5	3	1	2	50	0.6	32	2	1	1	0.1	2	1.165	0.87
C	$0eg$	2×10^{-4}	4×10^{-4}	1	0.5	3	1	2	50	0.6	32	2	1	1	0.1	2	1.165	0.87
D1	0	0	0	1	0.5	3	1	...	50	0.6	32	2	1	0.1	0.1	2	...	1
D2	$0g$	0	5×10^{-5}	1	0.5	3	1	...	50	0.6	32	2	1	0.1	0.1	2	...	1
D3	$0eg$	2×10^{-4}	5×10^{-5}	1	0.5	3	1	...	50	0.6	32	2	1	0.1	0.1	2	...	1

Table 1 Summary of parameters used for the numerical solutions of GSH, in the classical version without plastic deformation probabilities, $p_v = p_s = 0$, where m. indicates the model version used, and dots replace varied values. The last three columns contain the elastic stability limit g_e, and the analytical solution to the steady state for shear to normal elastic strain and stress, respectively.

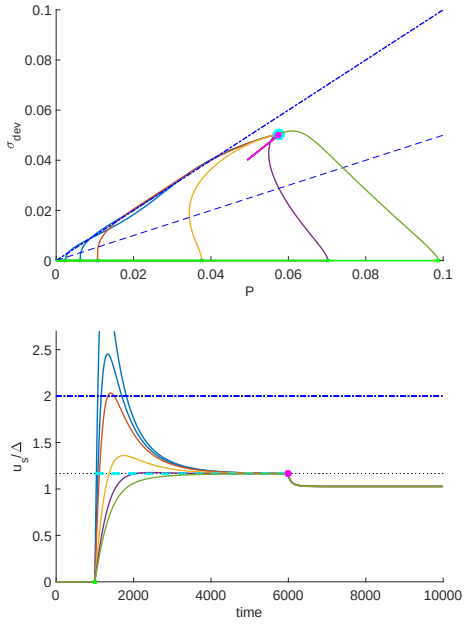

Fig. 9 Case B (model $0e$ with $T_e = 2.10^{-4}$): Same as in Fig. 8, with only difference the elastic dissipation active.

granular gas) to the static state (shorter magenta lines). Due the decreased T_g, in steady state, the other state variables Δ and u_s are increased, whereas their ratio is slightly decreased, see Eq. (97).

The effect of the new temperature production term with $f_g = 4.10^{-4}$ is then tested in Fig. 10 (case C), with otherwise the same settings as in case B. Only those cases that overshoot g_e are affected. One of them, the lowermost density case, is completely destabilized by the increase in T_g in the unstable regime, reaching a completely different steady state (far out of plot range), and returning rapidly to elastic stability as soon as the shear strain is stopped. Another case (second lowest density) remains above, but moves closer to g_e and remains there for some longer time before it reaches the analytically predicted steady state. This proofs that the production term of T_g, due to the elastic instability, allows to regularize the systems behavior by dynamic means: Counterintuitively, an increased generation of T_g can keep the system closer to the elastic instability, however, if too much T_g is produced, this destabilizes the system and allows it to explore the plastic, collisional steady state with very large T_g and – at the same time – comparatively small u_s and Δ (see the lower left corner in the upper panel and the out-of-bounds data in the lower panel).

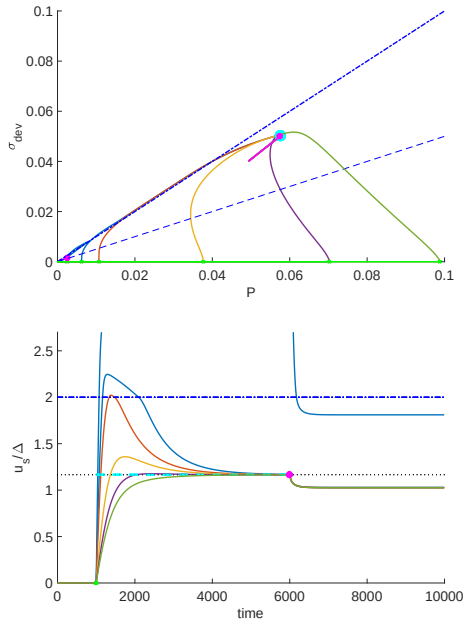

Fig. 10 Case C (model $0eg$ with $T_e = 2.10^{-4}$ and $f_g = 4.10^{-4}$): Same as in Fig. 8, with difference the elastic dissipation and the granular temperature creation both active.

5.2 Effect of dilatancy and dynamics

Next goal is to understand the behavior of the model at constant density, with different dilatancy parameters, α_1, and the effects of the elastic dissipation parameter T_e and the temperature regularization f_g.

The initial preparation starts from an un-jammed state at $\rho(0) = 0.58$, and is applied up to target density $\rho = 0.65$, during $t_p = 1000$. From this point on, pure shear is applied for $t_s = 5000$ and the final relaxation is applied for $t_r = 4000$, like before.

The values of α_1 are chosen such that a few of the data remain within the elastic instability limit $u_s/\Delta < g_e$, but a few overshoot, as can be seen in the lower panels of Figs. 11, 12, and 13.

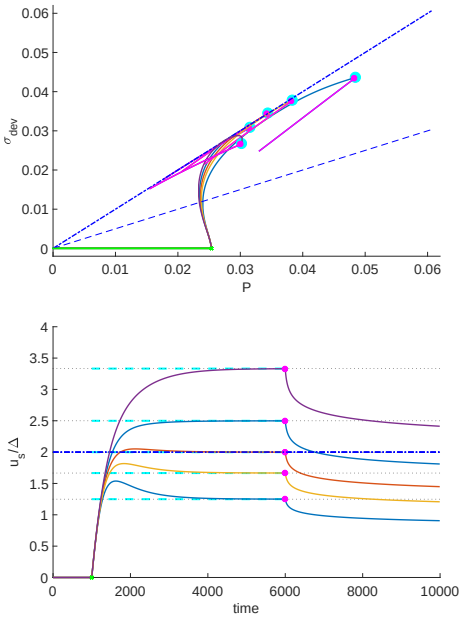

Fig. 11 Case D1 (model 0): Shear stress plotted against pressure (top) and deviatoric-to-isotropic elastic strain ratio plotted against time (bottom), for the same density, $\rho = 0.65$ for pure shear, with parameters given in table 1, in particular, for $T_e = 0$, and $f_g = 0$, for different values of $\alpha_1 = 0.75$, 1, 1.25, 1.5, 2 (from top to bottom). The green lines (on the horizontal) represent the isotropic preparation, the curves the evolution during pure shear up to the dots, representing the analytical steady state solution, $\sigma_{\rm dev} = \mu_0^{(ss)} P$, see Eq. (99), while the magenta lines show the final relaxation, starting from the dots, without shear. The slopes in the top panel correspond to $\mu_0^{(ss)} = 1$ and $\mu_c = 0.5$, to guide the eye, and the dashed horizontal lines in the lower panel represent the analytical values $g_e = 2$ (dash-dotted, blue) and various $g^{(ss)}$ (cyan and thin dots), see Eq. (97).

First, the effect of f_g on the system is studied in Figs. 11, 12, and later the effect of T_e in Fig. 13. Again, shear stress is plotted against pressure and the ratio of the deviatoric-to-isotropic elastic strains is plotted against time. In the former, Fig. 11, T_e and f_g are practically zero and have no effect at all, but an increasing dilatancy parameter, α_1 causes the system into decreasing levels of $g = u_s/\Delta$ during shear steady state (ss).

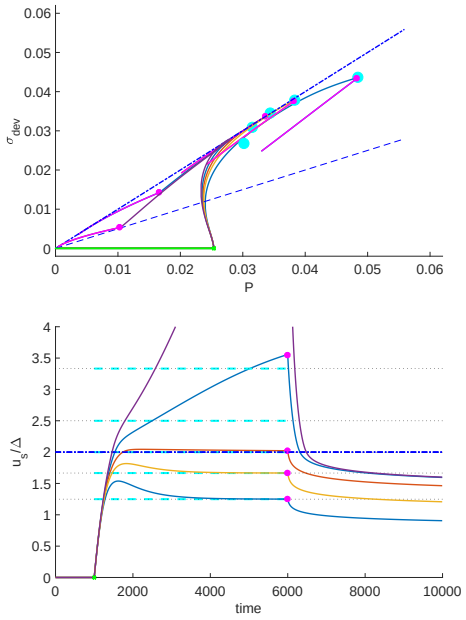

Fig. 12 Case D2 (model 0): Shear data as in Fig. 11, where all parameters are the same, except for $f_g = 5.10^{-5}$, which determines the granular temperature production in the instable regime, see Eq. (101) (not shown explicitly), which causes the different behavior of the upper curves.

The two lowermost curves remain within the elastic instability limit, the intermediate value $\alpha_1 = 1.25$ displays a slight overshoot but hits $g_e = 2$ in steady state, wheras the upper two curves are clearly beyond the elastically stable regime $g > g_e$. In the shear stress to normal stress plot, the different α_1 values lead to different steady states (thick dots) and a slow relaxation (magenta lines).

When temperature regularization is active in Fig. 12, the curves in the stable regime are not affected, the intermediate case is slightly modified and the upper two curves (smaller two α_1) are, again, considerably affected by the generation of T_g, i.e., the much larger T_g causes both elastic strains to relax towards the plastic limit – see the curves in the lower left corner of the shear to normal stress plot.

In the last Fig. 13, the finite T_e causes a reduced T_g in steady state, which results also in smaller $u_s^{(ss)}/\Delta$, see Eq. (97). During final relaxation, T_e is also causing a much more rapid (exponential) relaxation to the static state (shorter magenta lines).

Note that the elastic dissipation term, with finite T_e, is reducing granular temperature within and outside, whereas the thermal activation, f_g, increases T_g, but only outside the elastically stable regime.

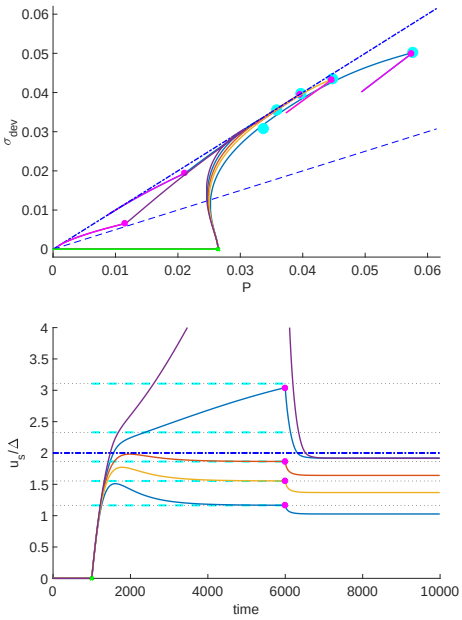

Fig. 13 Case D3 (model 0): Shear data as in Fig. 12, where all parameters are the same, except for $T_e = 2.10^{-4}$, which leads to slightly lower steady states, and a much more rapid (exponential) dissipation of energy.

6 DEM particle simulations

The particle simulations to be compared to the GSH solutions are the simplest possible element tests in a periodic cubical cell, with only diagonal components of the strain-rate active (isotropic compression/tension and pure shear). The $N = 4913$ frictionless particles ($\mu_p = 0$), with particle diameters drawn from a random homogeneous size distribution with maximum to minimum width, $d_p^{max}/d_p^{min} = 3$, are the same as used in Ref. [46], even though the simulations were re-run slower for the first compression and de-compression cycle, see Fig. 1.

6.1 Non-dimensionalization of DEM

The parameters given in the following with a prime, e.g., $\rho_p^{'} = 2000$ or $d_p^{'} = 2$, are used in the simulations shown in this paper. For working with units, there are two alternatives: Either one can read the numbers in chosen units [32] or the units are chosen based on physical properties to achieve *non-dimensional quantities*. The latter option is adopted here, i.e., the unit of length is chosen as the mean particle diameter, $x_u^{'} = \langle d_p^{'} \rangle = 2$, so that $\langle d_p \rangle = 1$ is the dimensionless diameter. The second unit is the material density, $\rho_u^{'} = \rho_p^{'} = 2000$, so that one has the dimensionless density, $\rho = \phi$, and thus the unit of mass, $m_u^{'} = \rho_u^{'}(x_u^{'})^3$, i.e., the particle mass, $m_p = (\pi/6)$. For the third unit one has several choices, where we adopt here the units of elastic stress, $\sigma_u^{'} = k_n^{'}/d_p^{'}$, with the linear normal contact stiffness, $k_n^{'} = 10^5$, which yields the dimensionless stress $\sigma = \sigma^{'} d_p^{'}/k_n^{'}$, and results in the unit of time $t_u^{'} = (m_u^{'}/k_n^{'})^{1/2} = 0.4$ [33]. In the chosen units, the dimensionless linear stiffness is $k_n = k_n^{'}(t_u^{'})^2/m_u^{'} = 1$, and the linear contact viscosity, $\gamma_n^{'} = 10^3$, becomes $\gamma_n = \gamma_n^{'} t_u^{'}/m_u^{'} = \gamma_n^{'}/[k_n^{'} t_u^{'}] = 4 \times 10^{-3}$, with background viscosity, $\gamma_b^{'} = 10^2$, or $\gamma_b = \gamma_b^{'} t_u^{'}/m_u^{'} = 4{\times}10^{-4}$.

The consequent *physically relevant properties* are the restitution coefficient $r = \exp(-\eta t_c) \approx 0.855$, with damping factor $\eta = \gamma_n/(2m_{12})$, reduced mass, $m_{12} = 0.063$, and contact duration, $t_c = \pi/\sqrt{k_n/m_{12} - \eta^2} = 0.79$, or $t_c^{'} = t_c t_u^{'} = 0.316$, all considered for a contact between the largest and the smallest particle, with the larger viscous damping time-scale, $t_v = 2m_{12}/\gamma_n \approx 5$, and the even larger background damping time-scale $t_b = 2m_{12}/\gamma_b \approx 50$. Note that this choice of units corresponds to setting $t_u^{'} \propto t_c^{'}$, which corresponds to collapsing different stiffness simulations in the elastic regime [72,113].

6.2 Calibration of GSH with DEM

The energy density has the same units as stress,

$$w_C^{'} = \frac{E_{pot}^{'}}{V^{'}} = \frac{\rho}{NV_p^{'}} \sum_{c=1}^{M} \frac{1}{2} k_n^{'} (\delta_c^{'})^2 \approx \frac{\rho C k_n^{'}}{4V_p^{'}} \langle (\delta^{'})^2 \rangle \ , \tag{102}$$

with the particle volume, $V_p^{'} = (\pi/6)\langle (d_p^{'})^3 \rangle$, and the contact number per particle $C = 2M/N$, given the total number of contacts, M. The fraction of rattlers, f_r, that relates C to the coordination number $Z = C/(1 - f_r)$, is not studied here, as it was discussed in detail in Ref. [46] and references therein.

The dimensionless energy density is thus:

$$w_C = w_C^{'} d_p^{'}/k_n^{'} = \frac{\rho C}{4V_p^{'}} d_p^{'} \langle (\delta^{'})^2 \rangle$$
$$\approx \frac{3\rho C \langle d_p \rangle}{2\pi \langle d_p^3 \rangle} \langle \delta^2 \rangle =: \frac{\rho C}{2} p_0 B_C \Delta^2 \ , \tag{103}$$

[32] Units could be, e.g., length, $x_u^{'} = 0.5 \times 10^{-3}$ m, time, $t_u^{'} = 10^{-5}$ s, and mass, $m_u^{'} = 1.25 \times 10^{-10}$ kg, to match experimental values: $\hat{d}_p = d_p^{'} x_u^{'} = 1$ mm, $\hat{\rho}_p = \rho_u^{'} \rho_p^{'} = 2000\,\mathrm{kg\,m^{-3}}$, etc., see Ref. [163], and section 5.

[33] The alternative dimensionless stress: $\sigma_\gamma = \sigma^{'}/[\rho_p^{'}(d_p^{'}\dot{\gamma}^{'})^2]$, with the unit of time set by the shear rate, $t_u^{'} = \dot{\gamma}^{'}$, is more useful for collisional shear flows, see Ref. [113], and is thus not adopted here fore the sake of brevity.

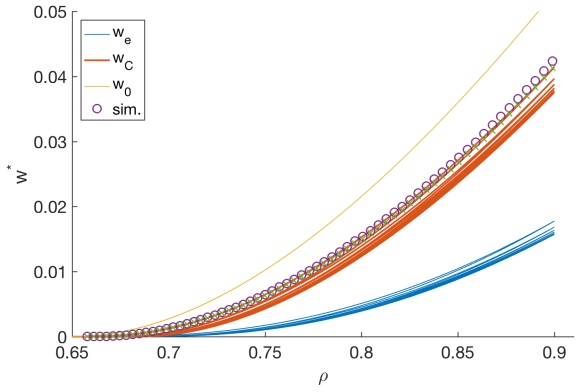

Fig. 14 Scaled energy density, $w^* = w/(p_0\rho C)$, plotted against density (volume fraction), $\rho = \phi$, for three models as introduced in sections 3.2.2 (Hertzian, w_e – thin lines) and 3.2.3, (granular, linear, w_C – thick lines), and perfectly elastic $w_0 = (1/2)B\Delta_0^2$ – light thin line – with $\Delta_0 = \log(\rho/\rho_{J0})$, with $\rho_{J0} = 0.65$ – all based on the same numerical solution of Δ, under six large-amplitude, isotropic, cyclic loading-unloading cycles, in subsection 4.1.1, and the explicit form of w inserted thereafter, while the symbols are taken from the particle simulations, scaled the same way.

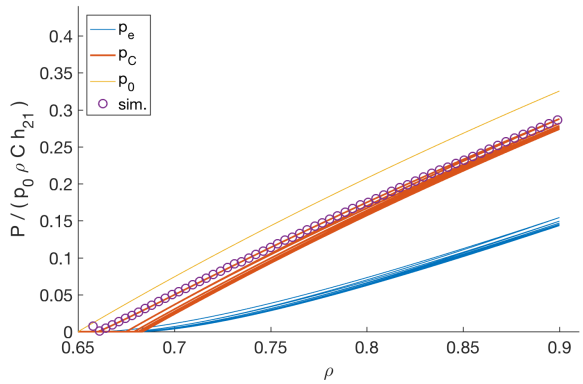

Fig. 15 Pressure scaled such that it resembles the isotropic elastic strain, $\Delta = P/(p_0\rho C h_{21})$ from the same data as in Fig. 14, where the uppermost line represents the perfectly elastic limit case, $\Delta = \log(\rho/\rho_{J0})$, with the minimal isotropic jamming density, $\rho_{J0} = 0.65$. For a zoom into the small pressure range, see Fig. 1

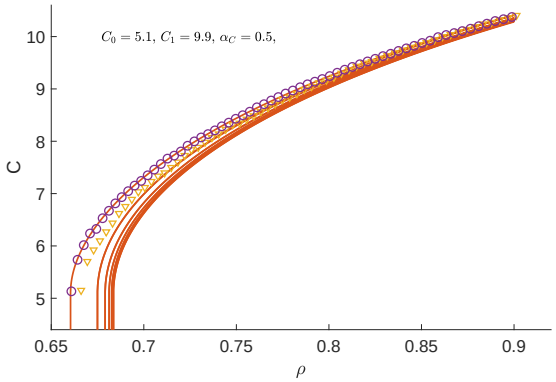

Fig. 16 Coordination number $C = C_0 + C_1\Delta^{\alpha_C}$, from the same data as in Fig. 14; circles and triangles correspond to the first loading and un-loading branch, respectively.

with all lengths non-dimensionalized by d_p', and $p_0 \approx \frac{3}{\pi}\frac{d_p d_2^2}{\langle d_p^3\rangle} \approx 0.766\, d_2^2 \approx 0.0704$, chosen such that $B_C = 1$, accounting for the third non-dimensional moment of the size distribution $\langle d_p^3\rangle \approx 1.245$ (equals unity for monodisperse particles), for more details see Refs. [30, 158,159,161,164].

From the present simulation data, one can identify (not shown) the (almost) constant ratios between overlap and elastic strain:

$$d_1 = h_{21}\langle\delta/d_p\rangle/\Delta^* = \langle\delta/d_p\rangle/\Delta \approx 0.24\,,$$

squared overlap and elastic strain:

$$d_2 = \langle(\delta/d_p)^2\rangle^{1/2}/\Delta^* \approx 0.31\,,$$

as well as overlap and squared overlap:

$$d_3 = h_1\langle\delta\rangle/(\langle\delta^2\rangle)^{1/2} \approx 0.79\,,$$

using the elastic strain deduced from the scaled, dimensionless pressure, $\Delta = \Delta^*/h_{21} = P/(p_0\rho C h_{21})$, with $p_0 = 0.0704$, and the large-overlap abbreviations $h_1 = 1-\langle\delta/d_p\rangle$ and $h_{21} = 1-\langle(\delta/d_p)^2\rangle/\langle\delta/d_p\rangle$, see Ref. [158]. This also allows to deduce the jamming density:

$$\rho_J = \rho/\exp(\Delta) \approx \rho\exp(\langle\delta/d_p\rangle/d_1)\,, \qquad (104)$$

which eventually allows to compare its evolution with the theoretical prediction, see Fig. 4.

7 Conclusion and Outlook

The focus of this paper was on yielding and unjamming/jamming of granular matter, a study inspired by the late Bob Behringer, to whom this work is dedicated. In an attempt to combine theoretical considerations with numerical/experimental observations on granular matter, the authors propose a minimalist macroscopic model to capture qualitatively all states of granular matter, and which even can be solved analytically in various special cases. Furthermore, the paper contains a review of literature on GSH as well as on particle simulation, which are compared in relation to each other and eventually used to quantitatively calibrate the GSH theoretical model with existing numerical results from a simple, frictionless, soft particle model.

The system considered was a representative volume element (RVE) of granular matter, homogeneous, i.e., without gradients and with no walls. The granular material was considered in fluid-like and solid-like states, as well as during continuous changes between these states. Particular focus was on the transition from elastically stable to instable, which is a novel contribution since the latter states can be highly dynamic, a situation that is not treatable by, e.g., standard elasto-plastic approaches or critical state theory.

Based on the rather complex, but versatile granular solid hydrodynamics (GSH), a much simplified qualitative model that includes un-jammed, gas- or fluid-like states as well as jammed solid-like states (elastically stable) was proposed and studied both analytically as well as numerically. Furthermore, various transitions and intermediate states could be identified and better understood in the framework of this simple GSH type model, which has only four state-variables, density, elastic strain (isotropic and deviatoric) and granular temperature, unifying all the states and transitions of granular matter that we could imagine. In order to keep this universal model attempt transparent, the model equations were often over-simplified by setting most parameters constant, so that the structure of the model equations rather than the consequences of additional constitutive assumptions could be tested. Analytical solutions of the model were possible for cases where either one or more state variables was fixed or set to zero, while other cases involved either purely isotropic or purely shear modes of deformation, which typically removes considerable fractions from the equations to render them solvable.

The model was generalized to include soft particle phenomenology, and even quantitative the rheology, elastic and dissipative responses, as inspired by recent soft particle simulations. Also a strictly non-thermal limit (removing the granular temperature) was considered, as well as perfectly plastic, elastic or intermediate states – possibly related to the critical state and the elastic instability, which was actually the main focus and reason to start this research. *A major open question about the size of the volume in which such instabilities occur, cannot be answered in this study, since we assumed homogeneity inside the RVE on the continuum theory level.*

Even though rather simple, the minimal universal model is capable of following the granular system from very low (dilute granular gas) to very high densities (dense jammed granular solid), including various transitions and all the transients. In order to limit complexity, the model was considered for a homogeneous (gradient-free) system that could be either seen as a RVE, or as material point of a full continuum model. *However, it is not clear which size this material element should have. From particle simulations with a few 1000 particles, it is clear (data not shown here) that the system is never really homogeneous, and that zones of plastic deformations can range from a few particles up to system spanning events. This inhomogeneity within the RVE was enclosed in the probabilities for plastic deformations that are an extension to the classical GSH.*
Considering jamming, we report a very slow, "half-hearted" transition to the jammed state, as observed in both particle simulations and GSH, where the true jamming density ϕ_J, is established above, not at the minimal possible jamming density $\phi_{J0} < \phi_J$, even in the absence of perturbations due to granular temperature, T_g, just due to the occurrence of plastic (irreversible) deformations that lead to better, more efficient packing during compression. A more detailed study of the rate dependence and thus dependence on T_g, was beyond the scope of this study.

7.1 Modes of un-jamming

Once jammed, the *first mode of isotropic un-jamming* appears trivial: decompression of the system makes the density decrease and un-jamming takes place when the elastic strain vanishes. However, the density at which un-jamming takes place is not the same as the jamming density, it rather depends on the history of the packing. Perturbations by tapping or over-compression both can result in un- and re-jamming densities considerably larger than the lowest possible, the random loose packing density. The longer/stronger the system is perturbed, the larger the jamming density will be, but the approach to this upper limit is realized very slowly, so slow that it requires very many cycles to be reached. *Whether there are well defined random loose and random close packing densities, below/above which the system cannot jam/un-jam anymore is an important open question. both limit densities are very sensible to the protocol one uses to approach and realize/measure them, especially in the absence of friction as relevant for soft, gel-like particles that resemble to many of the simulations referred to in this study.*

The *second mode of un-jamming is by plastic yielding*, which involves irreversible deformations/restructuring of the solid granular matter, but does not involve dynamics or granular temperature – at least not in the classical picture. Plastic events occur with a certain probability, see Ref. [46], which is larger the closer the system is to un-jamming or the larger the elastic

shear strain (and/or stress) is, which was previously accumulated. This mode involves the more classical world of elasto-plastic continuum mechanics and rheology for example see Refs. [165,29,4]. The evident lack of a dynamic state variable is at the origin of many difficulties with those elasto-plastic concepts, in particular when the deformation rates become larger and larger. Modern concepts like fluidity or non-local models have been proposed during the last years to overcome this problem [165,166,66,94,18,111], however, the proper account for the granular temperature in the elastic regime, and for unjamming, is still an open issue that is at least partly solved now.

The *third mode of un-jamming is a transition* occuring via an elastic instability, i.e., the loss of convexity, and then involves deformations of the solid granular matter that can occur without penalty (work), at the onset of concavity (elastic instability) or, are even activated/pushed by the external stresses (in the concave regime, or closeby). This mode is seemingly different from plastic yielding, since it allows for dynamics (granular temperature) to build up, grow, and eventually push back the system into a mechanically stable elastic state before/while it is dissipated.

How much different – if at all – plastic and elastic yielding really are has to be seen, and is subject of current ongoing research.

7.2 Outlook and open questions

Besides extending the theory to general, inhomogeneous systems with gradients, further research is also needed to:

- Generalize the present version to arbitrary tensorial form in three dimensions, involving also the so far lacking third invariant of the tensors.
- Connect quantitatively the granular gas and fluid (standard) kinetic theory with GSH.
- Determine the proper shape of the energy density for granular solids for realistic materials with friction, cohesion, polydispersity.
- Sort out if the present version of GSH without a micro-structural (fabric) tensor is sufficient or needs to be improved – is the elastic strain enough?
- Find the different mechanisms of relaxation, creation and destruction of energy in the elastic strain degrees of freedom as well as the dynamic, kinetic, granular ones.
- Identify the relaxation/evolution dynamics and the interplay of the multiple mechanisms, represented by the various different terms, of the state-variables below, above and during un-jamming/jamming?

Present research is aimed to address the remaining challenging questions: What are the differences and similarities of the driving forces/mechanisms? And, can they indeed all be combined in a single universal model as attempted in this study?

Acknowledgements We thank Sampann Arora for many GSH discussions and the first version of the simple GSH-solver, as well as Anthony Thornton, Thomas Weinhart, Itai Einav, Ken Kamrin and Felix Darve for many valuable discussions about GSH, flow, jamming and un-jamming, and Nishant Kumar, Kianoosh Taghizadeh and Vanessa Magnanimo for our collaboration and discussions on particle simulations in the context of continuum modeling.

Compliance with ethical standards

Conflict of interest: There is no conflict of interest.

References

1. J. P. Hansen and I. R. McDonald. *Theory of Simple Liquids*. Academic Press, 1986.
2. H. Di Benedetto and F. Darve. Comparison of rheological laws in rotational kinematics. *Journal de Mecanique Theorique et Appliquee*, 2(5):769, 1983.
3. R. I. Tanner. Review article: Aspects of non-colloidal suspension rheology. *Physics of Fluids*, 30:101301, 2018.
4. Alexandre Nicolas, Ezequiel E. Ferrero, Kirsten Martens, and Jean-Louis Barrat. Deformation and flow of amorphous solids: An updated review of mesoscale elastoplastic models. *Rev. Mod. Phys.*, 90(4):045006, 2018.
5. H. M. Jaeger, S. R. Nagel, and R. P. Behringer. The physics of granular materials. *Physics Today*, 49(4):32–38, 1996.
6. Heinrich M. Jaeger, Sidney R. Nagel, and Robert P. Behringer. Granular solids, liquids, and gases. *Rev. Mod. Phys.*, 68(4):1259–1273, 1996.
7. Thorsten Pöschel and Stefan Luding. *Granular gases*, volume 564. Springer Science & Business Media, 2001.
8. S. Luding. Towards dense, realistic granular media in 2D. *Nonlinearity*, 22(12):R101–R146, 2009.
9. M. Lätzel, S. Luding, H. J. Herrmann, D. W. Howell, and R. P. Behringer. Comparing simulation and experiment of a 2D granular Couette shear device. *Eur. Phys. J. E*, 11(4):325–333, 2003.
10. D. Bi, J. Zhang, B. Chakraborty, and R. P. Behringer. Jamming by shear. *Nature*, 480(7377):355–358, 2011.
11. Jie Ren, Joshua A. Dijksman, and Robert P. Behringer. Reynolds Pressure and Relaxation in a Sheared Granular System. *Phys. Rev. Lett.*, 110:18302, 2013.
12. Romain Mari, Ryohei Seto, Jeffrey F. Morris, and Morton M. Denn. Discontinuous shear thickening in brownian suspensions by dynamic simulation. *Proceedings of the National Academy of Sciences*, 112(50):15326–15330, 2015.
13. A. Singh, R. Mari, M. M. Denn, and J. F. Morris. A constitutive model for simple shear of dense frictional suspensions. *Journal of Rheology*, 62:457, 2018.

14. Dong Wang, Jie Ren, Joshua A. Dijksman, Hu Zheng, and Robert P. Behringer. Microscopic origins of shear jamming for 2d frictional grains. *Phys. Rev. Lett.*, 120(20):208004, 2019.
15. Itai Einav and Alexander M. Puzrin. Pressure-dependent elasticity and energy conservation in elastoplastic models for soils. *Journal of Geotechnical and Geoenvironmental Engineering*, 130(1):81–92, 2004.
16. R. G. Wan, M. Pinheiro, and P. J. Guo. Elastoplastic modelling of diffuse instability response of geomaterials. *Int. J. Numer. Anal. Meth. Geomech.*, 35(2):140–160, 2011.
17. M. L. Manning and A. J. Liu. Vibrational modes identify soft spots in a sheared disordered packing. *Phys. Rev. Lett.*, 107(10):108302, 2011.
18. Qiong Zhang and Ken Kamrin. Microscopic description of the granular fluidity field in nonlocal flow modeling. *Phys. Rev. Lett.*, 118:058001, 2017.
19. Alan A. Long, Dmitry V. Denisov, Peter Schall, Todd C. Hufnagel, Xiaojun Gu, Wendelin J. Wright, and Karin A. Dahmen. From critical behavior to catastrophic runaways: comparing sheared granular materials with bulk metallic glasses. *Granular Matter*, 21(4):99, 2019.
20. Julia Boschan, Stefan Luding, and Brian P. Tighe. Jamming and irreversibility. *Granular Matter*, 21(3):58, 2019.
21. Jasna Brujic, Ping Wang, Chaoming Song, David L. Johnson, Olivier Sindt, and Hernan A. Makse. Granular dynamics in compaction and stress relaxation. *Phys. Rev. Lett.*, 95(12), 2005.
22. Jasna Brujić, Chaoming Song, Ping Wang, Christopher Briscoe, Guillaume Marty, and Hernán A. Makse. Measuring the Coordination Number and Entropy of a 3D Jammed Emulsion Packing by Confocal Microscopy. *Phys. Rev. Lett.*, 98(24):248001, 2007.
23. Olukayode I. Imole, Maria Paulick, Vanessa Magnanimo, Martin Morgeneyer, Bruno E. Montes, Marco Ramaioli, Arno Kwade, and Stefan Luding. Slow stress relaxation behavior of cohesive powders. *Powder technology*, 293:82–93, 2016.
24. E. Ando, J. Dijkstra, E. Roubin, C. Dano, and E. Boller. A peek into the origin of creep in sand. *Granular Matter*, 21:11, 2019.
25. Pieter A. Vermeer. *Continuous and discontinuous modelling of cohesive-frictional materials*, volume 568. Springer Science & Business Media, 2001.
26. F. Alonso-Marroquin and H. J. Herrmann. Calculation of the incremental stress-strain relation of a polygonal packing. *Phys. Rev. E*, 66, 2002.
27. F. Alonso-Marroquin, S. Luding, H. J. Herrmann, and I. Vardoulakis. Role of anisotropy in the elastoplastic response of a polygonal packing. *Phys. Rev. E*, 71(5):051304, 2005.
28. Richard Wan and Nicot, Francois. Micromechanical Formulation of Stress Dilatancy as a Flow Rule in Plasticity of Granular Materials. *Journal of Engineering Mechanics*, 136(5):589–598, 2010.
29. Itai Einav. The unification of hypo-plastic and elastoplastic theories. *International Journal of Solids and Structures*, 49(11-12):1305–1315, 2012.
30. N. Kumar, S. Luding, and V. Magnanimo. Incremental stress and microstructural response of granular soils under undrained axisymmetric deformation. In Kenichi Soga, Krishna Kumar, Giovanna Biscontin, and Matthew Kuo, editors, *Geomechanics from Micro to Macro*, pages 115–121, Reggio Calabria (Italy), 14-18 September 2009, 2014. CRC Press/Balkema.
31. Joe D. Goddard. Continuum modeling of granular media. *Applied Mechanics Reviews*, 66(5):050801, 2014.
32. K. Kamrin and J. D. Goddard. Symmetry relations in viscoplastic drag laws. *Proc. R. Soc. A*, 470(2172):20140434, 2014.
33. J. D. Goddard and K. Kamrin. Dissipation potentials from elastic collapse. *Proc. R. Soc. A*, 475(2226):20190144, 2019.
34. F. Darve, E. Flavigny, and M. Meghachou. Yield surfaces and principle of superposition: revisit through incrementally non-linear constitutive relations. *International Journal of Plasticity*, 11(8):927–945, 1995.
35. F. Darve. Liquefaction phenomenon of granular materials and constitutive stability. *Int. J. Engineering Comput.*, 13(7):5–28, 1996.
36. N. Xu and C. S. O'Hern. Measurements of the yield stress in frictionless granular systems. *Phys. Rev. E*, 73:61303, 2006.
37. L. Sibille, F. Nicot, F. V. Donze, and F. Darve. Material instability in granular assemblies from fundamentally different models. *Int. J. Numer. Anal. Meth. Geomech.*, 31:457–481, 2007.
38. Luc Sibille, Francois Nicot, and Félix Darve. Analysis of failure occurrence from direct simulations. *European Journal of Environmental and Civil Engineering*, 13(2):187–201, 2009.
39. F. Nicot, A. Daouadji, F. Laouafa, and F. Darve. Second-order work, kinetic energy and diffuse failure in granular materials. *Granular Matter*, 13:19, 2011.
40. Waldemar Zylka. Gaussian approximation and Brownian dynamics simulations for Rouse chains with hydrodynamic interaction undergoing simple shear flow. *The Journal of Chemical Physics*, 94(6):4628–4636, 1991.
41. N. Hadda, L. Sibille, F. Nicot, and F. Darve. Failure in granular media from an energy viewpoint. *Granular Matter*, 18:50, 2016.
42. Antoine Wautier, Stéphane Bonelli, and Francois Nicot. Micro-inertia origin of instabilities in granular materials. *International Journal for Numerical and Analytical Methods in Geomechanics*, 42(9):1037–1056, 2018.
43. Silke Henkes and Bulbul Chakraborty. Statistical mechanics framework for static granular matter. *Phys. Rev. E*, 79:61301, 2009.
44. Yimin Jiang and Mario Liu. Applying GSH to a wide range of experiments in granular media. *The European Physical Journal E*, 38(3):15, 2015.
45. Yimin Jiang and Mario Liu. Why granular media are thermal, and quite normal, after all. *The European Physical Journal E*, 40(1):10, 2017.
46. Nishant Kumar and Stefan Luding. Memory of jamming-multiscale models for soft and granular matter. *Granular matter*, 18(3):1–21, 2016.
47. Kuniyasu Saitoh, Norihiro Oyama, Fumiko Ogushi, and Stefan Luding. Transition rates for slip-avalanches in soft athermal disks under quasi-static simple shear deformations. *Soft Matter*, 15:3487–3492, 2019.
48. Mehdi Pouragha, Jérôme Duriez, Antoine Wautier, Richard Wan, François Nicot, and Félix Darve. Preferential growth of force network in granular media. *Granular Matter*, 21(3):67, 2019.
49. Dapeng Bi and Bulbul Chakraborty. Rheology of granular materials: dynamics in a stress landscape. *Philosophical Transactions of the Royal Society of London A: Mathematical, Physical and Engineering Sciences*, 367(1909):5073–5090, 2009.

50. Brian Miller, Corey O'Hern, and R. P. Behringer. Stress Fluctuations for Continuously Sheared Granular Materials. *Phys. Rev. Lett.*, 77:3110–3113, 1996.
51. C. T. Veje, D. W. Howell, R. P. Behringer, S. Schöllmann, S. Luding, and H. J. Herrmann. Fluctuations and flow for granular shearing. In H. J. Herrmann, J. P. Hovi, and S. Luding, editors, *Physics of dry granular media - NATO ASI Series E 350*, page 237, Dordrecht, 1998. Kluwer Academic Publishers.
52. R. P. Behringer, Karen E. Daniels, Trushant S. Majmudar, and Matthias Sperl. Fluctuations, correlations and transitions in granular materials: statistical mechanics for a non-conventional system. *Philosophical Transactions of the Royal Society A: Mathematical, Physical and Engineering Sciences*, 366(1865), 2008.
53. M. R. Kuhn and A. Daouadij. Stress fluctuations during monotonic loading of dense three-dimensional granular materials. *Granular Matter*, 21:10, 2019.
54. Corey S. O'Hern, Andrea J. Liu, and Sidney R. Nagel. Effective temperatures in driven systems: static versus time-dependent relations. *Phys. Rev. Lett.*, 93(16), 2004.
55. Silke Henkes, Corey S. O'Hern, and Bulbul Chakraborty. Entropy and temperature of a static granular assembly: an ab initio approach. *Phys. Rev. Lett.*, 99(3):038002, 2007.
56. Ning Xu, Corey S. O'Hern, and Lou Kondic. Stabilization of nonlinear velocity profiles in athermal systems undergoing planar shear flow. *Phys. Rev. E*, 72(4):041504+, 2005.
57. M. M. Bandi, Prasenjit Das, Oleg Gendelman, H. George E. Hentschel, and Itamar Procaccia. Universal scaling laws for shear induced dilation in frictional granular media. *Granular Matter*, 21(3):40, 2019.
58. Fansheng Xiong, Philip Wang, Abram H. Clark, Thibault Bertrand, Nicholas T. Ouellette, Mark D. Shattuck, and Corey S. O'Hern. Comparison of shear and compression jammed packings of frictional disks. *Granular Matter*, 21(4):109, 2019.
59. R. P. Behringer, Dapeng Bi, B. Chakraborty, S. Henkes, and R. R. Hartley. Why do granular materials stiffen with shear rate? Test of novel stress-based statistics. *Phys. Rev. Lett.*, 101(26), 2008.
60. Bingyu Cui, Giancarlo Ruocco, and Alessio Zaccone. Theory of elastic constants of athermal amorphous solids with internal stresses. *Granular Matter*, 21(3):69, 2019.
61. Shuai Zhang and Xiaohui Cheng. Small-strain shear moduli modeling of sand: a non-equilibrium thermodynamic approach, including an application to leighton buzzard sand. *Granular Matter*, 21:68, 2019.
62. Meimei Wang, Dong Wang, Joshua E. S. Socolar, Hu Zheng, and Robert P. Behringer. Jamming by shear in a dilating granular system. *Granular Matter*, 21(4):102, 2019.
63. S. Athani and P. Rognon. Mobility in granular materials upon cyclic loading. *Granular Matter*, 20:67, 2019.
64. Pavel S. Iliev, Elena Giacomazzi, Falk K. Wittel, Miller Mendoza, Andreas Haselbacher, and Hans J. Herrmann. Behavior of confined granular beds under cyclic thermal loading. *Granular Matter*, 21(3):59, 2019.
65. Stefan Luding and Fernando Alonso-Marroqu'in. The critical-state yield stress (termination locus) of adhesive powders from a single numerical experiment. *Granul. Matter.*, 13:109–119, 2011.
66. J. Zhao and N. Guo. Unique critical state characteristics in granular media considering fabric anisotropy. *Géotechnique*, 63(8):695–704, 2013.
67. Hao Shi, Rahul Mohanty, Somik Chakravarty, Ramon Cabiscol, Martin Morgeneyer, Harald Zetzener, Jin Y. Ooi, Arno Kwade, Stefan Luding, and Vanessa Magnanimo. Effect of particle size and cohesion on powder yielding and flow. *KONA Powder and Particle Journal*, page 2018014, 2017.
68. G. D. R. MiDi. On dense granular flows. *Eur. Phys. J. E*, 14(4):341–365, 2004.
69. N. Berger, E. Azema, J.-F. Douce, and F. Radjai. Scaling behaviour of cohesive granular flows. *Europ. Phys. Lett.*, 112:64004, 2015.
70. Sudeshna Roy, Stefan Luding, and Thomas Weinhart. A general(ized) local rheology for wet granular materials. *New Journal of Physics*, 19:043014, 2017.
71. T. Weinhart, R. Hartkamp, A. R. Thornton, and S. Luding. Coarse-grained local and objective continuum description of three-dimensional granular flows down an inclined surface. *Physics of Fluids*, 25(7):070605, 2013.
72. A. Singh, V. Magnanimo, K. Saitoh, and S. Luding. Effect of cohesion on shear banding in quasistatic granular materials. *Phys. Rev. E*, 90(2):022202+, 2014.
73. T. Barker, D. Schaeffer, M. Shearer, and N. Gray. Well-posed continuum equations for granular flow with compressibility and $\mu(i)$-rheology. *Proc. R. Soc. A*, 473(2201):20160846, 2017.
74. J. D. Goddard and J. Lee. Regularization by compressibility of the $\mu(i)$ model for dense granular flow. *Physics of Fluids*, 30:073302, 2018.
75. David Schaeffer, Thomas Barker, Daisuke Tsuji, Pierre Gremaud, Michael Shearer, and JMNT Gray. Constitutive relations for compressible granular flow in the inertial regime. *J. Fluid Mech.*, 874:926–951, 2019.
76. James Baker, Francois Guillard, Benjy Marks, and Itai Einav. X-ray rheography uncovers planar granular flows despite non-planar walls. *Nature communications*, 9(1):5119, 2018.
77. M. Wiebicke, E. Ando, V. Smilauer, I. Herle, and G. Viggiani. A benchmark strategy for the experimental measurement of contact fabric. *Physics of Fluids*, 21(3):54, 2019.
78. Xiaohui Cheng, Shize Xiao, Alex Sixie Cao, and Meiying Hou. A review and analysis of granular shear experiments under low effective stress conditions. *Granular Matter*, 21(4):104, 2019.
79. J. Geng, D. Howell, E. Longhi, R. P. Behringer, G. Reydellet, L. Vanel, E. Clément, and S. Luding. Footprints in sand : The response of a granular material to local perturbations. *Phys. Rev. Lett.*, 87, 2001.
80. C. S. O'Hern, Langer, and S. R. Nagel. Force distributions near jamming and glass transitions. *Phys. Rev. Lett.*., 86:111–114, 2001.
81. K. E. Daniels and R. P. Behringer. Characterization of a freezing/melting transition in a vibrated and sheared granular medium. *J. Stat. Mech. - Theory and Experiment*, 2006, 2006.
82. T. S. Majmudar, M. Sperl, S. Luding, and R. P. Behringer. Jamming Transition in Granular Systems. *Phys. Rev. Lett.*, 98(5):058001+, 2007.
83. Stefan Luding. Granular matter: So much for the jamming point. *Nature*, 12(6):531–532, June 2016.
84. D. Vescovi, D. Berzi, and C. di Prisco. Fluid-solid transition in unsteady, homogeneous, granular shear flows. *Granular Matter*, 20:27, 2019.
85. Ryohei Seto, Abhinendra Singh, Bulbul Chakraborty, Morton M. Denn, and Jeffrey F. Morris. Shear jamming and fragility in dense suspensions. *Granular Matter*, 21(3):82, 2019.

86. S. Luding and E. S. Perdahciouglu. A Local Constitutive Model with Anisotropy for Various Homogeneous 2D Biaxial Deformation Modes. *Chemie Ingenieur Technik*, 83(5):672–688, 2011.
87. David M. Walker, Antoinette Tordesillas, Jie Ren, Joshua A. Dijksman, and Robert P. Behringer. Uncovering temporal transitions and self-organization during slow aging of dense granular media in the absence of shear bands. *Europhys. Lett.*, 107(1):18005, 2014.
88. Eduardo Rojas Parra and Ken Kamrin. Capturing transient granular rheology with extended fabric tensor relations. *Granular Matter*, 21(4):89, 2019.
89. Akhil Vijayan, Yixiang Gan, and Ratna Kumar Annabattula. Evolution of fabric in spherical granular assemblies under the inluence of various loading conditions through dem. *Granular Matter*, 22(1):34, 2020.
90. Nicolas Brodu, Joshua A. Dijksman, and Robert P. Behringer. Spanning the scales of granular materials through microscopic force imaging. *Nature communications*, 6:6361+, 2015.
91. Aghil Abed Zadeh, Jonathan Barés, Theodore A. Brzinski, Karen E. Daniels, Joshua Dijksman, Nicolas Docquier, Henry O. Everitt, Jonathan E. Kollmer, Olivier Lantsoght, Dong Wang, Marcel Workamp, Yiqiu Zhao, and Hu Zheng. Enlightening force chains: a review of photoelasticimetry in granular matter. *Granular Matter*, 21(4):83, 2019.
92. Jonathan Barés, Nicolas Brodu, Hu Zheng, and Joshua A. Dijksman. Transparent experiments: releasing data from mechanical tests on three dimensional hydrogel sphere packings. *Granular Matter*, 22(1):21, 2020.
93. Bernard Cambou, Felix Darve, and Francois Nicot. Particle methods in geomechanics. *International Journal for Numerical and Analytical Methods in Geomechanics*, 43:831–832, 2019.
94. D. L. Henann and K. Kamrin. A predictive, size-dependent continuum model for dense granular flows. *Proceedings of the National Academy of Sciences*, 110(17):6730–6735, 2013.
95. Somayeh Farhadi and Robert P. Behringer. Dynamics of sheared ellipses and circular disks: effects of particle shape. *Phys. Rev. Lett.*, 112(14):148301, 2014.
96. B. Nadler, F. Guillard, and I. Einav. Kinematic model of transient shape-induced anisotropy in dense granular flow. *Phys. Rev. Lett.*, 120(19):198003, 2018.
97. S. D. C. Walsh and A. Tordesillas. A thermomechanical approach to the development of micropolar constitutive models of granular media. *Acta mechanica*, 167(3):145–169, 2004.
98. N. P. Kruyt, O. Millet, and F. Nicot. Macroscopic strains in granular materials accounting for grain rotations. *Granul. Matter.*, pages 1–12, 2014.
99. A. Merkel and S. Luding. Enhanced micropolar model for wave propagation in ordered granular materials. *Int. J. of Solids and Structures*, 106-107:91–105, 2017.
100. Kuniyasu Saitoh, Rohit K. Shrivastava, and Stefan Luding. Rotational sound in disordered granular materials. *Phys. Rev. E*, 99(1):012906, 2019.
101. X. He, W. Wu, G. Cai, J. Qi, J. R. Kim, D. Zhang, and M. Jiang. Work-energy analysis of granular assemblies validates and calibrates a constitutive model. *Granular Matter*, 22(1):28, 2020.
102. Itai Einav and Mario Liu. Hydrodynamic derivation of the work input to fully and partially saturated soils. *Journal of the Mechanics and Physics of Solids*, 110:205–217, 2018.
103. Aaron S. Baumgarten and Ken Kamrin. A general fluid-sediment mixture model and constitutive theory validated in many flow regimes. *Journal of Fluid Mechanics*, 861:721–764, 2019.
104. Yimin Jiang and Mario Liu. Granular elasticity without the coulomb condition. *Physical Review Letters*, 91(14):144301, 2003.
105. Yimin Jiang and Mario Liu. Energetic instability unjams sand and suspension. *Physical Review Letters*, 93(14):148001, 2004.
106. Yimin Jiang and Mario Liu. From elasticity to hypoplasticity: dynamics of granular solids. *Physical Review Letters*, 99(10):105501, 2007.
107. Yimin Jiang and Mario Liu. Granular solid hydrodynamics. *Granular Matter*, 11(3):139, 2009.
108. L. D. Landau and E. M. Lifshitz. *Fluid Mechanics*. Butterworth-Heinemann, 1987.
109. J. T. Jenkins and S. B. Savage. A theory for the rapid flow of indentical, smooth, nearly elastic, spherical particles. *J. Fluid Mech.*, 130:187–202, 1983.
110. J. T. Jenkins. Dense shearing flows of inelastic discs. *Physics of fluids*, 18(10):103307, 2006.
111. D. Berzi and J. T. Jenkins. Fluidity, anisotropy, and velocity correlations in frictionless, collisional grain flows. *Phys. Rev. Fluids*, 3(9):094303, 2018.
112. Ramón Garcia-Rojo, Stefan Luding, and Javier J. Brey. Transport coefficients for dense hard-disk systems. *Physical review. E, Statistical, nonlinear, and soft matter physics*, 74(6 Pt 1), 2006.
113. Dalila Vescovi and Stefan Luding. Merging fluid and solid granular behavior. *Soft matter*, 12(41):8616–8628, 2016.
114. J. T. Jenkins and D. Berzi. Dense inclined flows of inelastic spheres: tests of an extension of kinetic theory. *Granul. Matter.*, 12, 2010.
115. L. D. Landau and E. M. Lifshitz. *Theory of Elasticity*. Butterworth-Heinemann, 1986.
116. Y. Duan and Z.-G. Feng. A new kinetic theory model of granular flows that incorporate particle stiffness. *Physics of Fluids*, 31:013301, 2019.
117. R. M. Nedderman. *Statics and kinematics of granular materials*. Cambr. Univ. Press, Cambridge, 1992.
118. Mario Liu. Thermodynamics and constitutive modeling. In Itai Einav & Eleni Gerolymatou, editor, *ALERT Doctoral School 2018: Energetical Methods in Geomechanics / Chapter 2: Thermodynamics and Constitutive Modeling,* `http://alertgeomaterials.eu/data/school/2018/2018_ALERT_school.pdf`, 2018.
119. D. Krijgsman and S. Luding. 2D cyclic pure shear of granular materials, simulations and model. In S. Luding and A. Yu, editors, *Powders Grains 2013*, pages 1226–1229, Sydney, Australia, 2013. Balkema.
120. N. Kumar, S. Luding, and V. Magnanimo. Macroscopic model with anisotropy based on micro-macro information. *Acta Mechanica*, 225(8):2319–2343, 2014.
121. D. Krijgsman and S. Luding. Simulating granular materials by energy minimization. *Comp. Part. Mech.*, 3(4):463–475, 2016.
122. J. Zhang, T. Majmudar, A. Tordesillas, and R. Behringer. Statistical properties of a 2D granular material subjected to cyclic shear. *Granul. Matter.*, 12(2):159–172, 2010.
123. Karin A. Dahmen, Yehuda Ben-Zion, and Jonathan T. Uhl. Micromechanical Model for Deformation in Solids with Universal Predictions for Stress-Strain Curves and Slip Avalanches. *Phys. Rev. Lett.*, 102:175501, 2009.

124. J. Bardeen. Critical fields and currents in superconductors. *Rev Mod Phys 34.667*, 34(4), 1962.
125. C. Liu and S. R. Nagel. Sound in a granular material: Disorder and nonlinearity. *Phys. Rev. B*, 48:15646, 1993.
126. A. S. J. Suiker, R. de Borst, and C. S. Chang. Micro-mechanical modelling of granular material. Part 1: Derivation of a second-gradient micro-polar constitutive theory. *Acta Mechanica*, 149(1), 2001.
127. E. Somfai, J. N. Roux, J. H. Snoeijer, M. van Hecke, and W. van Saarloos. Elastic wave propagation in confined granular systems. *Phys. Rev. E*, 72:21301, 2005.
128. B. P. Tighe and J. E. S. Socolar. Nonlinear elastic stress response in granular packings. *Phys. Rev. E*, 77(3):031303+, 2007.
129. X. Jia. Codalike multiple scattering of elastic waves in dense granular media. *Phys. Rev. Lett.*, 93(15):154303, Oct 2004.
130. Stefan Luding. Granular media: Information propagation. *Nature*, 435(7039):159–160, 2005.
131. Michael Mayer and Mario Liu. Propagation of elastic waves in granular solid hydrodynamics. *Physical Review E*, 82(4):042301, 2010.
132. Kianoosh Taghizadeh, Holger Steeb, Vanessa Magnanimo, and Stefan Luding. Elastic waves in particulate glass-rubber mixture: experimental and numerical investigations/studies. *EPJ Web of Conferences*, 140:12019, 2017.
133. Hongyang Cheng, Stefan Luding, Kuniyasu Saitoh, and Vanessa Magnanimo. Elastic wave propagation in dry granular media: Effects of probing characteristics and stress history. *Int. J. of Solids and Structures*, 2019. in press.
134. Lijin Wang, Andrea Ninarello, Pengfei Guan, Ludovic Berthier, Grzegorz Szamel, and Elijah Flenner. Low-frequency vibrational modes of stable glasses. *Nature Communications*, 10:26, 2019.
135. N. P. Kruyt. Three-dimensional lattice-based dispersion relations for granular materials. In J. Goddard, P. Giovine, and J. T. Jenkins, editors, *IUTAM-ISIMM Symposium on Mathematical Modeling and Physical Instances of Granular Flows*, pages 405–415, Reggio Calabria (Italy), 14-18 September 2009, 2010. AIP.
136. Rohit Kumar Shrivastava and Stefan Luding. Effect of disorder on bulk sound wave speed: a multiscale spectral analysis. *Nonlin. Processes Geophys.*, 24:435–454, 2017.
137. C. E. Maloney and A. Lematextasciicircumitre. Amorphous systems in athermal, quasistatic shear. *Phys. Rev. E*, 74:16118, 2006.
138. A. J. Liu and S. R. Nagel. Nonlinear dynamics: Jamming is not just cool any more. *Nature*, 396(6706):21–22, 1998.
139. Paul C. Martin, O. Parodi, and Peter S. Pershan. Unified hydrodynamic theory for crystals, liquid crystals, and normal fluids. *Physical Review A*, 6(6):2401, 1972.
140. H. B. Callen. *Thermodynamics and an introduction to thermostatistics*. John Wiley & Sons, 1985.
141. Peter Kostädt and Mario Liu. Three ignored densities, frame-independent thermodynamics, and broken Galilean symmetry. *Physical Review E*, 58(5):5535, 1998.
142. Oliver Müller, Mario Liu, Harald Pleiner, and Helmut R. Brand. Transient elasticity and polymeric fluids: Small-amplitude deformations. *Physical Review E*, 93(2):023113, 2016.
143. Oliver Müller, Mario Liu, Harald Pleiner, and Helmut R. Brand. Transient elasticity and the rheology of polymeric fluids with large amplitude deformations. *Physical Review E*, 93(2):023114, 2016.
144. K. Saitoh, V. Magnanimo, and S. Luding. Master equation for the probability distribution functions of overlaps between particles in two dimensional granular packings. *Soft Matter*, 11:1253–1258, 2015.
145. Mathias Tolomeo, Kuniyasu Saitoh, Combe Gaël, Stefan Luding, Vanessa Magnanimo, Vincent Richefeu, and Gioacchino Viggiani. Stochastic model for the micromechanics of jammed granular materials: experimental studies and numerical simulations. *EPJ Web of Conferences*, 140:02021, 2017.
146. D. Kolymbas. *Introduction to Hypoplasticity*. Balkema, Rotterdam, 2000.
147. Yimin Jiang and Mario Liu. Proportional paths, barodesy, and granular solid hydrodynamics. *Granular Matter*, 15(2):237–249, 2013.
148. D. P. Bi, J. Chang, B. Chakraborty, and R. P. Behringer. Jamming by shear. *Nature*, 480:355, 2011.
149. Somayeh Farhadi and Robert P. Behringer. Dynamics of sheared ellipses and circular disks: effects of particle shape. *Phys. Rev. Lett.*, 112:148301, 2014.
150. Yimin Jiang and Mario Liu. Stress- and rate-controlled granular rheology. In *AIP Conference Proceedings*, volume 1542, pages 52–59. AIP, 2013.
151. Y. Jiang and M. Liu. A brief review of granular elasticity. *The European Physical Journal E - Soft Matter*, 22(3):255, 2007.
152. Y. Jiang and M. Liu. Incremental stress-strain relation from granular elasticity: Comparison to experiments. *Phys. Rev. E (Statistical, Nonlinear, and Soft Matter Physics)*, 77(2):021306, 2008.
153. M. Mayer and M. Liu. Propagation of elastic waves in granular solid hydrodynamics. *Phys. Rev. E*, 82:042301, 2010.
154. B.O. Hardin and F.E. Richart. Elastic wave velocities in granular soils. *J. Soil Mech. Found. Div. ASCE*, 89: SM1:33–65, 1963.
155. Yimin Jiang and Mario Liu. Granular solid hydrodynamics (GSH): a broad-ranged macroscopic theory of granular media. *Acta Mechanica*, 225(8):2363–2384, 2014.
156. L. Bocquet, W. Losert, D. Schalk, T. C. Lubensky, and J. P. Gollub. Granular shear flow dynamics and forces: Experiment and continuum theory. *Phys. Rev. E*, 65(1):011307, Dec 2001.
157. V. Magnanimo and S. Luding. A local constitutive model with anisotropy for ratcheting under 2D axial-symmetric isobaric deformation. *Granul. Matter.*, 13(3):225–232, 2011.
158. F. Göncü, O. Durán, and S. Luding. Constitutive relations for the isotropic deformation of frictionless packings of polydisperse spheres. *C. R. Mécanique*, 338(10-11):570–586, 2010.
159. O. Durán, N. P. Kruyt, and S. Luding. Micromechanical analysis of deformation characteristics of three-dimensional granular materials. *International Journal of Solids and Structures*, 47(17):2234–2245, 2010.
160. V. Ogarko and S. Luding. Equation of state and jamming density for equivalent bi- and polydisperse, smooth, hard sphere systems. *Journal of Chemical Physics*, 136(12):124508, 2012.
161. Vitaliy Ogarko and Stefan Luding. Prediction of polydisperse hard-sphere mixture behavior using tridisperse systems. *Soft Matter*, 9(40):9530–9534, 2013.
162. Raffaele Cafiero, Stefan Luding, and Hans J. Herrmann. Two-dimensional granular gas of inelastic spheres with multiplicative driving. *Phys. Rev. Lett.*, 84:6014–6017, 2000.

163. S. Luding. Objective constitutive relations from DEM. In J. Grabe, editor, *Seehäfen für Containerschiffe zukünftiger Generationen*, pages 173–182, TUHH, Germany, 2008. GB.
164. M. R. Shaebani, M. Madadi, S. Luding, and D. E. Wolf. Influence of polydispersity on micromechanics of granular materials. *Phys. Rev. E*, 85(1):011301+, 2012.
165. Ken Kamrin. Nonlinear elasto-plastic model for dense granular flow. *Int. J. of Plasticity*, 26:167–188, 2010.
166. Ken Kamrin and Georg Koval. Nonlocal Constitutive Relation for Steady Granular Flow. *Phys. Rev. Lett.*, 108:178301, 2012.